Arabian Journal of Chemistry (2021) **14**, 103103

King Saud University

Arabian Journal of Chemistry

www.ksu.edu.sa
www.sciencedirect.com

ORIGINAL ARTICLE

The multi-dimensional approach to synergistically improve the performance of inorganic thermoelectric materials: A critical review

Y.S. Wudil [a,b], **M.A. Gondal** [a,b,*], **M.A. Almessiere** [c], **A.Q. Alsayoud** [d]

[a] *Laser Research Group, Physics Department, King Fahd University of Petroleum & Minerals (KFUPM), Mailbox 5047, Dhahran 31261, Saudi Arabia*
[b] *K.A.CARE Energy Research & Innovation Center, King Fahd University of Petroleum and Minerals, Dhahran 31261, Saudi Arabia*
[c] *Department of Biophysics, Institute for Research and Medical Consultations (IRMC) Abdulrahman Bin Faisal University, P.O. Box 1982, 31441 Dammam, Saudi Arabia*
[d] *Department of Mechanical Engineering, King Fahd University of Petroleum and Minerals (KFUPM), Dhahran 31261, Dhahran, Saudi Arabia*

Received 3 January 2021; accepted 21 February 2021
Available online 4 March 2021

KEYWORDS

Thermoelectric;
Thermal conductivity;
Power factor;
Power generation;
Seebeck coefficient;
Renewable energy

Abstract This review discusses the recent progress and persistent challenges toward achieving high thermoelectric (TE) figure of merit with inorganic TE materials. For decades, the interdependence between the relevant thermoelectric parameters has been the main impediment halting the large-scale usage of these materials for clean energy production. The thermoelectric performance can be improved by reducing the thermal conductivity or maximizing the power factor. We summarized the state-of-the-art methodologies adopted to reduce the lattice thermal conductivity to its amorphous limit, thus enhancing the figure of merit. The synergistic approach of utilizing valence band convergence, carrier filtering together with resonant levels formation has also been found to improve the power factor and the figure of merit of some TE materials. The work gives particular emphasis to systems in which spectacular advances have been demonstrated, such as chalcogenides, Heusler compounds, clathrates, and skutterudites. We further summarized different materials fabrication techniques with their success in tuning the TE performance. A discussion on future perspec-

---

[*] Corresponding author at: Laser Research Group, Physics Department, King Fahd University of Petroleum & Minerals (KFUPM), Mailbox 5047, Dhahran 31261, Saudi Arabia.
E-mail address: magondal@kfupm.edu.sa (M.A. Gondal).

Peer review under responsibility of King Saud University.

Production and hosting by Elsevier

https://doi.org/10.1016/j.arabjc.2021.103103

tive where both the power factor and the thermal conductivity can be significantly tuned via a multi-scale approach to yield high-performance TE materials for industrial applications has been presented.

1. Introduction

Energy generation for domestic and industrial applications through the conversion of waste-heat heat via thermoelectric effect has consistently received attention and aroused widespread interest globally due to the ever-growing environmental crisis such as global warming resulting from burning fossil fuels and a decline in energy resources (Wu et al., 2020). Thermoelectric materials can convert the thermal energy to electricity via the Seebeck effect, and they can be utilized for refrigeration and heating applications via the Peltier effect (Heo et al., 2019; Pavan Kumar et al., 2019; Hsieh et al., 2019; Ahmad et al., 2019). The performance of TE materials can be assessed by the dimensionless figure of merit ZT, given as $ZT = S^2T/\rho(\kappa_E + \kappa_l)$ where S is the Seebeck-coefficient, ρ is the electrical resistivity, T is the absolute temperature, $\kappa_E$andκ_l are electronic and lattice thermal conductivities respectively (Mao et al., 2019). Thus, TE material is expected to demonstrate high electrical conductivity and Seebeck coefficient while maintaining low thermal conductivity (Kleinke, 2010). The interdependence of the physical parameters makes it challenging to develop efficient TE systems.

For the past few decades, researchers have worked assiduously to improve the figure of merit using various techniques leading to decreased thermal conductivity or enhanced power factor $(PF = S^2/\rho)$ (Qian et al., 2019; Xi et al., 2018). However, the major challenge is the coupling between the relevant parameters, an impediment halting the large-scale applications of TE materials (Liu and Rajagopal, 2019; Salhi et al., 2018). For instance, high carrier concentration provides excellent electrical conductivity with reduced Seebeck coefficient and higher thermal conductivity. Therefore, although metals have high electrical conductivity due to large charge carriers, they exhibit small ZT value resulting from low Seebeck coefficient and increased thermal conductivity. On the contrary, insulators cannot be utilized for TE energy generation since they have zero electrical conductivity, which implies almost zero TE figure of merit. Typically, TE materials are neither insulators nor metals, but small bandgap semiconducting compounds with optimum carrier density between 10^{19} – 10^{21} cm^{-3} (Nolas, 2019).

Recently, a remarkable increase in ZT has been accomplished through lattice thermal conductivity minimization resulting from all length-scale phonon scattering by hierarchical architecture via mesoscale grain boundaries, second phase nanoscale endotaxial precipitates, intrinsic bond anharmonicity, and solid solution point defects. Increased Seebeck coefficient has also been achieved due to the convergence of degenerate electronic band valleys, band energy offset minimization, and resonance state formation in the electronic bands caused by alloying and carrier engineering. Another essential feature determining the quality of TE materials is the complexity of the crystal structure, as it promotes the thermopower due to the presence of spikes in the density of state (DOS), which gives rise to large first-derivative of the DOS, thus improving the thermopower as depicted by Mott Jone's equation (1) (E represents energy and E_F is the Fermi energy) (Wudil et al., 2020). The reduction in the value of κ in complex materials is a consequence of phonons scattering assisted by the plenty of grain boundaries, thus, decreasing the phonons' mean free path length (Mott and Jones, 1958; Rao et al., 2006).

$$S \propto \frac{1}{DOS(E_F)} \left| \frac{\partial [DOS(E)]}{\partial E} \right| E = E_F \tag{1}$$

Furthermore, the nanoinclusion of domains has been employed to reduce the intrinsic lattice thermal conductivity as well. In such a case, the structure impedes the phonons' motion only but transparent to electron flow. The concept is termed phonon-glass-electron-crystal (PGEC), a typical behavior whereby materials act like crystal with respect to electron scattering (high electrical conductivity) and behave like glass with respect to phonon scattering (low thermal conduction) (Slack, 1997). Furthermore, compounds made of heavy elements are principally known to possess low intrinsic lattice thermal conductivity resulting from the constituent atoms' minimized vibrational frequencies. Such elements generally form contemporary thermoelectrics (Wei et al., 2019).

In the near future, it is expected that advanced thermoelectric devices could produce sufficient energy from the waste-heat lost in industries, automobiles, and domestic appliances, thereby replacing the currently operational alternators (Wudil et al., 2019; Mahmoudinezhad et al., 2020; Angeline et al., 2019; Elmoughni et al., 2019; Karthick et al., 2019; Pourkiaei et al., 2019; Zhou et al., 2020; Kong et al., 2019; Yang et al., 2019; Rodrigo et al., 2019; Choi et al., 2019; Kanimba and Tian, 2019; Mohammadnia et al., 2020; Houshfar, 2020; Cui et al., 2019; Allison and Andrew, 2019; Zhao et al., 2019; Karthick et al., 2019; Yuan et al., 2019; Marefati and Mehrpooya, 2019). Thermoelectric materials find applications in almost all sectors of human endeavor. They can be used for power generation, refrigeration, or thermal energy sensors. They are used continuously in fields where efficiency is uniquely essential, like medicine, aerospace, biology, military, and industries.

Even the heat generated from human body can be used to energize low-power electronics such as wrist-watch on a smaller scale. In addition to photovoltaics, thermoelectric generators can generate electricity from solar thermal energy at long wavelengths (Toberer, 2016). The projected current thermoelectric efficiency of different p-types and n-types compounds is presented in Fig. 1a and 1b, respectively, according to their operation temperatures (Beretta et al., 2019). The compounds are grouped as low, medium, and high-temperature materials using blue, brown, and red colors respectively. For the thermoelectric devices to completely replace the existing freon compressors and other environmentally degrading energy sources in the global market, a ZT value

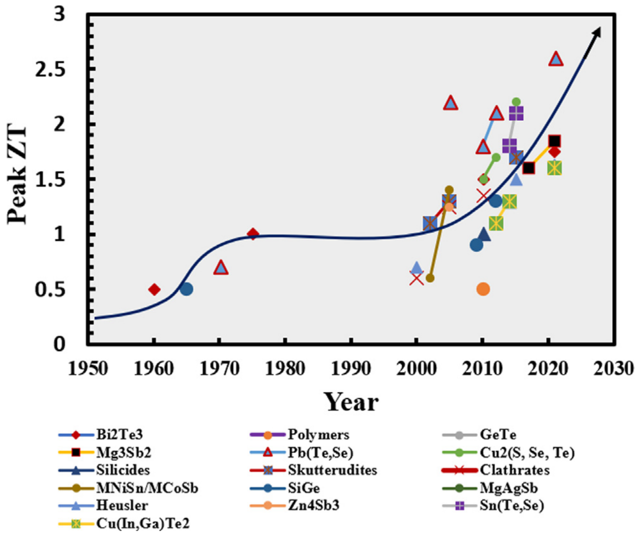

Fig. 1 Evolution of thermoelectric figure of merit for different high-performance TE materials within their optimal operation temperatures. Generated from refs (Beretta et al., 2019; Zhao et al., 2013; Biswas et al., 2012; Ma et al., 2021; Bos, 2021; Tsai et al., 2021; Yang et al., 2016; Song et al., 2019; Wu et al., 2019)

above unity is required to ensure maximum energy extraction from waste-heat (He et al., 2019). Fig. 2 summarizes TE generators' relative performance compared with other conventional solar, nuclear, and coal engines.

Owing to the diversity in thermoelectric research, which covers materials investigation, processing and design, theoretical research and device assembly, we report in this review only recent advances and existing challenges hitherto in the development of inorganic thermoelectric materials (chalcogenides, complex materials, and Heusler compounds) using cutting-edge approaches. These approaches include nanostructuring, intra-matrix band engineering, and all-scale hierarchical architecture. We have demonstrated the mechanisms to simultaneously apply these techniques additively and synergistically to improve the figure of merit. Different materials fabrication techniques have also been highlighted as they relate to ZT enhancement. A discussion of the challenges to further advance these new insights to achieve optimum ZT has also been presented.

2. Challenges in improving the TE figure of merit

The ideal thermoelectric materials are expected to the electrically short-circuited and thermally open-circuited due to their PGEC properties, i.e., thermoelectric materials are expected to acquire crystal behavior with respect to electrical conduction and glass behavior with regards to thermal conduction. The coupling existing between the transport parameters makes ZT enhancement somewhat tedious since any effort to improve one term could negatively affect the other (Wudil et al., 2020). The conventional approach to improving the figure of merit is either to enhance the power factor or to reduce the lattice thermal conductivity (Bell, 2008). While the former is achieved by optimizing charge carrier concentration, the latter is usually accomplished by creating scattering centers. TE parameters are generally defined by the carrier mobility (μ), the effective mass of the charge-carriers (m*), and the scattering factor (r). The interdependence of these parameters has marked an upper bound to ZT to around unity for bulk materials.

The kinetic definition of the Seebeck coefficient describes it as the difference between the average energy of the charge-carriers and the Fermi energy (Pichanusakorn and Bandaru, 2010). Nevertheless, both the Fermi energy and the energy of

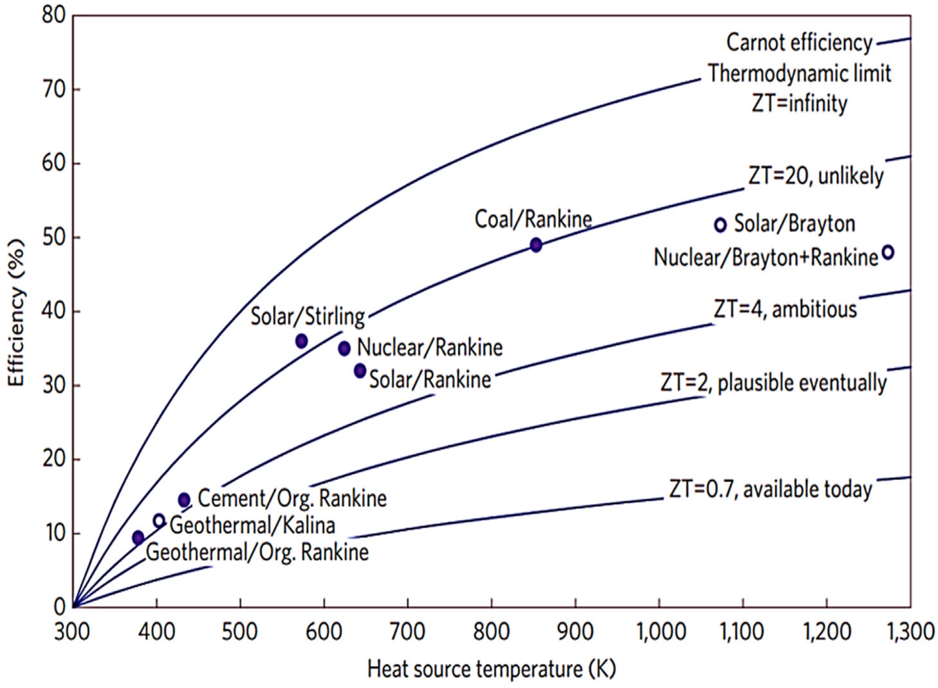

Fig. 2 Comparison of the conventional engines with optimistic TE efficiencies. Adapted from Vining, 2009

the mobile charge carriers increase with carrier concentration (n). However, the rise in the latter is less significant compared to the Fermi energy. Thus, an attempt to improve ZT by increasing the concentration of n could drag S down, reducing the overall power factor except for optimum concentration of n, where both the electrical conductivity and the thermopower are improved. Hence, for most of the homogeneous materials, increased carrier concentration improves the electrical conductivity (σ) and drags down the Seebeck coefficient. Consequently, the energy-independent scattering approximation requires that for most of degenerate semiconductors and metals, S can be defined as (Alam and Ramakrishna, 2013).

$$\frac{S}{T} = \frac{8\pi^2 k_B^2 m^* T}{(3eh^2)} \left(\frac{\pi}{3n}\right)^{\frac{2}{3}} \tag{2}$$

The high charge-carrier effective mass m* improves the thermopower which consequently enhances the power factor, as depicted in equation (2). Generally, materials with high effective mass possess low charge carrier mobility, limiting the value of the power factor, which can equally be expressed as ($m^{*3/2}\mu$). Noteworthy, there is nothing like an optimal effective mass. However, there exist low effective mass high mobility semiconductors (GaAs, SiGe) and high effective mass low mobility polaron semiconductors (chalcogenides, oxides) as well (Snyder and Toberer, 2010).

To lower the lattice thermal conductivity, defects are usually introduced to the material's matrix to scatter-off phonons, which are responsible for the lattice contribution to heat transport. Nevertheless, electrons too can get scattered in the process, causing reduced carrier mobility. Thus, the ratio $\frac{\mu}{k_{th}}$ can be used to ascertain how efficiently ZT is enhanced (D.R.-Crcp.B. Raton, undefined, 2005). Experimentally, the ratio is usually improved through reduced k_{th} instead of enhanced μ, which requires deeper exploitation of the fundamental mechanisms governing the process.

According to the Wiedemann-Franz law, the electronic contribution to the thermal conduction is proportional to the electrical conductivity of the material as (Snyder and Toberer, 2010)

$$k = \sigma L T \tag{3}$$

Where L represents the Lorenz number. The electrical conductivity can also be expressed in terms of the chemical potential, electronic charge, and carrier concentration as:

$$\sigma = \mu n e \tag{4}$$

Thus, the electronic contribution to the thermal conduction becomes

$$k_e = \sigma L T = \mu n e L T \tag{5}$$

It can, therefore, be deduced that although the low concentration of the charge carriers results in low thermal conductivity, typical of what is needed for better ZT, it also amounts to low electrical conductivity, which in turn lower the figure of merit. Similarly, equation (5) reveals that for enhanced electrical conduction, high mobility carriers are required. It is pertinent to note that equation (2) signifies that increased charge carrier effective mass improves the value of S. However, it has a negative consequence on the mobility of the charge carriers, which ultimately decreases the electrical conductivity and the figure of merit. For narrow bandgap semiconductors, carriers' thermal excitation from the valence to conduction bands generates electrons and holes, but the majority carrier's concentration does not change significantly. When two different charge carriers are present, the bipolar effect exists, which is critical for thermoelectrics (Goldsmid, 2009).

In summary, the electronic contribution to the thermal conductivity is always enhanced while improving electrical conductivity. To minimize this impact, k_{th} needs to be significantly reduced using various means. However, the most widely employed method, i.e. through defect incorporation, lowers the carrier mobility and σ. These are the most significant challenges for TE materials being addressed for decades. Until recently, the emphasis was mainly given to the nanostructuring approach by producing low dimensional TE materials and phonon engineering in bulk TE compounds.

3. Current strategies employed to improve the thermoelectric figure of merit

3.1. Nanostructuring

There exist two main classes of nanostructured TE materials. The first consists of a large assembly of nanoparticles as a single-phase material while the second constitutes a dominant bulk materials alloyed with a minor nanostructured second phase, generally introduced through precipitation or solid solutions (Dylla et al., 2019; Ge et al., 2019; Alagar Nedunchezhian et al., 2019; Wang et al., 2019; Wu et al., 2019). The bulk material may not necessarily be at the nanoscale. Nucleation and growth of a second phase is the primary method of introducing such nanostructures to the parent. The secondary phase nanostructures are expected to be completely soluble in the liquid state but insoluble in the solid-state. Rapid cooling of the melt by quenching causes the second phase to precipitate since it exceeds the solid-solution limit. For large-scale thermoelectric applications, either nanostructured bulk-materials or thin-films are employed depending on the current need. For example, thin-films show more promise in Peltier micro-chips applications, while nanostructured bulk materials are considered more appropriate for stand-alone materials.

Multiple reports have indicated that a reduction in k_{latt} is the main reason for enhancing thermoelectric performance in nanostructured bulk materials. The phonons with a varying wavelength in solid crystalline materials contribute to the heat transport at different scales. The lattice thermal conductivity is minimized due to the increased scattering of the heat-carrying phonons by the interfacial boundaries.

Thermal conductivity minimization through nanostructuring was observed in the bulk thermoelectric systems by Kanatzidis et al. (Hsu et al., 2004). They studied $AgPb_mSbTe_{2+m}$ systems and found the nanostructures embedded in the matrix of the parent compound. They attributed the decrease in the thermal conductivity to the ubiquitous and spontaneous nanoscale precipitation of the secondary phase in the host material. Generally, the nano-crystals are embedded in the matrix endotaxially with a low lattice mismatch (Kang et al., 2020). A schematic of the typical interface boundaries depicting carriers' motion is presented in Fig. 3.

Low-dimensional materials possess an excellent potential for improving the power factor or lowering the thermal conductivity. While the former is usually achieved through quan-

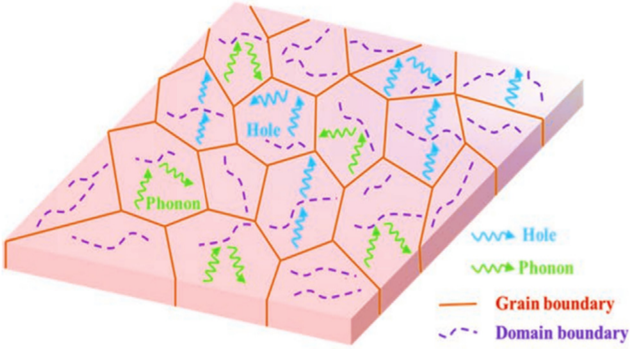

Fig. 3 A schematic of the material's grain boundaries illustrating the motions of holes and phonons. Adapted from ref (Zhang et al., 2019).

tum confinement formation by the nanostructures, the latter could be accomplished by introducing intrinsic interfaces to impede phonon transport. Higher thermopower could be realized in nanomaterials due to the increased density of states around the Fermi level. Anisotropic Fermi surfaces in nanomaterials of multi-valley cubic-semiconductors are critical to achieving delta doping and modulation doping. Nanomaterials with a delta-like density of states do not obey the Wiedemann-Franz law, thus, making them promising candidates for improved thermoelectric performance (Venkatasubramanian et al., 2001).

Due to the change in the density of states with spatial confinement of charge-carriers, theoretical predictions on ZT enhancement via nanostructuring were based on the power factor modification and the electronic contribution to the thermal conductivity. These studies mainly used the bulk values for k_{ph} by ignoring the phonon spatial confinement. However, it is essential to mention that due to mini-Umklapp mechanisms and mini-band formation, the phonon transport can be modified even for superlattice of similar compounds. The relaxation rate of the phonons is affected mainly by the phonon confinement effect, which caused the significant difference between the thermal properties of bulk materials and nanostructured materials (Balandin and Wang, 1998).

There exist multiple attempts to improve the efficiency of TE materials using low-dimensional structures. Recently, Guodong et al. (Li et al., 2019) reported an exciting twin boundary mechanism to reduce the lattice thermal conductivity of Mg_2Si without adversely affecting the electrical transport properties such as the Seebeck coefficient and electrical conductivity. They introduced the concept of nano-twinning and validated it through the density functional theory approach. A significant reduction of thermal conductivity ~ 90% was recorded (Fig. 4), which they attributed to higher phonon scattering rate, short phonon lifetime, Mg-Mg pair rattling, and lower phonon velocities. The authors suggested the possible extension of this technique to other low-thermal conductivity desired materials.

Yuan et al. (Wang et al., 2019) realized a significant improvement in the peak ZT value from 0.7 at 470 K to 1.1 for nanostructured Bi_2Te_3. They employed a non-equilibrium reaction triggered by spark plasma sintering to suppress the Te-vacancies in order to lower the carrier concentration, which eventually led to low electronic thermal conductivity. The authors suggested that the method could be utilized to control point defects in TE materials.

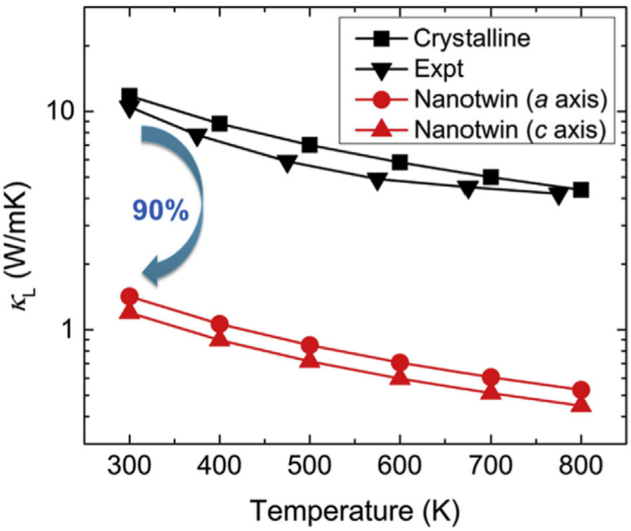

Fig. 4 Comparison of the nano-twinned Mg_2Si lattice thermal conductivity with crystalline Mg_2Si and experimental result for bulk Mg_2Si. Adapted from Li et al., 2019

Recently, Wenke et al. (He et al., 2019) reported a significant improvement in the value of ZT through selenium inclusion in tin sulfide (SnS) material to form environmentally-friendly and low-cost $SnS_{0.91}Se_{0.09}$. They observed an appreciable decrease in the lattice thermal conductivity with an enhanced thermoelectric power factor leading to a ZT of ~ 1.6 at 873 K (Fig. 5). Such remarkable performance was accomplished through electronics band manipulation, which allows synergistic optimization of charge-carrier mobility and effective-mass.

Xiaoming et al. (Hu and Hu, 2019) developed highly uniform and porous p-type $Bi_{0.4}Sb_{1.6}Te_3$ bulk material using resistance pressing sintering. A significant decrease in thermal and electrical conductivities was observed with increasing porosity. However, the reduced electrical conductivity was compensated by the decreased thermal conductivity, thereby attaining a high ZT of ~ 1.1 at 343 K, about 20% enhancement compared to the pure dense sample. The authors proposed that the porous structures' uniformity is critical for enhanced thermoelectric performance and mechanical properties.

Jian et al. (Zhang et al., 2019) investigated chalcopyrite $CuGaTe_2$ due to its remarkable power factor. They prepared a complex nano-scaled quinary system of $Cu_{1-x}Ag_xGa_{0.4}In_{0.6}$-$Te_2$ ($0 \leq x \leq 0.4$). They achieved an impressive reduction in thermal conductivity from 6 W m^{-1} K^{-1} to 1.5 W m^{-1} K^{-1} (-for × = 0.4) via alloying of Ag and In isoelectronic elements to provide scattering sites. Consequently, an outstanding ZT of 1.6 was realized for the chalcopyrite $Cu_{0.7}Ag_{0.3}Ga_{0.4}In_{0.6}Te_2$ at 873 K, about 37% enhancement compared with the pristine $CuGaTe_2$ (Fig. 6). The authors propose that such isoelectronic multi-element alloying can significantly reduce chalcopyrite compounds' thermal conductivity and improve its overall thermoelectric performance.

Elsewhere, Zhou et al. (Zhou et al., 2005) fabricated Bi_yTe_{1-y} nanowires on Al_2O_3 membrane at different ratios. Compared to the bulk phase, improved thermopower was observed at

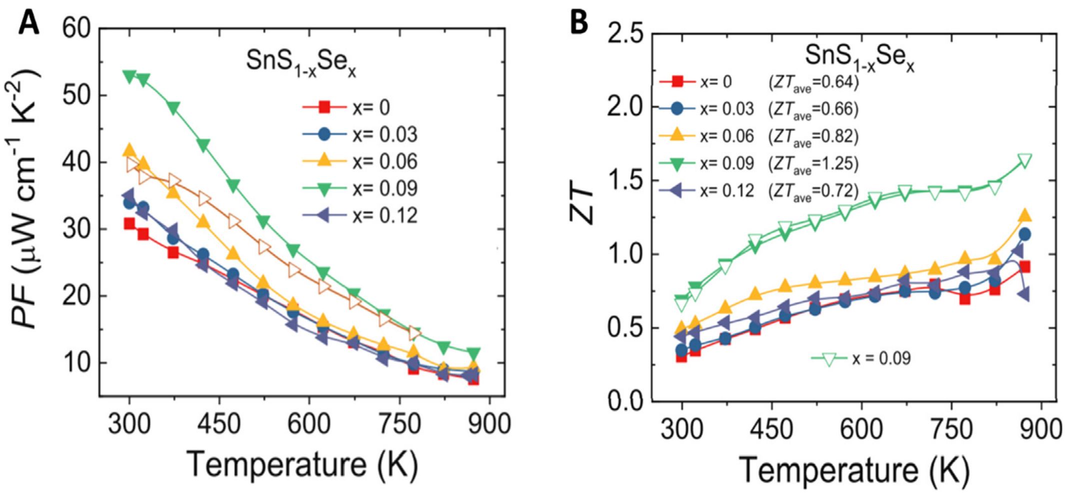

Fig. 5 (a) The thermoelectric power factor for Se-doped SnS (b) Temperature-dependent ZT of Se-doped SnS. Adapted from ref (He et al., 2019).

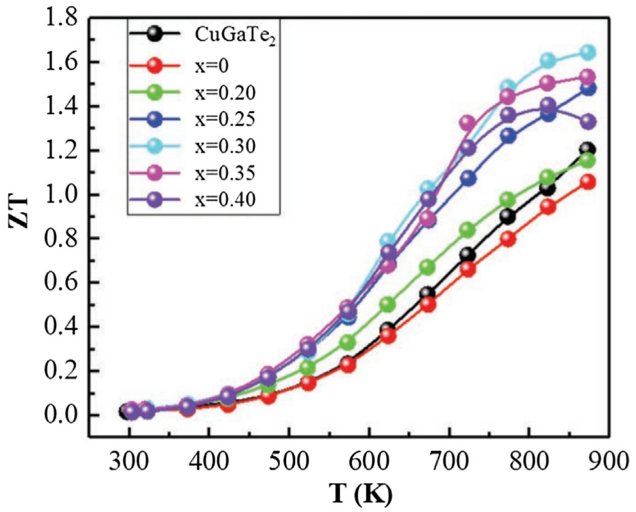

Fig. 6 Temperature dependence of ZT values for pure $CuGaTe_2$ and samples of $Cu_{1-x}Ag_xGa_{0.4}In_{0.6}Te_2$ (x = 0, 0.20, 0.25, 0.30, 0.35, 0.40). Adapted from ref (Zhang et al., 2019).

300 K when y = 0.46. However, a higher value of y showed decreased thermopower. The average surface-roughness of the nanowires (~1nm) was believed to contribute to the reduction of the intrinsic lattice thermal conductivity without deteriorating the electronic conductivity despite the wavelength of electrons is of the order of 10 nm while for the phonons is of the order of 1 nm. Similarly, the thermal conductivity of $Si_{0.8}Ge_{0.2}$ prepared by pressure sintering was found to be below that of its bulk crystalline powder due to the presence of defects. However, a simultaneous decrease in ZT was observed, which was harmful to ZT enhancement. Several of these cases have been reported where a decrease in k could not improve the value of ZT for one reason or the other (Lee et al., 1997). Kim et al. (Kim et al., 2006) reported the epitaxial embedding of ErAs into $In_{0.53}Ga_{0.47}As$ where they observed a decrease in the lattice thermal conductivity with an increased electronic contribution to the thermal conductivity due to phonon scattering and electron–phonon scattering, respectively. ErAs was assumed to provide more scattering-mechanism for low to high wavelength phonons. Hitherto, the fundamental explanation of how and why thermal conduction of crystalline materials is reduced through nanostructuring is still not sufficient. . Nano-structuring has opened a new window for thermal conductivity suppression apart from using the complex structures as the interdependence of the transport properties which are difficult to control in bulk materials becomes relatively more comfortable to deal with (Wang et al., 2020; Marinho et al., 2019; Sivaprahasam et al., 2019; Dylla et al., 2019; Gainza et al., 2019; Fitriani et al., 2016; Yin et al., 2019).

3.2. Mass fluctuations

The concept of mass fluctuations is yet another promising technique employed to reduce the lattice thermal conductivity. Once the difference between the masses of the dopant atom and the host element is large, the lattice periodicity is disturbed and consequently increases phonon scattering, thereby minimizing the lattice thermal conductivity (Lu et al., 2019).

Elsewhere (Hooshmand Zaferani et al., 2019), reduced lattice thermal conductivity was observed while using heavy masses with large unit cells and low spring constants. Similarly, solid-solution alloying has been reported to lower the lattice thermal conductivity due to mass fluctuations (Biswas et al., 2019). For the alloying approach, the constituent alloys' mass ratio significantly determines the scattering rate, and the random vacancies produced serves as the typical scattering regions.

Wenqi et al. (Lu et al., 2019) reported a remarkable ZT of 1.85 for lead and sulfur co-doped tin selenide at 873 K. They claimed that co-doping has widened the bandgap and consequently reduced the bipolar thermal conductivity. They observed a record low thermal conductivity of 0.13 $W\,m^{-1}\,K^{-1}$, resulting from the synergistic approach of thermal conductivity minimization and mass fluctuations triggered by nanoprecipitates and sulfur incorporation, as depicted in Fig. 7. The authors proposed that high thermoelectric performance could be accomplished by introducing large mass fluctuations, suppressing bipolar thermal conductivity, and tailoring the band structure.

The introduction of mass fluctuations to half Heusler materials is yet another critical mechanism to reduce kth (Kang et al., 2020). For example, ZrNiSn having a crystal structure of MgAgAs family possesses bandgaps of about 0.20 – 0.25 eV. Their crystal structure consists of three interpenetrating face-centered cubic sublattices and a nickel sub-lattice vacancy. Shen et al. (Shen et al., 2001) introduced Hf on Zr site, causing phonon mass-fluctuations scattering, which led to the decrease in the value of k. They also studied the effects of introducing Sb on the Sn sites where they observed a significant increase in the thermopower due to the reduction of electrical resistivity without deteriorating the Seebeck coefficient. Also, they investigated the effect of isoelectronic incorporation of palladium in nickel sites on the overall thermal conductivity. Finally, a thermal conductivity value of 4.5 W/mK and a power factor of 22.1 μW/K^{2}cm were obtained at room temperature for the composite $Hf_{0.5}Zr_{0.5}Ni_{0.8}Pd_{0.2}Sn_{0.99}Sb_{0.01}$. On the other hand, Browning et al. (Browning et al., 1999) suggested that although chemical substitutions immensely alter the chemical properties of ZrNiSn, the effect on the enhancement of the figure of merit is insignificant.

3.3. *All-scale hierarchical architecture*

The all-scale hierarchical approach involves the simultaneous scattering of heat-carrying phonons through the full-spectrum range of their mean free path, via defect incorporation, nanoscale precipitation, and mesoscale grain boundary creation integrated to reduce the lattice thermal conductivity synergistically (Zhao et al., 2013). The strategy is robust enough to bring the thermal conductivity to its amorphous limit. Generally, nanostructured bulk thermoelectric materials contain some atomic defects either due to the dissolution of the dopants or partial dissolution of the second phase. Acoustic phonons are majorly responsible for the thermal transport in crystalline materials, and the phonons can be defined in terms of their mean free path and wavelength, each of which contributes to the heat transport (Biswas et al., 2012).

Atomic defects can quickly scatter the phonons with a mean free path between 0.1 and 1 nm due to defect-induced local bond-strain or mass contrast. Meanwhile, the phonons with a mean free path in the range 1–100 nm can be scattered by the nanoprecipitates. Such scattering predominantly occurs at the interface between the matrix and the precipitates or due to mass contrast. However, the phonons with a mean free path in the range 0.1–1 μm are mostly unaffected. Thus, the need to devise a means to suppress the long-wavelength phonons becomes necessary (Kang et al., 2020). To scatter the long mean free path phonons, there is a need to break the crystal to a mesoscopic scale (0.1 – 5 μm) followed by sintering of the fine powders to facilitate scattering at the interfacial regions. Elsewhere, it is reported that Si/Ge alloys grain sizes of 4 μm facilitated thermal resistance up to 26% due to grain boundary scattering (Zhao et al., 2014).

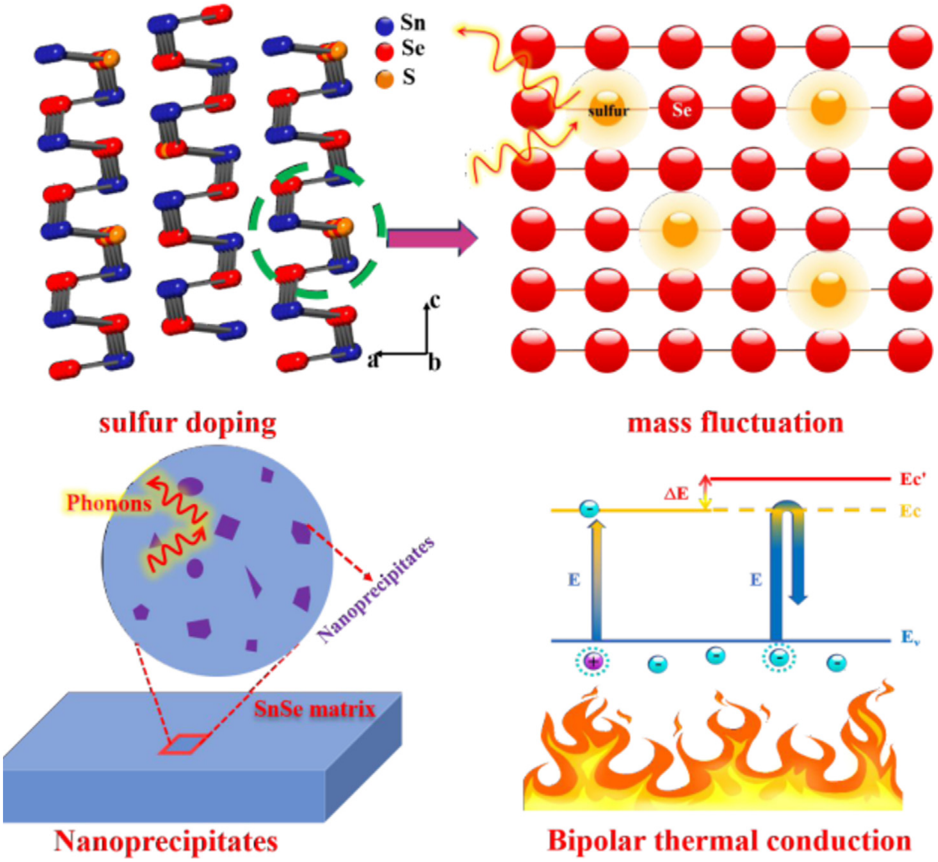

Fig. 7 Schematic description of thermal conductivity suppression due to Pb and Se co-doping. Adapted from ref (Lu et al., 2019).

Therefore, to scatter the phonons through all mean free path ranges, from the nanoscale to microscale, the solid solution atomic defects, nanostructuring, and mesoscale approach must be integrated into a single sample as presented in Fig. 8. Fig. 8b shows the phonons distribution according to their mean free path and consequently assigned to their preferred mode of scattering. Biswas et al. (Biswas et al., 2012) applied the all-scale architectural approach to study the thermoelectric properties of PbTe-SrTe (4 mol%) composite doped with 2 mol% Na prepared by melting reactions of the solid precursors, followed by spark plasma sintering of the crushed ingots. They recorded a 30 – 50% enhancement in ZT compared to the melt-processed samples. They achieved a record high ZT of 2.2 at 915 K, underscoring the significance of the multiscale approach to effectively reduce the lattice thermal conductivity, thus remedying the challenge of improving ZT.

Recently, Priya et al. (Kang et al., 2020) reported the successful implementation of the all-length-scale hierarchical approach on $(Hf_{0.6}Zr_{0.4})NiSn_{0.99}Sb_{0.01}$ half-Heusler material doped with tungsten nanoprecipitates prepared using RF induction melting and spark plasma sintering to produce the required pellets. At the atomic scale, the multi-element alloying at M site facilitated reduced thermal conduction due to scattering at point defects within the lattice. At the nanoscale, hafnium nano precipitates were generated at the half-Heusler matrix due to the rapid fabrication process involved, contributing to the scattering of the medium range (1–100 nm) mean free path phonons. Finally, the long-scale mean free path phonons were scattered by the mesoscale grain boundaries resulting from sintering the sample. The integrated approach triggered an ultra-low thermal conductivity for the half-Heusler material, which consequently yielded ZT of 1.4 at 773 K and a ZT average of 0.93 between 300 K and 973 K. The material also exhibited a power density of 13.9 W/cm When used as in thermoelectric generator.

Elsewhere (Zhao et al., 2013), a ZT of 2.0 at 823 K was achieved for PbTe-MgTe composites doped with 2% Na via the all-scale hierarchical architecture. The Mg endotaxial nanostructures, coupled with the mesoscale microstructure, facilitated the reduction in the lattice thermal conductivity. Further decrease in the thermal conductivity was enhanced by Mg alloying, which increases the energy gap of PbTe, thus lowering the effect of thermally excited minority carrier diffusion, which increases the bipolar thermal conductivity.

Tingle et al. (Li, n.d.) found out that the thermoelectric properties of Sn_2Bi can be significantly enhanced through fluorination. They observed a record-low thermal conductivity of 0.19 W m^{-1} K^{-1} and ultra-high ZT of 1.70 and 2.45 at 300 K for p-doped and n-doped compounds, respectively higher than the reported ZT of $Bi_{0.48}Sb_{1.52}Te_3$ (ZT ~ 1.4 at 475 K) and $Bi_2Te_{2.79}Se_{0.21}$ (ZT ~ 1.2 at 357 K). They attributed such improvement to the enhanced anharmonicity, reduced group velocity, and increased three-phonon scattering phase space.

3.4. Electronic band engineering

The preceding sections have discussed various ZT enhancement mechanisms through lattice thermal conductivity minimization, including nanostructuring, mass fluctuations, and an all-scale hierarchical approach. Herein, we discuss the power factor enhancement strategies by mainly boosting the Seebeck coefficient through intra-matrix band engineering via band convergence, band alignment, or resonance level formation. We demonstrated that a simultaneous increase in the Seebeck coefficient and electrical conductivity could be achieved at optimum carrier concentration.

3.5. Band convergence

Lead and tin chalcogenides exhibit a fascinating valence band structure. Apart from the conventional light hole valence band existing at the high-symmetry L-point of the Brillion zone, they possess an additional valence sub-band at the (Σ) point, known as the heavy valence-band, at a relatively lower energy level (Banik et al., 2015).

At high temperatures, the p-type charge carriers can be accommodated into the two valence sub-bands. Due to their cubic symmetry, the two bands exhibit high degeneracy, which ultimately improves the thermopower. Previously, the literature suggested that while the Σ-band remains roughly at a constant energy level with respect to the conduction band, the L-band moves down gradually as temperature increases, depend-

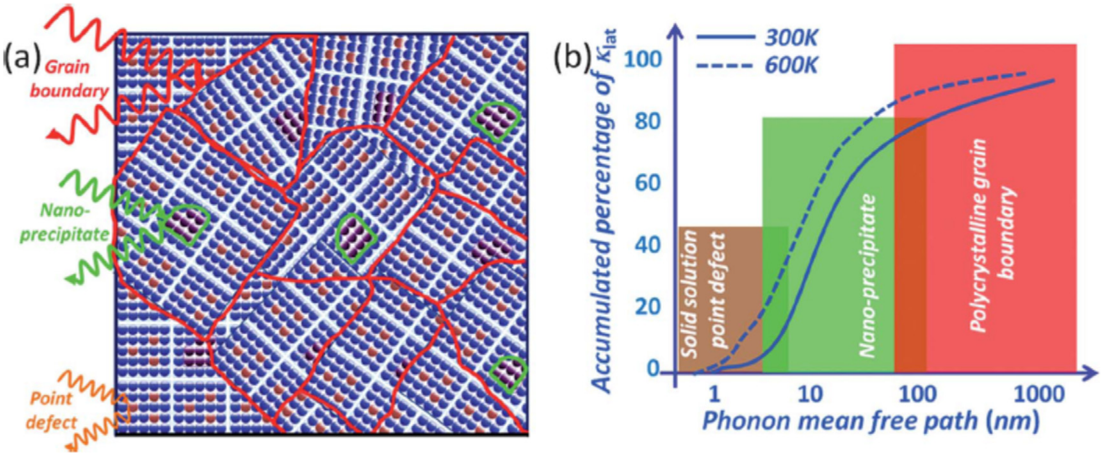

Fig. 8 The all-scale hierarchical approach to minimize the lattice thermal conductivity showing (a) atomic defects, nano-precipitate, and mesoscale grain boundary (b) Phonons distribution according to their mean free path. () Adapted from Zhao et al., 2014

ing on the energy offset between the two valence sub-bands, and passes the Σ-band edge at a specific temperature (see Fig. 9) (Zhao et al., 2014). This model implies that the material rapidly changes from a direct gap to an indirect gap semiconductor with increasing temperature. However, recent studies have challenged this proposition. Hall-effect investigations revealed that the proposed convergence does not occur up to 1000 K temperature. Experimental results showed that PbTe maintained its direct gap behavior up to 800 K (Biswas et al., 2012), indicating the absence of valence band convergence with increasing temperature.

This new perspective implies that as the temperature increases, the difference in energy between the two valence sub-bands may decrease. However, the L-band does not cross below the energy level of the Σ-band. Thus, there exists a little controversy that needs to be rectified experimentally. In this notion, as the energy difference between the two valence sub-bands decreases, the heavy valence sub-band contribution to the transport increases due to the thermal excitation of the holes from the L to the Σ band. Generally, heavy doping facilitates the heavy valence band's contribution to the Seebeck coefficient as it lowers the Fermi energy and minimizes the energy offset between the two valence sub-bands. Therefore, the contribution of the Σ sub-band can be realized at low temperatures via heavy doping.

As depicted in Fig. 10, at a given carrier concentration, p-type PbTe exhibited a remarkably larger Seebeck coefficient than the n-type PbTe, especially at higher temperatures. Specifically, the Seebeck coefficient of the n-type PbTe is −180 μV/K, while that of the p-type PbTe with the same carrier concentration is + 270 μV/K (Pei et al., 2012; Lalonde et al., 2011). The excesses in the Seebeck coefficient can be attributed to the contributions from the heavy valence band. The n-type materials could not demonstrate such improvement due to the single-nature of the conduction band. The production of holes at the Σband further enhances the Seebeck coefficient due to their large effective mass, as shown in equation (2). On the other hand, both p- and n-type PbSe exhibited nearly the same Seebeck coefficient at room temperature. However, the Seebeck coefficient of the p-type PbSe increased dramatically with rising temperatures. For instance, at 920 K, the value of the Seebeck coefficient for p-type PbSe is + 250 μV/K, while for n-type, it is −100 μV/K at the same carrier concentration (Zhao et al., 2013). The increase in the Seebeck coefficient for the p-type PbSe is attributed to the role played by the Σ band at higher temperatures. For the PBS system, both the n-type and the p-type samples exhibited a similar Seebeck coefficient up to 900 K temperature demonstrating the lesser impact of the heavy valence band (Zhao et al., 2011). This unique characteristic different from PbSe and PbTe may be attributed to the considerable energy offset between the light and heavy hole valence bands (about 0.4 eV).

Elsewhere, Shenoy et al. (Shenoy and Bhat, 2019) have demonstrated that Bi-doping in SnTe also facilitated valence band convergence. They reported an optimized ZT of 1.32 at 840 K due to the increase in the Seebeck coefficient. Similarly, Biswas et al. (Banik et al., 2015) have reported an increased Seebeck coefficient in SnTe resulting from Mg-alloying. They

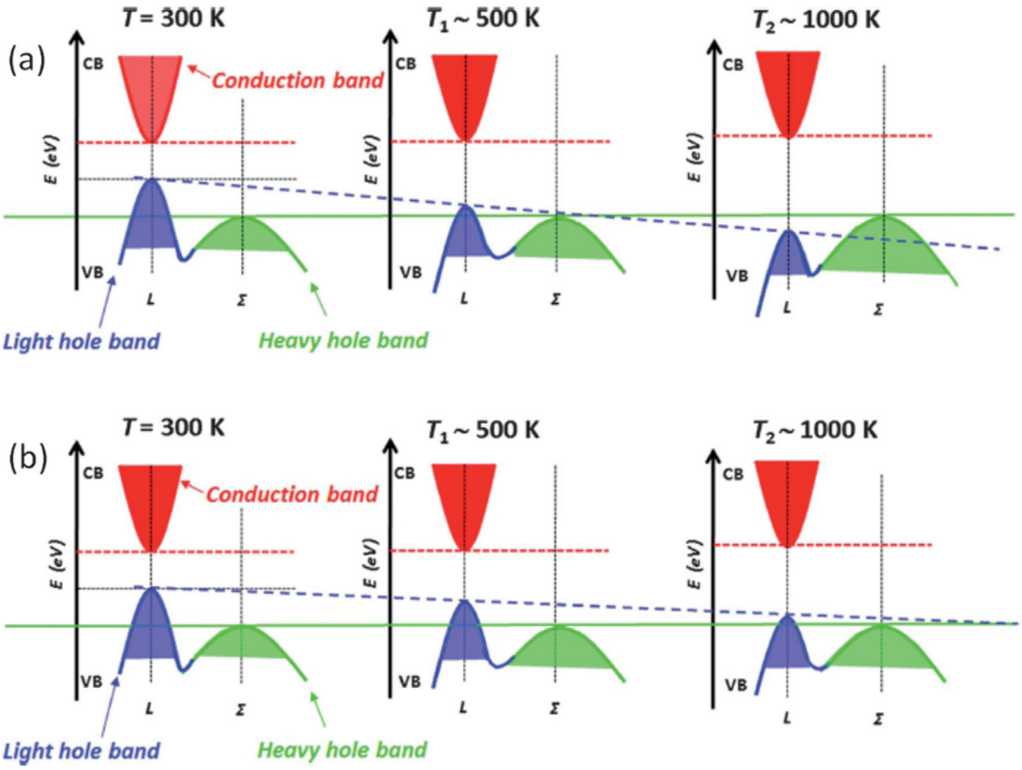

Fig 9 The two proposed models for the valence band convergence in the PbTe system as a function of temperature (a) The light hole band crosses below the heavy hole band (b) The second model showing the slow convergence with the L-band above the Σ-band. () Adapted from Zhao et al., 2014

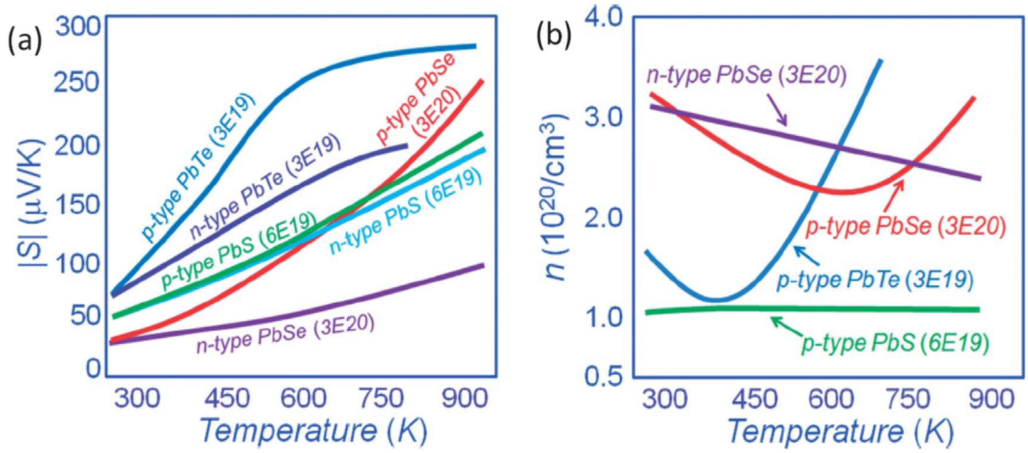

Fig. 10 (a) Seebeck coefficient as a function of temperature for lead chalcogenides showing the enhancement in p-type samples except for PbS which remains almost the same up to 900 K (b) Carrier concentration as a function temperature, the upturn shows the onset of Σ-band contribution.

achieved a ZT of 1.2 at 860 K temperature. In summary, doping lead and tin chalcogenides with Hg, Mg, Cd, Ca, and Mn has resulted in valence band convergence (Banik et al., 2015).

DFT calculations demonstrate that the compositional alloying of these compounds $Pb_{1-x}A_xQ$ (Q = Se and Te) with metals may trigger the convergence of the two valence sub-bands (D'Souza et al., 2020). As the solid solution fraction of A increases, both the L- and Σ sub-bands lower their energies with the L-band moving faster than the Σ sub-band, thus, narrowing their energy offset. Noteworthy, if the second phase has a larger bandgap, the principal bandgap (L- point to conduction band) will increase with the increase in the second phase. In general, such calculations suggest that the energy level of the Σ sub-band does not change significantly. Hence, alloying via a solid solution is a practical approach to improve the Seebeck coefficient.

3.6. Resonance level formation

The distortion in the density of state can significantly enhance the Seebeck coefficient of thermoelectric semiconductors. Some group III impurities induce specific characteristics in IV-VI semiconducting materials related to the creation of deep and resonance energy levels. The discovery of this phenomenon has opened a new window for manipulating the thermoelectric properties of IV-VI compounds. The Fermi level is mainly pinned at the impurity states. The origin of the doping-induced virtual energy levels is still a subject of research. They are ascribed to either existence of an additional Fermi surface, or hybridization between neighboring Te-state (for Tellurides) and an excited resonant atom, or due to valence fluctuation (Heremans et al., 2008).

The electronic properties of different compounds doped with a particular group III elements turned out to be diverse. Meanwhile, doping the same compound with different group III elements also yielded different results. The critical factor here determining the expected outcome is the region in the electronic spectrum in which the impurity states exist. For instance, indium acts as a donor in PbTe, creating impurity levels near the conduction band, pinning the chemical potential in this part of the electronic spectrum. However, it forms a resonant state within the valence band of SnTe and therefore acts as an acceptor element (Heremans et al., 2012).

Generally, the formation of resonant states influences the thermoelectric transport properties due to two main reasons: (1) The distortion of the electronic density of states, which translates itself as increased DOS near a characteristic energy level, and (2) Enhanced scattering resulting from the resonance of carriers between the conduction band of the host matrix and the localized impurity states from the dopants. To achieve maximum performance, extrinsic doping is often necessary to optimize the figure of merit because usually, intrinsic defects do not provide the optimum carrier density. Another viable means of improving the performance of materials doped with resonant elements is to control the carrier concentration via the introduction of an extrinsic (non-resonant) element to independently tune the carrier density for optimum ZT (Zhou et al., 2016).

Several works have been conducted to improve the TE performance of IV-VI compounds by forming resonant energy levels (virtual states). For example, Zhang et al. (Zhang et al., 2013) reported a high ZT of 1.1 for resonant In-doped SnTe at 873 K. Similarly, Heremans et al. (Heremans et al., 2008) observed a high ZT of 1.5 at 773 K for resonant Tl-doping in PbTe for $Tl_{0.02}Pb_{0.98}Te$. Recently, Shenoy et al. co-doped SnTe with two resonant atoms (Bi and Zn). They observed remarkable improvement in the performance, with ZT reaching 1.6 at 840 K and a record high figure of merit of 0.86 between 300 K and 840 K. Thus, this unveils a novel strategy to improve the performance of the Pb-free compound further. Elsewhere, Zhang et al. (Ma et al., 2019) reported a dramatic increase in the figure of merit of SnTe resulting from Pd-In co-doping, where indium facilitated the formation of resonant levels while Pd stimulated valence band convergence.

3.7. Substructure approach

Another distinctive approach to mitigate the PGEC difficulty is via the substructure approach, where each region serves a different purpose (Zhu et al., 2019; Zhang et al., 2019). An insulating

Table 1 Summary of the materials fabrication techniques.

Fabrication Technique	Materials produced	Precursors used	Remarks	Refs.
Solvothermal process	Nanoflowers of Bi_2Te_3	Na_2TeO_3, $Bi(NO_3)_3{\cdot}5H_2O$, acetone, ethanol, PVP K30, and formic acid	Low-cost. defective nanoflowers yielded medium performance (ZT = 0.68). The authors observed that the nucleation process of thermoelectric compounds is controlled by the type of solvent used.	(Guo et al., 2016); (Liang et al., 2011) (Deng, 2002)
	Single crystals of Bi_2Te_3 nanostructures	Ethylene glycol, sodium dodecyl benzene sulfonates, EDTA, NaOH, Na_2TeO_3, and $BiCl_3$	Optimum TE power conversion was realized due to increased phonon scattering which lowers the thermal conductivity.	(Zhang et al., 2013)
Chemical method (solution process)	single crystal of SnSe	Ethylenediamine, SnSe powder, and acetonitrile,	A remarkable power factor was obtained emanating from the synergistic effect of the textured-microstructure due to transitions from 2D $SnSe_2$ to SnSe phases	(Heo et al., 2019)
	Bi_2Te_3 nanoparticles	hydrazine hydrate, glycol, ethylene, $BiCl_3$, and Te powder	The authors recorded high ZT as a consequence of reduced thermal conductivity.	(Srivastava and Singh, 2012)
Facile solution	Nanocrystalline Bi_2Se_3 and Bi_2Te_3	[$BiCl_3$], $NaBH_4$, methanol, Se, powder, [$Bi(NO_3)_3$] and [$Bi(CH_3COO)_3$]	They carried out microstructural characterization and obtained spherically shaped Bi2Se3.	(Mntungwa et al., 2014)
Hydrothermal method	nanorods, nano-plates, and nanotubes of Bi_2Te_3	Te powder, $BiCl_3$, Na_2-EDTA	-	(Kim et al., 2012)
	Bi_2Te_3-flakes	$BiCl_3$ and Te powder assisted by $NaBH_4$ and NaOH	SEM revealed non-uniform structures, enhanced carrier mobility led to an increase in the overall TE performance	(Li et al., 2011)
Hydrothermal method	2D nanoplates of Ge-doped SnSe	-	Incredible TE performance was achieved, ZT of ~ 2.1 at 873 K, resulting from an increased flow of p-type carriers induced by Ge	(Chandra and Biswas, 2019)
Large-scale zone melting technique	Zn and Cu-doped $Bi_2(Te_{0.9}Se_{0.1})_3$ ingots	–	High ZT of 1.10 and 1.15 was recorded for the Zn and Cu loaded ingots, resulting from decreased thermal conductivity.	(Wang et al., 2013)
Molecular-Beam-Epitaxy	$PbTe/Pb_{1-x}Eu_xTe$	–	A Remarkable increase in ZT to 2.0 at 300 K temperature was observed	(Tan et al., 2016)
Bridgman technique	single-crystalline Bi_2Te_3	–	Anisotropic transport properties induced by the growth mechanisms were observed.	(Nassary et al., 2009)
RC-sputtering	$Fe_2V_{1-x}W_xAl$ thin film samples		An incredible TE figure of merit above 5.0 was accomplished for the Heusler materials.	(Hinterleitner et al., 2019)
High-pressure torsion	NbFeSb and $Ti_{0.5}Zr_{0.5}NiSn$-based materials	–	ultra-low κ resulting from deformation-induced defects + lattice stiffening caused by the torsion method was realized.	(Rogl et al., 2020)
Arc-melting technique	(Ti, Hf, Zr)CoSb composites	–	Fe-inclusion in the Co sites to make $TiFe_xCo_{1-x}Sb$ (at × = 0.15) has improved the TE performance of such material	(Sekimoto et al., 2005)
Ball-milling followed by dc-current hot-pressing	$Zr_{0.5}Hf_{0.5}CoSb_{0.8}Sn_{0.2}$	–	Increased phonon scattering reduces κ, however, high agglomeration gives rise to larger grains scattering electrons at the detriment of the charge-carrier mobility.	(Yan et al., 2011)
Czochralski technique	$Ba_8Ga_{16}Ge_{30}$	–	They obtained homogeneous crystal with a larger Ga/Ge ratio due to higher pressure and larger pulling, plus low κ.	(Hou et al., 2009)

oxide layer could be used to separate free charge-carriers encapsulated to planar Cu-O sheet. The oxide layer accommodates the dopant-atoms that produce electrons to the planar Cu-O sheet. The isolation of the conducting region from the doping region ensures effective screening of the charge-carriers from the dopants, thus, avoiding a decrease in mobility due to carrier-trapping. In this proposed configuration, the phonon-glass region accommodates the dopant atoms and disordered-structures without deteriorating the electron-crystal region. The dimension of the electron-crystal regions is desired to be in the order of angstroms or nanoscale to facilitate electron filtering, thereby enhancing the Seebeck coefficient. Additionally, phonons with short mean free-path can be scattered within the phonon-glass region. $Ca_xYb_{1-x}Zn_2Sb_2$ is a promising thermoelectric material that uses the substructure approach. However, its thermal conductivity is relatively high (about 1.5 W/mK) compared with the state-of-the-art materials (Gascoin et al., 2005). For heat transport, a wide range of phonons are involved, and hence the need to introduce a large-scale disorder to scatter long-wavelength phonons. Combining the nanostructuring and substructure approach could be crucial in improving the thermoelectric performance.

We have summarized in table 2, those materials that have exhibited an excellent thermoelectric figure of merit together with some important remarks on the potential reasons behind their performance.

3.8. Synergistic integration of multiple mechanisms

The most effective way to realize a cutting-edge figure of merit in thermoelectric materials is to devise a means of strategically integrating the multiple approaches in a single sample. The electronic structure engineering tactics can enhance the power factor while the thermal conductivity can be minimized by considering the all-length scale hierarchical techniques. However, such synergistic improvements are not easy to apply. For example, when extrinsic dopants are introduced to regulate the carrier density stimulate band convergence, they tend to increase the electronic thermal conductivity and reduce the figure of merit. Similarly, when nano precipitates are injected to scatter the medium wavelength phonons, the low energy charge carriers produced affect the Seebeck coefficient's value adversely. Therefore, the systematic improvement of one parameter without inducing a deleterious impact on the rest is the field's future research trend.

Recently, many groups have attempted to combine as many of the approaches as possible to achieve high ZT. Kanatzidis et al. (Zhao et al., 2016) reported a remarkable improvement in ZT for the SnTe system nanostructured with SrTe and doped with several elements (Ga, Bi, and In). They successfully lowered thermal conductivity and enhanced electrical transport properties. Similarly, Kang et al. (Kang et al., 2020) achieved a ZT of 1.4 at 773 K for half Heusler $(Hf_{0.6}Zr_{0.4})NiSn_{0.99}Sb_{0.01}$ via a synergistic effect of carrier filtering integrated with all-scale hierarchical phonon scattering. Furthermore, Zhao and his team (Zhao et al., 2013) achieved a ZT of 2.0 for Na-doped PbTe in 6% MgTe. They ascribed the high performance to the simultaneous increase in the power factor through valence band convergence, a decrease in the lattice thermal conductivity via an all-scale hierarchical approach, and bipolar thermal conductivity suppression.

Some groups combined binary thermal conductivity minimization and enhancement of the carrier transport properties (Khitun et al., 2000; Balandin and Lazarenkova, 2003). They achieved such a milestone using Quantum-dot-superlattice (QDS) to improve the quantum confinement of carriers. For the QDS materials, the electronic conduction occurs due to the hopping between the dots, mainly characterized by low-mobility. Therefore, with QDS, the electrical transport properties should be equally a matter of concern as the thermal transport. The formation of 3D extended mini bands through regimentation and strong coupling was proposed instead of localizing the quantum-dot states. The fabrication of 3D regimented quantum dot superlattices of Ge grown on Si was suggested (Balandin and Lazarenkova, 2003). Typically, due to the spatial confinements, an improved phonon relaxation rate was observed, resulting from substantial modification in phonon group velocity. Multiple works indicated a considerable reduction in the lattice thermal conductivity of Ge/Si QDS than their bulk counterparts (Khitun et al., 2000).

The use of superlattices as promising thermoelectric materials also enables the application of multiple approaches to improve ZT. A superlattice system of Si/SiGe multiple-quantum-well (MQW) structured samples was studied by Dresselhaus et al. (Dresselhaus et al., 1999), where they recorded a dramatic increase in the power factor. Similarly, $PbTe/Pb_{1-x}Eu_xTe$ MQW was grown using the MBE technique at different quantum well's width (Hicks and Harman, 1996). A remarkable increase in ZT to 2.0 at 300 K temperature was realized. Generally, compared with their bulk counterparts, the 2D MQW structures demonstrate an improved figure of merit with narrowed quantum well's width, which causes a hike in charge carriers' density per unit volume. In summary, the thermoelectric power factor can be enhanced by the carrier pocket engineering (CPE), and the Seebeck coefficient can be boosted through trapping of cold charge-carriers by the band discontinuities in the quantum wells (Dresselhaus et al., 2007). It was established that CPE could be employed to adjust the barrier thickness and the quantum well's width to set the energies of the L and X point sub-bands to below the lowest gamma point sub-band, thereby increasing the density of states of the L and X point sub-bands. This phenomenon was typical in the whole superlattice materials like GaAs/AlAs. A figure of merit of 0.41 was obtained for the whole superlattice GaAs/AlAs at room temperature, which is more than 40 times that of GaAs. Experimentally, the enhancement in $Z_{3D}T$ was observed for several superlattices such as Si/SiGe, $PbTe/Pb_{1-x}Eu_xTe$, and Bi_2Te_3/Bi_2Se_3. However, their power factor did not reflect the quantum carrier-confinement enhancement effect (Dresselhaus et al., 1999).

4. Multiple techniques for thermoelectric materials fabrication

In this section, different sample fabrication techniques for various high-performance TE materials have been summarized together with their significant achievement to provide a clear insight into the choice of the synthesis process for efficient thermoelectric power conversion efficiency.

Several PGEC materials have been studied for improved TE figure of merit (Pavan Kumar et al., 2019; Hsieh et al., 2019; Parbatani et al., 2019; Li et al., 2019; Li et al., 2018; Vikram and Johnson, 2018; Chen et al., 2018; Ge et al.,

Table 2 Different TE materials with a thermoelectric figure of merit above unity.

Materials	Synthesis method	ZT	Temp.	Remark	Ref.
$Fe_2V_{0.8}W_{0.2}Al$ thin-films	Sputtering + DFT	6.0	393 K	The authors attributed the high ZT value to mass fluctuations, their DFT suggested the films to be at metastable states.	(Hinterleitner et al., 2019)
Bi_2Te_3/Sb_2Te_3 superlattice	–	2.4	300 K	The potential barrier served as phonon scattering centers to lower the value of lattice thermal conductivity	(Venkatasubramanian et al., 2001)
Bi_2Te_3 nanostructures	Hydrothermal technique	1.16	300 K	High thermopower was achieved leading to increased ZT	(Wu et al., 2013)
nanoplates of Ge-doped SnSe	Hydrothermal + spark plasma sintering	2.1	873 K	Ge-inclusion facilitated p-type carrier supply thereby boosting the TE power factor	(Chandra and Biswas, 2019)
Zn and Cu-doped $Bi_2(Te_{0.9}Se_{0.1})_3$	Large-scale zone melting technique	1.15	300 K	Metal doping helps scatter phonons which are the major contributors to thermal conductivity	(Wang et al., 2013)
$PbTe/Pb_{1\text{-}x}Eu_xTe$	Molecular-Beam-Epitaxy	2.0	300 K	Narrowed MQW creates a spike in the DOS near the Fermi level which improves the Seebeck coefficient	(Hicks and Harman, 1996)
hole-doped SrTe-alloyed PbTe	Chemical method	2.5	923 K	Enlargement of the bandgap due to the heavily Sr-doped into the matrix of PbTe enhances TE performance	(Tan et al., 2016)
CdSe-modified PbSe	–	1.4	870 K	High ZT achieved through synergistic optimization of thermal and electrical transport properties	(Qian et al., 2019)
$Ba_8Ga_{16}Ge_{30}$	Czochralski technique (Hou et al., 2009)	1.3	1000 K	Reduced thermal conductivity with elevated electrical conductivity at a high Ga/Ge ratio was recorded	(Bentien et al., 2004)
$Ba_8Cu_xGa_{16\text{-}x}Sn_{30}$	Sn-flux method	1.35	540 K	Different Cu concentration at Ga sites yielded high ZT.	(Deng and Saiga, 2010)
$Yb_{0.3}Co_4Sb_{12}/0.05CoSi$ composite	In-situ precipitation	1.5	873 K	Enhanced low-energy carrier filtering at the potential barrier improved Seebeck coefficient	(Qin et al., 2019)
$Ba_{0.08}La_{0.05}Yb_{0.04}Co_4Sb_{12}$	Induction melting	1.7	800 K	The introduction of ions to the structure facilitates electron transfer to the cations for charge-balancing	(Shi et al., 2011)
Se-doped $Mg_{3.2}Sb_{1.5}Bi_{0.5}$	Ball milling and hot pressing	1.7	700 K	Mn, Co inclusion enhances charge carrier scattering mechanisms	(Zhang et al., 2019)
$SnS_{0.91}Se_{0.09}$	DFT	1.6	873 K	A remarkable increase in ZT achieved through the synergistic optimization of carrier mobility and effective mass	(He et al., 2019)
$Bi_{0.4}Sb_{1.6}Te_3$	Resistance pressing sintering	1.1	343 K	The authors observed a decrease in both κ and σ due to an increase in porosity.	(Hu and Hu, 2019)
chalcopyrite $Cu_{0.7}Ag_{0.3}Ga_{0.4}In_{0.6}Te_2$	Ball-Milling and hot-pressing	1.6	873 K	The authors propose that isoelectronic multi-element alloying reduces the value of κ for chalcopyrite compounds	(Zhang et al., 2019)
S,Pb-co-doped SnSe	Facile hydrothermal method	1.85	873 K	They claim that co-doping widens the bandgap and consequently reduced the bipolar thermal conductivity	(Lu et al., 2019)
F-doped Sn_2Bi	DFT	2.45	300 K	High ZT achieved via enhanced anharmonicity, reduced group velocity and increased three-phonon scattering phase space	(Li, n.d.)
Bi_2Te_3	Non-equilibrium reaction triggered by spark plasma sintering	1.1	470 K	Appreciable ZT achieved by suppressing Te-vacancy to control point defect	(Wang et al., 2019)

2018). Researchers have also employed different synthesis methods to develop such materials to control the structures down to the nanoscale. Efficient thermoelectric compounds are often intensively researched, e.g., group IV-VI materials like SnTe, PbS, PbSe, SiGe, PbTe, BiTe, and GeTe. Pb's toxicity, coupled with the shortage of Ge, enables materials such as BiTe and SnSe (Jin et al., 2018) to dominate the thermoelectric field (He et al., 2019).

The two main approaches used to fabricate nanomaterials are the bottom-up and top-down mechanisms. In the former, nanostructures are grown by bringing pieces together (Ramirez et al., 2020). However, in the latter, bulk materials are broken down into nanostructure level (Mamur et al., 2018). For over a decade, the bottom-up approach has outshined the top-down approach and is becoming more promising for different nanoscale applications as it enhances nanostructured-materials development with highly stoichiometric compositions and fewer defect records. For the bottom-up approach, generally, the growth processes are categorized into chemical and physical methods. The former comprises solvothermal processes, electrolysis deposition, laser chemical vapor, electrochemical, wet chemical method, chemical oxidation, facile solution, and biomolecule-assisted hydrothermal. The physical growth methods include spray pyrolysis, pulsed laser deposition, sputtering, and thermal evaporation methods.

Bulk Bi_2Te_3-based compounds have exhibited promising thermoelectric performance compared with their counterparts. There have been several efforts to increase the TE efficiency of these materials via a nano-structuring approach where low-dimension nanocomposites such as nanoplates, nanorods, nanosheets, nanoflowers, nanotubes, and nanowires are developed using different fabrication techniques. For example, Rama et al. (Venkatasubramanian et al., 2001) obtained a remarkable ZT ~ 2.4 in a thin film-based superlattice of p-type Bi_2Te_3/Sb_2Te_3, which is an incredible improvement compared to the state-of-the-art Bi_2Te_3 materials. They attributed the enhancement in the figure of merit to the relative advantage of thin-film materials over the bulk TE compounds since quantum confinement of charge carriers is feasible in the former.

Guo et al. (2016) used a solvothermal process to prepare hierarchical nanoflowers of Bi_2Te_3 with additive nanostructured defects. They used precursors such as Na_2TeO_3, $Bi(NO_3)_3\cdot 5H_2O$, acetone, ethanol, PVP K30, hydrazine monohydrate, and formic acid. Highly stoichiometric Bi_2Te_3 was realized under energy dispersive spectroscopy (EDS). X-ray diffraction analysis of their sample matched well with the rhombohedral crystal structure of Bi_2Te_3, and the crystalline lattice fringe was obtained through a high-resolution transmission electron microscope (HRTEM) as 0.31 nm Field emission scanning electron microscopy revealed structures consisting of nanoflowers with an average diameter of about 550 nm. Their thermoelectric characterizations yielded a maximum ZT value of 0.68 at 475 K. Finally, the authors inferred that the optimum efficiency of the defective nanoflowers provides for a new dimension to utilizing nanomaterials as thermoelectric power generation and refrigeration applications.

Similarly, Zhang and his team (Zhang et al., 2013) used a low-temperature solvothermal synthesis method to fabricate single crystals of Bi_2Te_3 nanostructures. Morphological and structural characterizations of their samples showed a uniform surface having rhombohedral geometry and near stoichiometric compositions. They used starting materials such as ethylene glycol, sodium dodecyl benzene sulfonates, EDTA, NaOH, Na_2TeO_3, and $BiCl_3$. The authors realized several hexagonal nanostructures and nanosheets for different experimental conditions. The nanostructures' sharp edges demonstrated the samples' high-crystallinity, while HRTEM images vividly depicted the structurally uniform lattice fringes having about 0.21 nm spacing. The authors suggested that the Bi_2Te_3 microstructure could be affected by many factors, including the type of surfactants, NaOH concentration, the reaction temperature, etc. Lastly, they studied the transport properties of hot-pressed bulk samples where they observed a significant reduction in the thermal conductivity resulting from increased phonon scattering at the interfaces.

Also, Liang et al. (Liang et al., 2011) fabricated Bi_2Te_3 from Bi_2O_3 and Te powder using a solvothermal approach. For the preparation method, the two starting materials were added to the solution of ethylene glycol and polyvinylpyrrolidone without NaOH. The authors obtained a hexagonal crystal structure with lattice parameters a = 0.4395 nm and c = 3.044 nm. Similarly, TEM images revealed the anticipated hexagonal lattice fringes with an average spacing of 0.22 nm, indicating the material's single crystalline phase. Besides, they obtained infrared-active mode with Raman spectroscopy indicating the presence of forbidden structure in the bulk crystal.

Furthermore, Deng and coworkers (Deng, 2002) employed a solvothermal reaction to fabricate nanostructured Bi_2Te_3. They carried out a reaction of hydrated bismuth (III) chloride ($BiCl_3\cdot 2H_2O$), KBH_4, Te powder, and KOH with N,N-dimethyl formamide as solvent at temperatures between 100 and 180 °C. The authors suggested two mechanisms to obtain the material. First is the reduction of Te to Te^{2-} followed by a reaction with Bi^{3+}. The second approach is through the direct combination of the metals where Bi ions would be easily reduced to Bi metal by KBH_4 to produce the nanocrystalline Bi_2Te_3. Consequently, they highlighted that the first mechanism would likely occur for low reaction temperatures or short reaction times while the second mechanism would likely dominate at higher temperatures or longer reaction times. They observed the dependence of the samples' morphology on the reaction and the growth temperature as well. Furthermore, structural characterization revealed rhombohedral geometry with lattice parameters a = 0.438 nm and c = 3.050 nm, and they achieved excellent stoichiometric compositions under energy dispersive spectroscopy. Finally, the authors observed a significant effect of the type of solvent used in the nucleation process of thermoelectric compounds.

Recently, Sueng et al. (Heo et al., 2019) prepared a highly-textured and hole-doped single crystal of SnSe thin-films using a scalable and low-cost solution process. They recorded a remarkable power factor of $4.2\ \mu W/cm^{-1}K^{-2}$ at 550 K more than the previously obtained value for single-crystal SnSe. They attributed such improvement in the thermoelectric performance to the uniformity of the film, high-stoichiometry, and synergistic effect of the textured-microstructure, which were achieved through the transitions of 2D $SnSe_2$ to SnSe phases.

A facile solution technique was used by Mntungwa and his team (Mntungwa et al., 2014) to synthesize nanocrystalline Bi_2Se_3 and Bi_2Te_3. Their starting materials were bismuth carbonate salts [$Bi_2(CO_3)O_2$], toluene, tri-n-octylphosphine (TOP), bismuth chloride [$BiCl_3$], hexadecylamine (HDA), $NaBH_4$, methanol, deionized water, bismuth nitrate [$Bi(NO_3)_3$], and bismuth acetate [$Bi(CH_3COO)_3$]. Their method involves Te-reduction by $NaBH_4$ and high-temperature thermolysis in alkylamine. They realized spherically oriented crystals having an average diameter of about 25 nm with oleylamine and hexadecylamine as capping agents over the temperature ranges. They observed a microstructure having distinct lattice fringes with an average spacing of 0.34 nm under HRTEM, in tandem with the high-intensity planes of Bi_2Te_3 rhombohedral geometry.

Wu and his team (Wu et al., 2013) prepared the alloy nanostructures of Bi_2Te_3 using a hydrothermal technique. The precursors used were $NaBH_4$, NaOH, EDTA, Te-powder/Na_2TeO_3, and $BiCl_3$. The experiment was carried out in an open beaker, and a magnetic stirrer was employed for thorough mixing. The X-ray diffraction peak matched well with the rhombohedral crystal geometry of the Bi_2Te_3 without any observed impurity, although different Te sources were used during the synthesis. However, they observed a slight broadening in the diffraction peaks attributed to the small particles' sizes evident from the FESEM images. On the other hand, the SEM images exhibited varying morphological characteristics. Finally, the authors recorded a high ZT value of 1.16 resulting from high electrical conductivity and thermopower coupled with low thermal conductivity. These findings would be useful to produce cost-effective and large-scale thermoelectric materials with a high figure of merit.

On the other hand, nanostructured thermoelectric Bi_2Te_3 powders with varying morphological characteristics (nanorods, nanoplates, and nanotubes) were prepared using a hydrothermal approach by Kim et al. (Kim et al., 2012). During the preparation process, Te powder was mixed with $BiCl_3$ and Na_2-EDTA at different temperatures. According to the authors, the growth temperatures and the stabilizing agents influence the morphology greatly. Interestingly, X-ray diffraction confirms the rhombohedral geometry of Bi_2Te_3 with lattice parameters a = 0.4381 nm and c = 3.0460 nm for all the different morphologies. The authors proposed that the formation of Bi_2Te_3 could be explained as; The Bi^{3+} ions regulated by Na_2-EDTA while the reduction of Te by $NaBH_4$ produced Te^{2-} and consequently, the target materials are constructed.

Li and coworkers (Li et al., 2011) used hydrothermal and chemical oxidation techniques to synthesize Bi_2Te_3-flakes. The authors fabricated the compound through the mechanical blending of $BiCl_3$ and Te powder assisted by $NaBH_4$ and NaOH to regulate the P^H parameter. The structural study using XRD indicated the hexagonal phase of Bi_2Te_3 without any traceable impurity. However, the FESEM images revealed non-uniform structures with dimensions ranging from 20 to 500 nm. Finally, they observed the enhancement of the thermoelectric power factor at elevated temperatures, which could be attributed to improved carrier mobility.

Chandra and his team (Chandra and Biswas, 2019) synthesized 2D nanoplates of Ge-doped SnSe using a hydrothermal approach followed by spark plasma sintering and realized a peak ZT of ~ 2.1 at 873 K. Also, a peak anisotropic ZT of 1.75 parallel to the pressing direction was obtained at the same temperature. They attributed such a figure of merit improvement to the supply of p-type charge-carriers induced by Ge inclusion, which ultimately increased the power factor. Ultra-low thermal conductivity was also observed due to the plenty of interfaces and high anharmonicity in the lattice.

A biomedical-assisted hydrothermal technique was utilized by Mi et al. (2010) to grow Bi_2Te_3-based nanostructures for enhanced thermoelectric performance. The chemicals used by the team include K_2TeO_3, NaOH, $BiCl_3$, and alginic acid. The sample was grown at 220 °C temperature for 24 h. Their morphological studies showed a cluster of plate-like structures with average thickness and diameter of 10 and 100 nm respectively. The NaOH density was found to play a significant role in tuning the morphology of the material. Furthermore, their thermoelectric properties study revealed high room-temperature performance.

Additionally, Zhao et al. (Zhao and Wang, 2010) fabricated Bi_2Te_3 with different morphologies such as flakes, flower-like clusters, nanotubes, and nanowires using a hydrothermal approach. They used precursors such as Te powder and $BiCl_3$, while $NaBH_4$ was used as a reducing agent, and NaOH was used to control the P^H level. The XRD peaks were all indexed to the hexagonal Bi_2Te_3 without any traceable phase. Their SEM images revealed irregular flakes with dimensions ranging between 60 and 400 nm. The authors have emphasized the importance of temperature and reaction time in their experiment to achieve the nano-structuring of these materials to improve their thermoelectric figure of merit.

Wang and his team (Wang et al., 2013) used a large-scale zone melting technique to prepare Zn and Cu-inclusions in $Bi_2(Te_{0.9}Se_{0.1})_3$ ingots. Their surface and chemical characterizations revealed that the metal elements were embedded at the interfacial grain boundaries influencing the thermal transport. They reported appreciable enhancement in the ZT value resulting from the increased density of state effective mass even though Zn acted as a weak donor. The authors reported a significant increase in the power factor for Cu nanoinclusion coupled with a decrease in the lattice thermal conductivity resulting from increased phonon scattering. A ZT value of 1.10 and 1.15 was recorded for the Zn and Cu loaded ingots, respectively, indicating a 21% increase relative to the commercially doped ingots. Such an increase in the thermoelectric figure of merit makes the technique suitable for TE materials' commercial-scale production.

Chen and coworkers (Chen et al., 2012) utilized a cryogenic grinding technique to fabricate nanostructures of Bi_2Te_3 from its powdered coarse particles having an average size of 5 mm. Their XRD studies revealed more textured materials from the ingots compared to the grinded particles. They observed more defects along the basal plane during the manufacturing phase. Furthermore, they presented a comparative analysis between their work and others that utilized spark plasma sintering (SPS) and high energy ball milling (HEBM) techniques, results of which signals the high potential of their synthesis process to produce finer and high-quality nanostructures.

A refluxing method was used by Gupta et al. (2012) to grow nanostructured Bi_2Te_3. They used precursors such as KOH, EDTA, BiCl3, NaBH4, and Te powder. Morphological studies of their samples revealed a nanorod-like structure of 100 nm length and a 10 nm radius. They observed a reduction in the particles' dimension with increased KOH concentration. The authors suggested that a substantial variation in the particle form and sizes could be realized by changing the reaction parameters.

A low-cost chemical method was employed by Srivastava et al. (Srivastava and Singh, 2012) to fabricate Bi_2Te_3 nanoparticles at 50 °C. They used starting materials; hydrazine hydrate, glycol, ethylene, $BiCl_3$, and Te powder. X-ray diffraction analysis of the samples revealed the polycrystalline rhombohedral crystal geometry of Bi_2Te_3 nanostructures with an average crystallite size of 30 nm. The authors recorded a high thermoelectric figure of merit consequence of low thermal conductivity at room temperature. Similarly, Kim et al. (Kim et al., 2010) used a simple chemical method to fabricate Bi_2Te_3 nanostructures. The precursors used include TeCl4, BiCl3, and polyol solvent of ethylene–glycol. X-ray diffraction analysis revealed the rhombohedral geometry of Bi_2Te_3 with an average grain size of 300 nm. The authors observed significantly low thermal conductivity, which consequently improved the thermoelectric figure of merit for the Bi_2Te_3 nanomaterials.

Nanoparticles of Bi_2Te_3 were prepared by Kim and his colleagues (Kim et al., 2011) using a wet chemical reduction approach. They started with chemicals such as $(Bi(NO_3)_3)$ and Te powder, while ascorbic acid and ethylene diamine tetraacetic acid were used to stabilize the precursors as reducing agents. They realized the rhombohedral geometry of the materials with uniform crystallite dimensions. Their thermoelectric transport properties yielded significantly low thermal conductivity, which eventually improved the compound's thermoelectric figure of merit.

Scheele et al. (Scheele et al., 2009) employed a Schlenck technique to synthesize Bi_2Te_3 nanostructures in the inert atmosphere. Single-crystalline bismuth telluride of 10 nm average crystallite sizes was realized. Their x-ray diffraction spectroscopy revealed the rhombohedral crystal geometry of the material with slight peak broadening indicating the particles' small size. The authors observed polycrystalline behavior from the selected area electron diffraction fringe patterns. Their thermoelectric transport properties measurements demonstrated a low concentration of charge carriers leading to small electrical and thermal conductivities.

The mechanical alloying technique was employed by Zakeri and coworkers (Zakeri et al., 2009) to fabricate Bi_2Te_3 nanocrystals by using Bi and Te as initial materials. They accomplished the nanocrystalline material only after 5 h of milling, although the complete process takes about 25 h. The hexagonal crystal structure of the material was realized and the Scherrer formula was used to estimate the average domain size (9 – 10 nm). Morphological studies revealed flakes-like structures scattered across the sample. The stability of the synthesis phase at high temperature (500 °C) was realized during the heating of the ball-milled particles with differential thermal analysis.

$PbTe/Pb_{1\text{-}x}Eu_xTe$ multiple-quantum-well-structured samples were prepared using the Molecular-Beam-Epitaxy technique with varying quantum well's width at × = 0.07 (Hicks and Harman, 1996). A remarkable increase in ZT to 2.0 at 300 K temperature was observed, which they attributed to enhanced power factor. Similarly, Tan et al. observed a record ZT of ~ 2.5 at 923 K in a heavily hole-doped SrTe-alloyed PbTe beyond its solubility limits (less than 1 mol%). They attributed the enhancement of the TE performance to the bandgap's enlargement due to the high Sr doped into the matrix of PbTe, which significantly intensified the power factors (Tan et al., 2016).

Qian et al. (Qian et al., 2019) reported an exciting work on the modification of PbSe to replace the costly and less abundant moderate-temperate thermoelectric PbTe. They introduced CdSe, which possesses a larger bandgap and similar crystal structure compared with PbSe leading to improved effective-mass through conduction band flattening, and suppression of both the bipolar and lattice thermal conductivities due to bandgap enlargement and the presence of nano-defects respectively. They achieved a high ZT of ~ 1.4 at 870 K resulting from synergistic optimization of thermal and electrical transport properties, making the material a promising candidate for moderate-temperature TE applications.

Nassary and his team (Nassary et al., 2009) used the Bridgman technique to grow single crystalline Bi_2Te_3. The authors studied the dependence of electrical conductivity on temperature, Hall coefficient, and other thermoelectric properties for two crystallographic directions. Their investigations revealed a positive sign of the Hall coefficients and Seebeck parameters, implying that holes are the dominant charge carriers, and hence the material is a p-type. On the other hand, they observed the transport properties to be completely anisotropic. They reported three distinct regions in their Hall effect measurement curve; extrinsic, transition, and intrinsic regions between 163 and 293 K, 293 – 388 K, and 388 – 528 K respectively. They attributed the scattering process in the material to some faults and stoichiometric vacancies. Finally, they suggested that increased defects existed at higher temperatures.

The effects of 0-D defects such as antisites, dopants, interstitials and vacancies, 1-D defects like a screw and edge dislocations, 2-D defects e.g. grain boundaries, and 3-D defects like nanoinclusion of structures on the performance of TE materials was investigated by Liu and his colleagues (Liu et al., 2016). They suggested that the defects should be drastically minimized for better TE efficiency since the Seebeck coefficients, electrical and thermal conductivities are reflections of phonon and charge transports. An alternative approach to enhance the thermoelectric efficiency of these materials was developed in their experiments.

Elsewhere (Ashalley et al., 2015), a detailed review of the fabrication and characterization of Bi_2Te_3 compounds of 0D, 1D, and 2D was presented. Their work encompasses the synthesis method, nanostructure control, and thermoelectric properties studies. Furthermore, the interconnection between the topological insulating characteristics of the Bi_2Te_3-based materials and the enhancement of their thermoelectric figure of merit was highlighted. The authors suggested that Bi_2Te_3-based nanomaterials would continue to be the leading next-generation thermoelectric energy harvesters.

Another important class of high-temperature thermoelectric materials is the half Heusler compounds (HHM). They possess a simple rock salt structure generally represented by ABY, as depicted in Fig. 11. Where A and Y form the material structure and element B occupies a position (1/4, 1/4, 1/4)

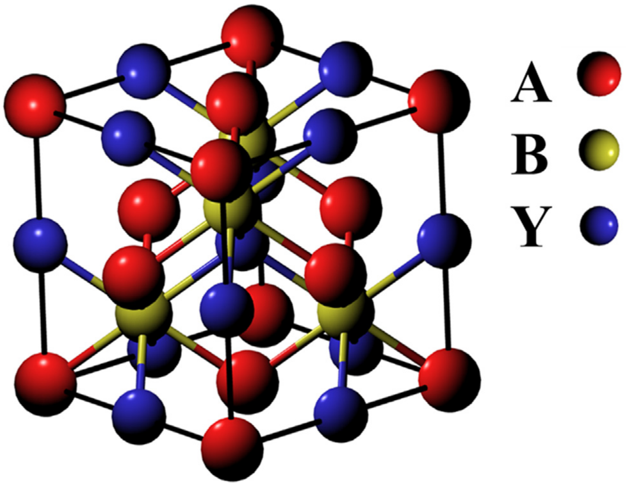

Fig. 11 Schematic representation of the unit cell of the half-Heusler crystal structure.

along the body diagonal (Liu et al., 2012). On the other hand, the full Heusler compounds can be denoted by A_2BY structure. A and B are generally transition metals, while Y is the main group element, as represented in Fig. 12. The HHM exhibit excellent chemical and mechanical stability and a high thermoelectric power factor resulting from their high electrical conductivity and thermopower. However, the relatively large thermal conductivity (~10 W/mK) impedes the improvement of the figure of merit (Bhattacharya et al., 2000). These challenges were tackled via increased phonon scattering through nanograins inclusion and chemical substitutions.

The latest report in the development of Heusler compounds with a record maximum thermoelectric figure of merit reaching above 5.0 was carried out by Hinterleitner et al. (2019). They fabricated a series of $Fe_2V_{1-x}W_xAl$ thin film samples using RC-sputtering and investigated the thermoelectric properties with $Fe_2V_{0.8}W_{0.2}Al$ demonstrating the best thermoelectric performance. They also studied the electronic structure using the density functional theory as implemented in the VASP package. Their incredible thermoelectric measurements are presented in Fig. 13.

Gerda et al. (Rogl et al., 2020) used high-pressure torsion to prepare several p-type and n-type HHM for enhanced thermoelectric performance. NbFeSb-based and $Ti_{0.5}Zr_{0.5}NiSn$-based compounds exhibited ultra-low thermal conduction resulting from deformation-induced defects, i.e. dislocations and vacancies. They carried out density functional theory studies coupled with Raman spectroscopy, where they observed induced lattice stiffening caused by the torsion method. A significant reduction of the thermal conductivity coupled with enhanced power factor has improved the figure of merit of the half-Heusler compounds.

Shan et al. (Li et al., 2019) reported the fabrication of a novel HHM TaCoSn with thermal conductivity ~ 5.7 W/mK at 300 K, which is relatively low compared to other HHM counterparts. They observed from DFT calculations that the large Gruneisen parameter, Debye temperature, and low phonon velocity are the primary causes of low thermal conductivity. Also, strong phonon scattering was induced by incorporating Nb at Ta sites, which also lowered the thermal conductivity. A ZT value of more than 0.7 was realized at 973 K for the $Ta_{0.6}Nb_{0.4}CoSn_{0.94}Sb_{0.06}$.

TiCoSb is an interesting HHM that is sensitive to the sites of Co and Ti due to the existence of the 3d orbitals of Co and Ti atoms in its valence and conduction bands. It also has the highest bandgap among the half Heusler compounds reaching 0.95 eV. Sekimoto and his team (Sekimoto et al., 2005) used an arc-melting technique to prepare (Ti, Hf, Zr)CoSb composites. They recorded the highest ZT of 0.025 on TiCoSb at 920 K. However, they observed substantial improvement in the figure of merit reaching 0.45 following the inclusion of Fe to make $TiFe_xCo_{1-x}Sb$ (at × = 0.15), a relatively high value for a half-Heusler compound. The Seebeck coefficient was also found to rise to 300 μV/K at 850 K. Interestingly, they observed a shift in the material's behavior changing from n-type to p-type with small Fe inclusion. The electrical conductivity also was enhanced due to the Fe introduction in the presence of randomly dispersed TiO2. Remarkably, a decrease in the thermal conductivity was observed due to strain-field and mass fluctuations resulting from the substitution of Co by Fe. However, in comparison to the state-of-the-art thermoelectric compounds like Bi_2Te_3, the thermal conductivity is still high (3.7 W/mK) at 850 K.

Wu et al. (Wu et al., 2009) reported improved electrical conductivity and Seebeck coefficients of TiCoSb with Ge inclusion. Notably, the sign of the Seebeck coefficient of the $TiCoGe_{0.15}Sb_{0.85}$ changed from negative to positive with Ge doping at 850 K, indicating a transition in the compound's

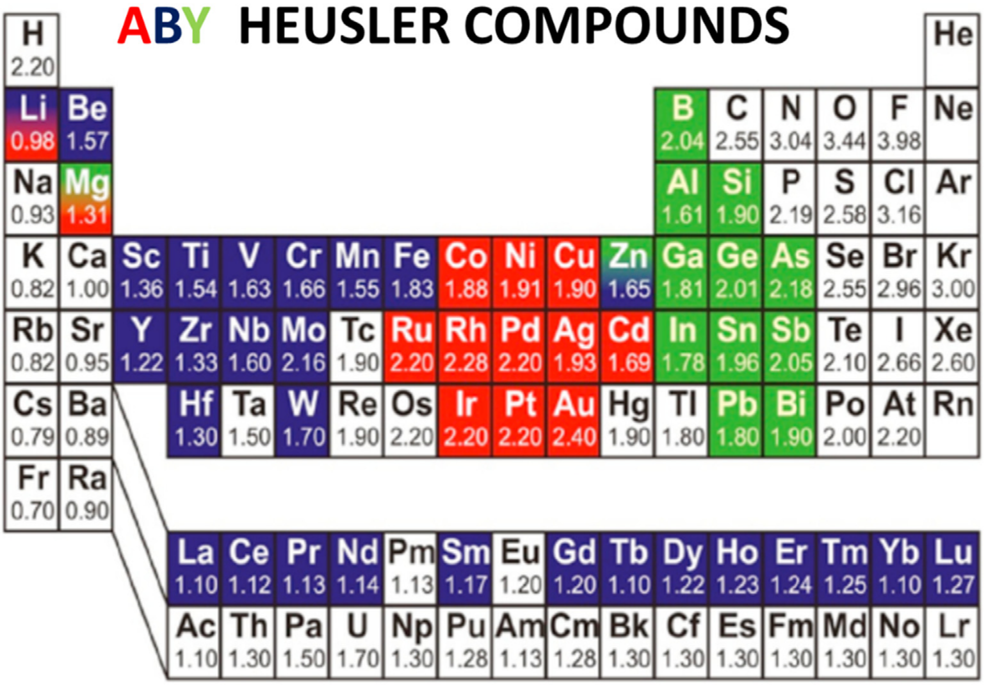

Fig. 12 Periodic table of elements showing different possible Heusler compounds configuration according to the assigned colors. Adapted from ref (Beretta et al., 2019).

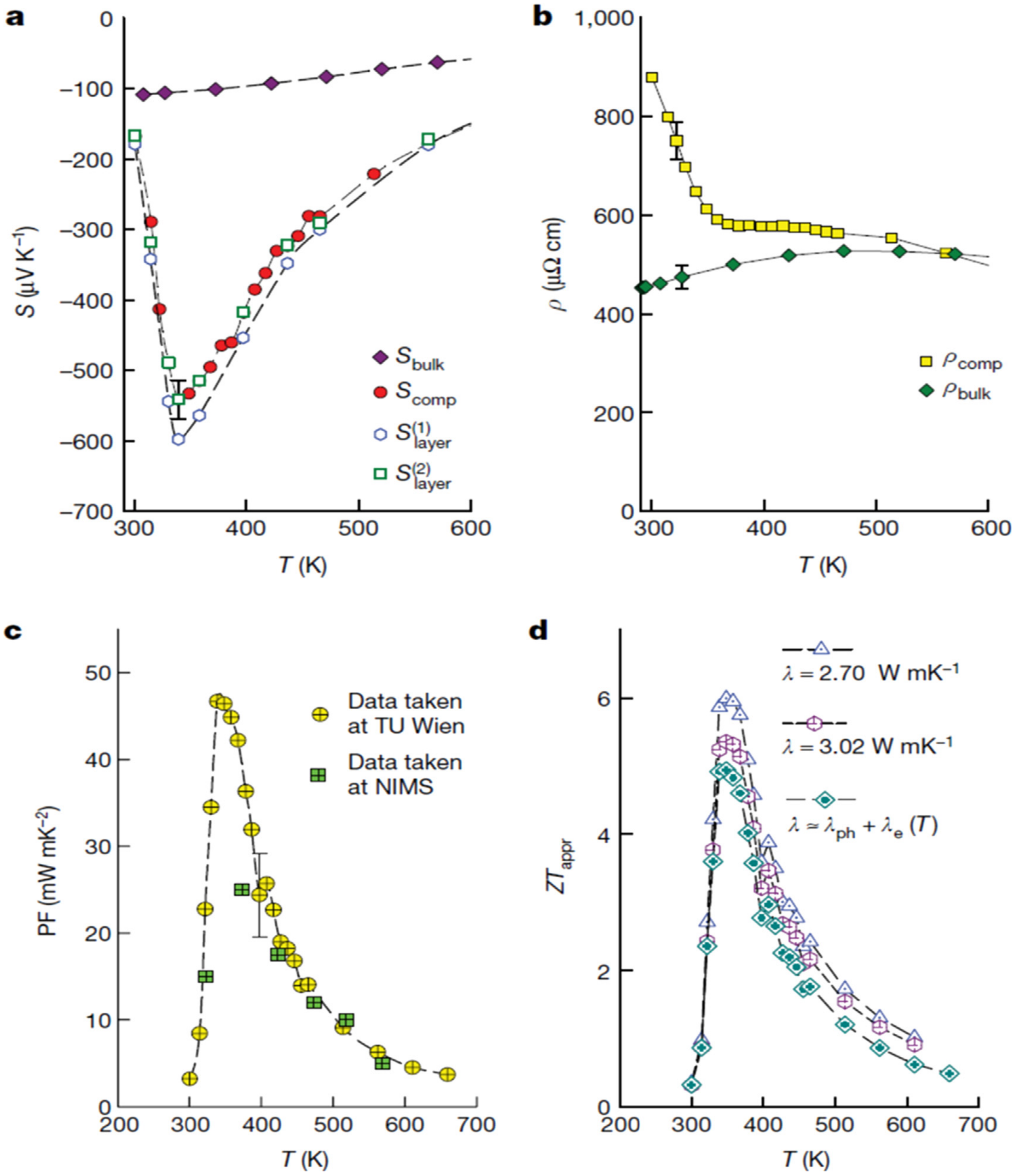

Fig. 13 Temperature-dependent transport measurements of Heusler thin-film $Fe_2V_{0.8}W_{0.2}Al$ with (a) Seebeck coefficient (b) electrical resistivity (c) power factor (d) figure of merit. Adapted from Hinterleitner et al., 2019

behavior from n-type to p-type. Furthermore, they attributed the significant reduction in the thermal conductivity to the intensive phonon scattering induced by the Ge substitution in the Sb sites and strain field fluctuation. However, the thermal conductivity is still high compared to other counterpart materials. On the other hand, Qiu et al. (2009) reported an appreciable TE performance in TiCoSb materials through Zr substitution in the Ti sites to produce $Ti_{0.5}Zr_{0.5}CoSb$. They observed a decline in the electrical and thermal conductivities, while the Seebeck coefficient demonstrated considerable improvement reaching up to − 420 µV/K at 600 K. On the contrary, Ni substitution in Co sites yielded a high ZT of 0.7 at 900 K resulting from the simultaneous increase in the thermopower and electrical conductivity. Beside (V, Nb, Ta)CoSn and (Ti, Zr, Hf)NiSn, there exist several other slightly explored HHM like ZrCoBi, YNiSb, NdCoSn, LaPdBi for n-type and NbFeSb, VFeSb, ZrCoBi, NbRhSn, NbCoSn for p-type materials. Typically, spark-plasma sintering and arc melting techniques are widely employed to fabricate half Heusler compounds (Wudil et al., 2019; Chauhan et al., 2019; Voronin et al., 2019; Van Du et al., 2019; El-Khouly et al., 2020; Luo et al., 2020).

Yan and his team (Yan et al., 2011) obtained an improved figure of merit in p-type HHM by reducing the average domain sizes to 1 µm. They recorded a 60% increase in ZT for $Zr_{0.5}Hf_{0.5}CoSb_{0.8}Sn_{0.2}$ when the average domain size was reduced to 200 nm by ball-milling the solid ingots to nano-powders followed by DC hot-pressing them to create dense bulk material.

Such ZT improvement is usually a consequence of reduced lattice thermal conductivity. The key issue with the ball-milling approach is the increased agglomeration of the grains, causing larger grain sizes. Apart from scattering the phonons, the created interfaces scatter the electrons at the detriment of the charge-carrier mobility.

Interestingly, for $Zr_xHf_{1-x}NiSn$ and $Zr_xHf_{1-x}CoSb$, it was revealed that despite reducing the grain sizes from micro to nanoscale, no decline in charge-carrier mobility was recorded, suggesting that even further decrease in the grain sizes to about 30 nm could improve the figure of merit. On the contrary, nanostructured skutterudite $Co_{0.9}Ni_{0.09}Sb_3$ was prepared by He et al. (2008) to obtain plenty of grain boundaries to enhance phonon scattering. They recorded a ZT of 0.7 at 800 K resulting from lowered thermal conductivity.

Several reports indicated appreciable enhancement in the figure of merit while using complex bulk-materials such as Zintl phases, clathrates, and skutterudites. A couple of research teams realized a low value of k_{th} by creating disorder in the unit-cell, such as partial occupancies or interstitial sites. For instance, due to plenty of random vacancies, low thermal conductivity was observed in rare-earth chalcogenides ($La_{3-x}Te_4$) with Th_3P_4 structure (Wood, 1988).

Many researchers have employed complex structures such as skutterudites and clathrates as potential thermoelectric materials with high-temperature applications (Graziosi et al., 2019). The leading impediment to these materials' use is their relatively high thermal conductivity resulting from their simple order and strong bonding. A novel method to investigate better thermoelectric materials whereby the constituent atoms of the cage compounds are encapsulated in a large-sized unit cell and exhibited low thermal conductivity resulting from the rattling of the atoms inside the voids was suggested by Slack et al. (SLACK, G. A., New Materials and Performance Limits for Thermoelectric Cooling, CRC Handb. Thermoelectr., 1995). The doping of charge-carriers was also proposed to enhance electron–phonon interactions. Furthermore, the thermal conductivity can also be reduced through alloying with transition metals. The ample space present in clathrates or skutterudites for the filling atoms enhances the rattling mode and causes soft-phonon mode, which also lowers the thermal conductivity. Filling the voids with heavy atoms or rare-earth atoms can also reduce the thermal conductivity.

Complex variants can also modify the state-of-the-art bulk Bi_2Te_3 to form compounds like $CsBi_4Te_6$, demonstrating lower thermal conductivity than Bi_2Te_3. The Cs atom causes structural complexity with its layers and Bi-Bi bond. The bandgap was found to decrease due to the Bi-Bi bond formation, which enables the acquisition of the peak ZT at lower temperatures compared to the Bi_2Te_3. The anisotropic effective mass of $CsBi_4Te_6$ enhances its thermopower with a small decrease in carrier mobility. The ordered homologous compounds of XTe/ Bi_2Te_3 (X = Pb, Sn, Ge) variants are also known to exhibit remarkable thermoelectric efficiency. However, only a few works exist on these materials with doping (Nolas et al., 2006). Reduced thermal conduction can also be achieved using thallium-based compounds such as $TlBiTe_6$ and Ag_3TlTe_3 due to the thallium's soft bonding uniqueness in addition to the cell-structure complexity (Kurosaki et al., 2005).

Clathrates are an important class of materials having the general formula $X_aY_bZ_{46-b}$. Y and Z are tetrahedrally coordinated to form a framework around atom X (Kim et al., 2000). some examples of clathrate candidates include $X_8Y_{16}Z_{30}$ (with X = Sr, Ba, Ca; Y = Al, Ga, In; Z = Si, Ge, Sn) and $X_8Y_8Z_{38}$ (with X = Na, K, Rb; Y = Al, Ga, In; Z = Si, Ge, Sn). Enhanced carrier mobility is achieved for these materials due to the covalent bonding existing in the anionic frameworks. As depicted in Fig. 14, the crystal structure of type 1 clathrates constitutes six tetrakaidecahedra (X_{24}) and two pentagonal dodecahedra (X_{20}) per unit cell (Okamoto et al., 2006).

$Sr_8Ga_{16}Ge_{30}$ is one of the state-of-the-art compounds demonstrating n-type semiconducting characteristics with the diamond-lattice structure of Ge at the four corners and enclosing Sr within the cage. It might be expected that the encapsulated metals release electrons to the frame, which consequently gets scattered by the rattling ions, thereby lowering the electrical conductivity. Noteworthy, $Sr_8Ga_{16}Ge_{30}$ would be deprived of its PGEC behavior if Sr is ionized. Thus, it would be a disadvantage if the electrical conduction occurs through Sr. It was demonstrated experimentally that low thermal conductivity (0.9 W/mK) coupled with high Seebeck coefficient (-320 μV/K) could be accomplished using $Sr_8Ga_{16}Ge_{30}$ compound, which is attributed to the sharp density of states around the Fermi-level (Nolas et al., 1998). However, such a high density of states could increase the electronic contribution to the overall thermal conductivity. It was also demonstrated that the Sr in the clathrate structure is practically neutral and that it does not influence the transport coefficient since it is not firmly bound to the cages (Iversen et al., 2000).

Another important clathrate material is $Ba_8Ga_{16}Ge_{30}$. Beintein and his team (Bentien et al., 2004) reported that with excess Ga concentration, the material's behavior has shifted to p-type semiconductor while the thermal conductivity was near that of isostructural $Sr_8Ga_{16}Ge_{30}$ and $Eu_8Ga_{16}Ge_{30}$. In a study conducted by Hou et al. (2009), varying Ga/Ge ratios were used to fabricate $Ba_8Ga_{16}Ge_{30}$ materials using the Czochralski technique. They obtained homogeneous crystals with a larger Ga/Ge ratio due to higher pressure and larger pulling. Also,

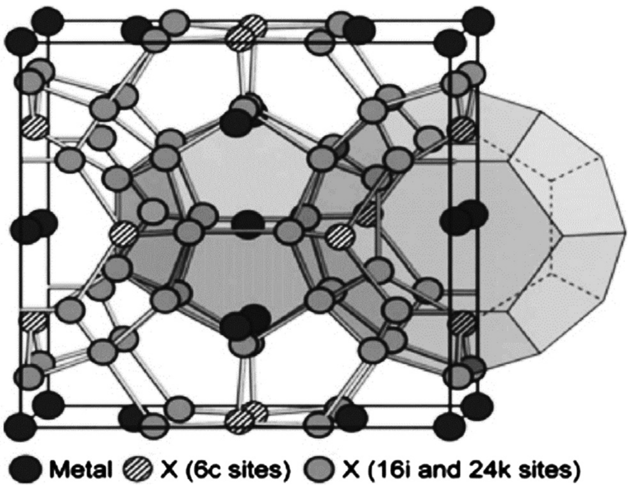

Fig. 14 The crystal structure of type-I clathrates with the shaded circles representing the atoms in the 6c sites and the dodecahedron (X_{20}) shown at the center of the unit cell with the tetrakaidekahedra by its side. Adapted from ref. (Alam and Ramakrishna, 2013)

they observed a reduced thermal conductivity with elevated electrical conductivity at a high Ga/Ge ratio without deteriorating the thermopower. Consequently, a ZT of 1.3 was realized at 1000 K. At elevated temperatures above 800 K, the vaporization of Ga contents shifted the material to its typical n-type behavior and demonstrated lowered electrical conductivity with enhanced thermopower. Notably, the vaporization of the Ga contents from the crystal has reduced significantly after heat-treating above 1000 K with a negative influence on the ZT. In contrast, as presented elsewhere (Wang et al., 2009), the variation of the Ga/Ge ratio in $Sr_8Ga_{16}Ge_{30}$ worked in the opposite route. The thermopower was decreasing, and the electrical conductivity was increasing with a decreased Ga/Ge ratio. However, there was no significant change to the thermal conductivity. Finally, they achieved a ZT of 0.8 at 650 K for the minimum Ga/Ge ratio. On the other hand, Deng et al. (Deng et al., 2010) conducted an impressive study where he observed an increase in the thermopower for Al substitution at Ga sites in $Ba_8Ga_{16}Sn_{30}$ resulting from its metallic characteristics with regards to the electrical resistivity. The overall figure of merit realized for the type viii clathrate material ($Ba_8Al_xGa_{16\text{-}x}Sn_{30}$) was 1.2 at 500 K temperature with × = 6. They claimed that even higher ZT could be accomplished by controlling the Sn and Al compositions. It was demonstrated in a similar work that substitution of Cu at Ga sites in $Ba_8Ga_{16}Sn_{30}$ yielded ZT as high as 1.35 at 540 K (Deng and Saiga, 2010). In summary, while clathrate I compounds have been relatively well-researched, class II clathrates have not been thoroughly investigated due to the difficulty accompanying their fabrication methods in a reliable and reproducible passion (Bobev and Sevov, 2001). Finally, type I clathrate materials showed more promise regarding thermal conductivity than the type II counterparts.

Skutterudites are also important compounds used in high-temperature thermoelectric applications with the general formula AB_3. As presented in Fig. 15, their cubic structure generally contains 32 atoms in a cell. Some skutterudite materials include $IrSb_3$, $IrAs_3$, Irp_3, $RhSb_3$, $RhAs_3$, $CoSb_3$, $CoAs_3$, and CoP_3. Contrary to clathrate materials, the skutterudites structure possesses some voids even without guest atoms. They possess substantial electron-crystal property resulting from high carrier mobility due to the covalent bonding, which is favored by the low electronegativity differences as in $IrSb_3$ and $CoSb_3$. The most significant challenge with these materials is to reduce the lattice thermal conductivity caused by the simple order and strong bonding. However, rattling inducement through doping the material has been discovered to solve the challenge. For increased stability of the skutterudite structure, filling the voids with electropositive ions and replacing neighboring anions showed a great promise (Shi et al., 2005).

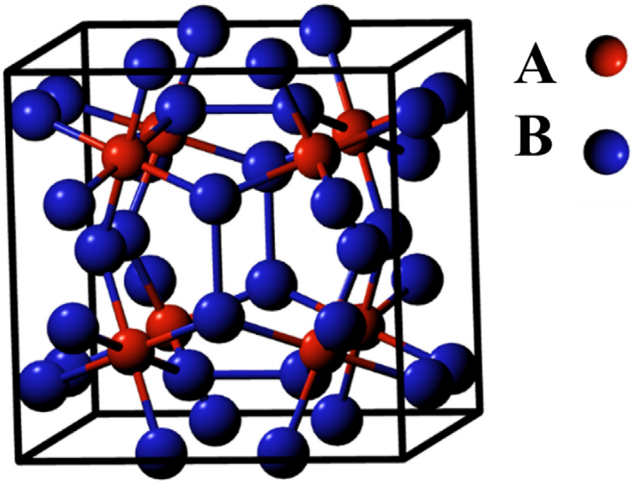

Fig. 15 Schematic representation of the unit cell of the skutterudite crystal structure.

Recently, n-type skutterudite material having isotype n/n BHJ structure was synthesized by Nie et al. (Nie et al., 2019). They used two entropy alloys $Yb_{0.1}Ca_{0.1}Al_{0.1}Ga_{0.1}In_{0.1}Fe_{0.25}Co_{3.75}Sb_{12}$ and $Yb_{0.3}Ca_{0.1}Al_{0.1}Ga_{0.1}In_{0.1}Fe_{0.25}Co_{3.75}Sb_{12}$ in 50:50 percentage ratio. They observed a decrease in the lattice thermal conductivity by ~ 15% and power factor enhancement by ~ 20% compared with the single phases separately. Finally, an average ZT value of 0.92 was achieved for the composite between 600 °C and 100 °C, about 30% improvement compared to separate phases of the compounds.

Dandan et al. (Qin et al., 2019) prepared a filled skutterudite composite $Yb_{0.3}Co_4Sb_{12}/0.05CoSi$ by embedding nanostructures of CoSi into grains of $Yb_{0.3}Co_4Sb_{12}$ using the in-situ precipitation technique. They observed an ultra-low thermal conductivity resulting from increased heat-carrying phonons scattering at the interfaces. Enhanced low energy carrier filtering at the potential barrier between the nanoprecipitates of CoSi and the material was observed, which ultimately improved the Seebeck coefficient and the power factor. Finally, a peak ZT of 1.5 was recorded at 873 K temperature. The authors propose that the nanostructured precipitates improved the composite's mechanical tolerance, making it competitive for practical applications.

Elsewhere (Tanahashi et al., 2002), $CeFe_3CoSb_{12}$ was prepared using CoSb3 with Ce and Fe. Thermoelectric characterizations revealed high thermopower and low thermal conductivity in the range 350 – 800 K. A peak ZT of 0.6 was realized at 600 K. Moreover, $Sn_zCo_4Sb_{11.2}Te_{0.8}$ was investigated at different temperatures from 350 to 700 K (J. Junga, S. Urb, I.K.-J. of C.P. Research, undefined, 2009). The Te species existed as electron-donors by replacing the Sb atoms. The material exhibited an n-type transport phenomenon over the temperature range. A peak ZT of 0.61 was obtained at 700 K after which it started to decline due to increased thermal conduction. In the same vein, a report on $CoSb_3$ filled with multiple elements (Yb, La, and Ba) showed a maximum ZT of 1.7 above 800 K for $Ba_{0.08}La_{0.05}Yb_{0.04}Co_4$Sb12 (Shi et al., 2011). In short, the introduction of ions to the structure facilitates electron transfer to the cations for charge-balancing and creates disorder in the lattice. For example, Co^{3+} can be partially substituted by Fe^{2+} in $CoSb_3$ compound (Snyder and Toberer, 2010).

Fan et al. (Zhang et al., 2019) recorded a dramatic increase in ZT from ~ 1.4 to ~ 1.7 around 700 K (Fig. 16) for Se-doped $Mg_{3.2}Sb_{1.5}Bi_{0.5}$-based Zintl TE materials through the incorporation of Mn and Co to manipulate the carrier scattering mechanisms which are critical to the enhancement of the TE power factor. An appreciable average ZT of 1.18 was recorded between 300 and 550 K temperatures resulting from the reduced thermal conductivity due to increased scattering centers. The authors suggested that such an exciting performance makes the material competitive to the commercially available Bi_2Te_3-based TE devices.

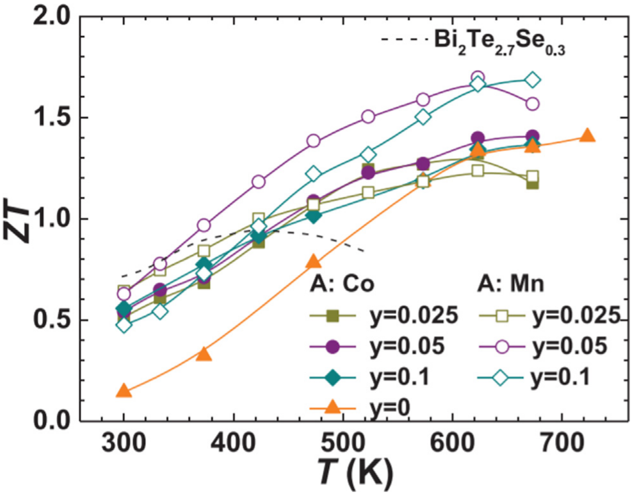

Fig. 16 Temperature-dependent ZT of Co, Mn incorporated $Mg_{3.2}Sb_{1.5}Bi_{0.5}Se_{0.01}$. Adapted from ref (Zhang et al., 2019).

In an attempt to produce low-cost thermoelectric material for Peltier applications, Jun et al. (Mao et al., 2019) prepared Zintl Mg_3Bi_2-based compounds to replace the widely used Bi_2Te_3-based compounds, which contain costly and scarce tellurium species. They obtain a comparatively high ZT of ~ 0.90 at 80 °C. A temperature difference of ~ 90 K was realized with the material as a Peltier device, which is remarkable for refrigeration applications.

Table 1. summarizes the different techniques employed by various groups to fabricate a multitude of thermoelectric materials, as presented in this review. In some cases, the precursors used in the experiments are highlighted.

5. Applications of thermoelectric materials

Thermoelectric devices being solid-state devices with no moving parts and which possess incredible reliability, durability, simple structure, and long operation lifetime, can be used in different fields for various applications. They can be utilized as refrigerators by converting DC-current into temperature gradient and can be used as thermoelectric generators (TEG) by transforming temperature gradient into useful electricity (Mohammadnia et al., 2020; Rahman et al., 2020; Luo et al., 2020; Riahi, 2020; Sargolzaeiaval et al., 2020; Jia and Guo, 2020; Kishore et al., 2020; Ishaq et al., 2020; Araiz et al., 2020; Lv et al., 2020).

In principle, thermoelectric modules consist of n-type and p-type TE materials arranged thermally in parallel and electrically in series as TE junctions (Sargolzaeiaval et al., 2020). The materials' selection is based upon their physical and thermoelectric properties, as elaborated in this review. A thermoelectric module system contains supporting components for optimum performance, such as a cooling device, which removes heat from the cold region, and heat sinks to absorb from the hot region of the module. For a typical TE module, the difference in temperature between low and high-temperature sides can reach 70 °C (Riffat and Ma, 2003). A single module's power output can reach as high as 125 W and can be modularly constructed to generate up to 5 KW. The schematic of the thermoelectric module architecture is presented in Fig. 17. Generally, those materials with a high figure of merit, above unity, at room temperatures are used for refrigeration applications while high-temperature thermoelectric materials are used in electricity generation.

5.1. Power generation

Electrical energy generation via thermoelectric modules exhibits an edge over the conventional power generation mechanisms being environmentally friendly, silent in operation, highly reliable, and does not contain heavy mechanics (Hamid Elsheikh et al., 2014). As a manifest of the facts mentioned above, TEGs development received much attention for applications in military, biomedical, remote power, and aerospace departments as a standalone power source (Brito et al., 2020; Shoeibi et al., 2020; Cai et al., 2020; Zhao et al., 2020; Wang et al., 2020; Meng et al., 2020; Gholikhani et al., 2020). The advancements in the field have made it feasible to develop such TEGs on different surfaces with a high degree of flexibility, as presented in Fig. 18.

Recently, there has been an increase in the use of TEGs for body-mounted low-powered devices such as portable electronics used for communication purposes like smart mobile phones, iPods, and MP3 players. Others also include those for medical applications like cardiac pacemakers and hearing aids. Fig. 19 shows a TE module prototype embedded in an armband and T-shirt to harvest thermal energy to power wearable sensors such as the electrocardiogram. These devices' typical power demand ranges between 5 microwatts to 1 W, and their life expectancy is around five years. Therefore, an auton-

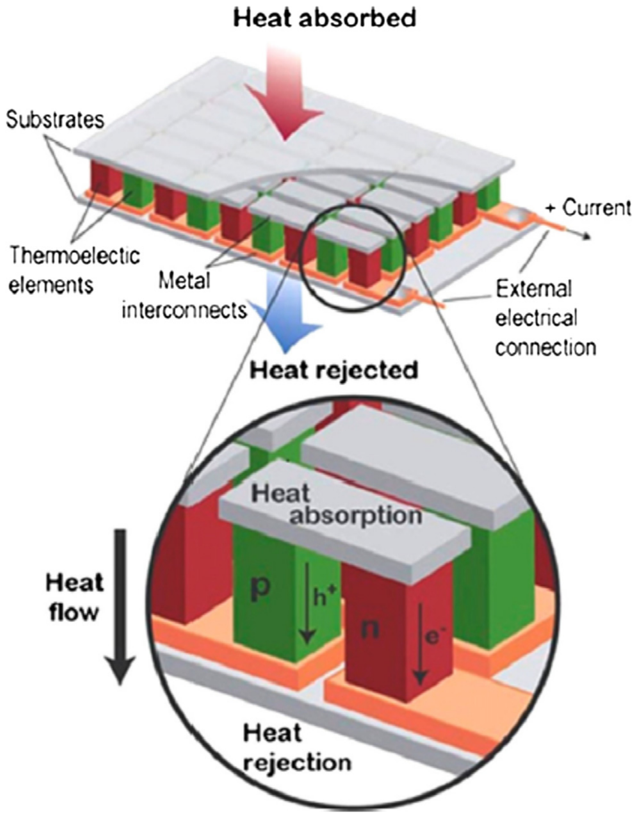

Fig. 17 Schematic of the thermoelectric module array. () Adapted from Saidur et al., 2012

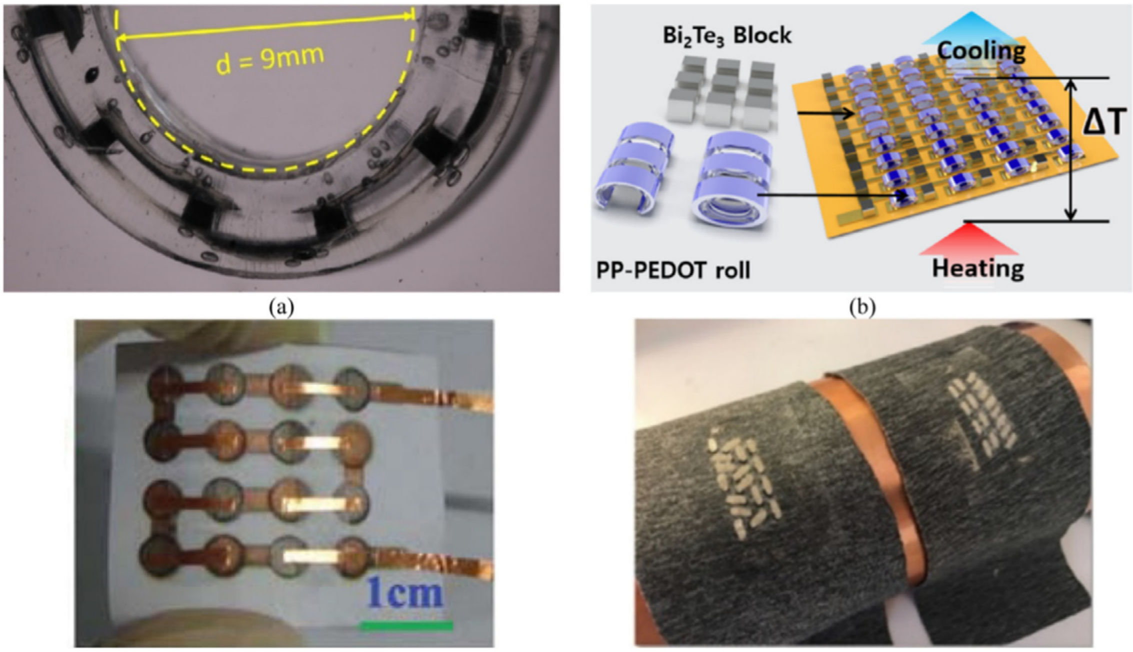

Fig. 18 Flexible TEGs fabricated on the surface of (a) polymer (b) polyamide (c) cellulose fiber (d) fabric. Reprinted from (Jaziri et al., 2019)

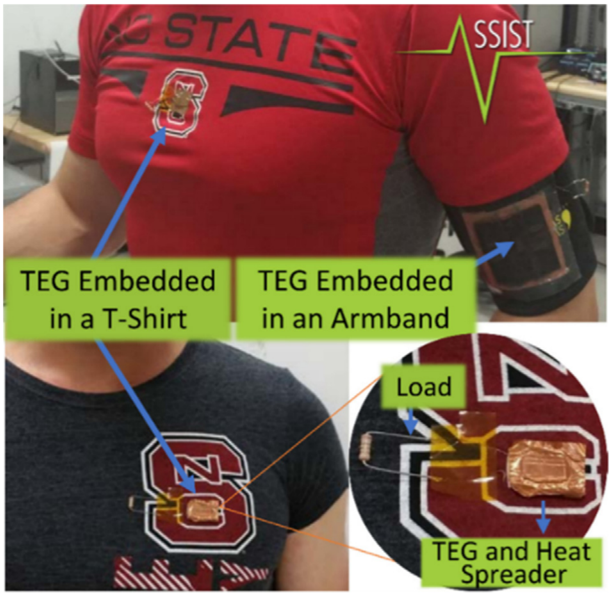

Fig. 19 Thermal energy harvesting module embedded in an armband and a T-shirt. Adapted from Hyland et al., 2016

omous and portable power-source will make them as compact and convenient as human gadgets (Saha et al., 2020; Yu et al., 2020; Pryds and Bjørk, 2020; Rodriguez et al., 2019). At present, the dominant energy source of such devices is a battery. Despite the recent improvement in batteries' power output, their presence in smart electronics has posed a constraint on their portability and operational cost (Vullers et al., 2009).

Furthermore, unlike batteries that contain environmentally unfriendly materials like cadmium, nickel, lead, lithium, zinc mercury, and sulfuric acid, TEGs can be safely incorporated into these devices without any risk of toxicity. Another remarkable body-mounted thermoelectric device is the TE-wristwatch, powered by the heat generated by the human body. One such watches produced by Seiko manufacturers typically generates 300 millivolts voltage from a 1.5 K temperature gradient (Hamid Elsheikh et al., 2014). The concept of a typical TE wrist-watch is presented in Fig. 20. The back-plate acts as a thermal collector from the human body, transferring it to the TEG, while the top case acts as a heat sink by radiating the heat to the atmosphere.

On the other hand, high power generation is also feasible through waste-heat recovery and solar thermoelectric generators. Each of the traditional means of electricity generation, such as hydropower generation, nuclear sources, and the burning of fossil fuels, posed some threats to environmental safety (Wang et al., 2019; Yin et al., 2019; Soleimani et al., 2020; Sharma et al., 2020; Wolf et al., 2019; Jaziri et al., 2019). For example, the nuclear source subjects the environment to nuclear meltdown while fossil fuel sources cause environmental pollution and global warming. Technically, electricity generation through thermoelectric materials does not only produce useful energy through renewable means but utilizes waste-heat generated from automobiles and steel industries, thereby reducing the effect of such heat on the environment to prevent global warming (Saha et al., 2020; Jiang et al., 2020; Nozariasbmarz et al., 2020; Zhang and Park, 2019; Cai et al., 2019). Having recognized the potential of waste-heat, those industries have been the main driving force behind the thermoelectric generator's development and commercialization. Currently, several leading automobile companies such as BMW, Ford, Volvo, and Volkswagen have integrated TEGs into their products to reduce fuel consumption of their engines (Hamid Elsheikh et al., 2014). Despite the currently small power generation efficiency of the TEGs, with effective

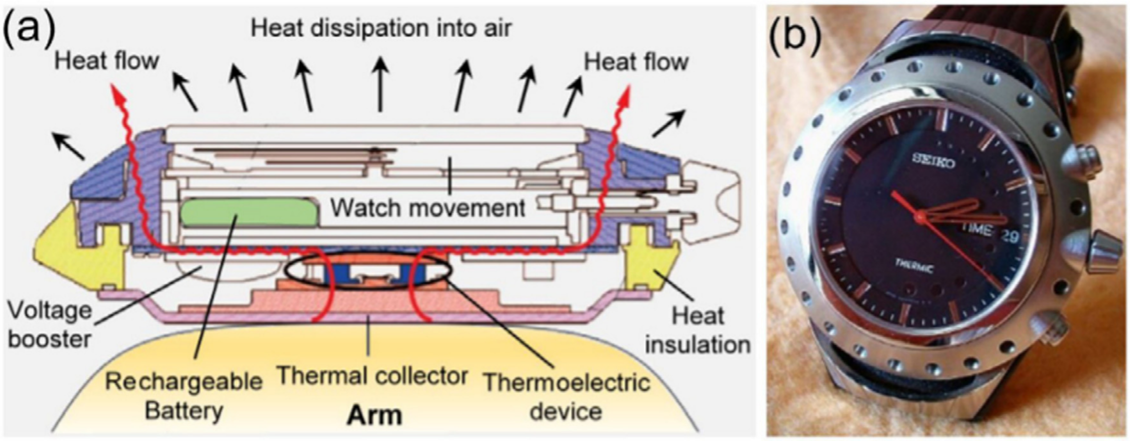

Fig. 20 (a) A schematic of the TE wristwatch concept (b) Real TE watch manufactured by Seiko. () Adapted from Nozariasbmarz et al., 2020

waste-heat harvesting and strategic design and diligent maintenance, the TEGs technology becomes imperative and attracts such manufacturers for investment. For example, a TEG with 10% efficiency and 1.25 figure of merit can be used to harness ~ 38% of the energy released through the exhaust at 250 °C temperature, which can generate a useful power that can, at least, power the electronics of the car and improves the operation of the vehicle, thereby improving fuel economy by almost 15% (Yu and Chau, 2009). Most TEGs employ BiTe-based materials since they can accomplish a high thermoelectric figure of merit below 500 K with these materials (Zhou et al., 2020; Kong et al., 2019; Yu et al., 2020). Thus, research on the development of such materials has been exhaustive. Hsu et al. (Hsu et al., 2011) came up with a 24 TEG module that can convert the waste-heat through automobile exhaust to useful electrical energy. They achieved a power output of 12 W when the temperature gradient was 30 °C. Karri and his team (Karri et al., 2011) conducted a comparison test between a TEG containing quantum-well material and Bi_2Te_3. They placed the generators at the exhaust streams of a vehicle and that of a conventional gas-powered generator under similar conditions. The relative fuel economy in both cases was higher in the quantum-well TEG compared to the Bi_2Te_3. However, they realized abrupt fluctuation in the output power with changing temperature, which can be inimical to electronic devices (Gou et al., 2013).

Some thermoelectric generators can also harness solar energy to produce electricity. Solar TEGs were initially employed for space applications because of their reliability and durability coupled with their capability to absorb abundant sunlight in outer space. The solar TEG system comprises two main parts, the solar thermal collector and the ordinary TEG. The thermal collector receives and concentrates solar irradiation as heat thereafter transmits it to the TEG through a fluid pipe or other means of heat transportation. The temperature gradient is thus determined by the thermal resistance of the TEG, which will be proportional to the heat flux from the collector to the fluid. Finally, electricity will be produced by the TEG as a consequence of the temperature gradient (Pourkiaei et al., 2019; Toberer, 2016). Elsewhere (Suter et al., 2010), a 4-leg TEG module was designed by Suter and his team. They used n-type $CaMn_{0.98}Nb_{0.02}O_3$ and p-type $La_{1.98}Sr_{0.02}CuO_4$ legs placed between Al_2O_3 ceramic cold/hot plates and exposed to focused solar irradiation. However, their analysis revealed a significant loss in solar heat, as more than 60% of such heat is re-radiated, and some portion is lost through convection from the absorber, while about 20% is lost via conduction through the legs of the solar TEG. He et al. (2012) carried further experimental and theoretical studies to overcome such thermal leakages using glass evacuated tube solar collectors. Their work revealed that the thermal losses could be minimized by about 55%.

Meanwhile, Wang et al. (Miljkovic and Wang, 2011) developed a hybrid solar TEG that passively transfers heat to the bottoming cycle using a thermosyphon with a structure like an evacuated tube sunlight collector. The hybrid system contains a parabolic-shaped mirror to focus the solar irradiation on a surface-coated with TE material and a thermosyphon to maintain the cold-temperature side and spread the extra heat to the bottom cycle as depicted in Fig. 21. The performance of such devices depends on the TE materials incorporated. While bismuth telluride-based materials are efficient for low-temperature applications, filled skutterudites are equally useful for medium -temperature usage up to 500 °C. with increasing demand for cleaner sources of energy and perpetual emergence of novel TE systems, solar TEGs employing hybrid and multi-stage configurations will have a great prospect.

5.2. Cooling applications

Thermoelectric devices can be used for cooling applications via the Peltier effect. The unique features of such devices include less noise, low weight, flexibility in packaging, and reliability (Wang et al., 2019; Yin et al., 2019; Jaziri et al., 2019; MohanKumar et al., 2019; Li et al., 2019; Liu and Wang, 2019; Zhang et al., 2019; Eklund et al., 2019; Li et al., 2020; Sun et al., 2019; Putri et al., 2019; Zhao et al., 2019; Di Liu et al., 2020). Thermoelectric coolers (TEC) are commonly used for electronics applications to transport heat from a surface whose temperature is above the ambient temperature (Chein and Huang, 2004). For a junction in an electronic system, the TEC ensures that its temperature is low enough for safe operation. For computing systems, the demand for integrated

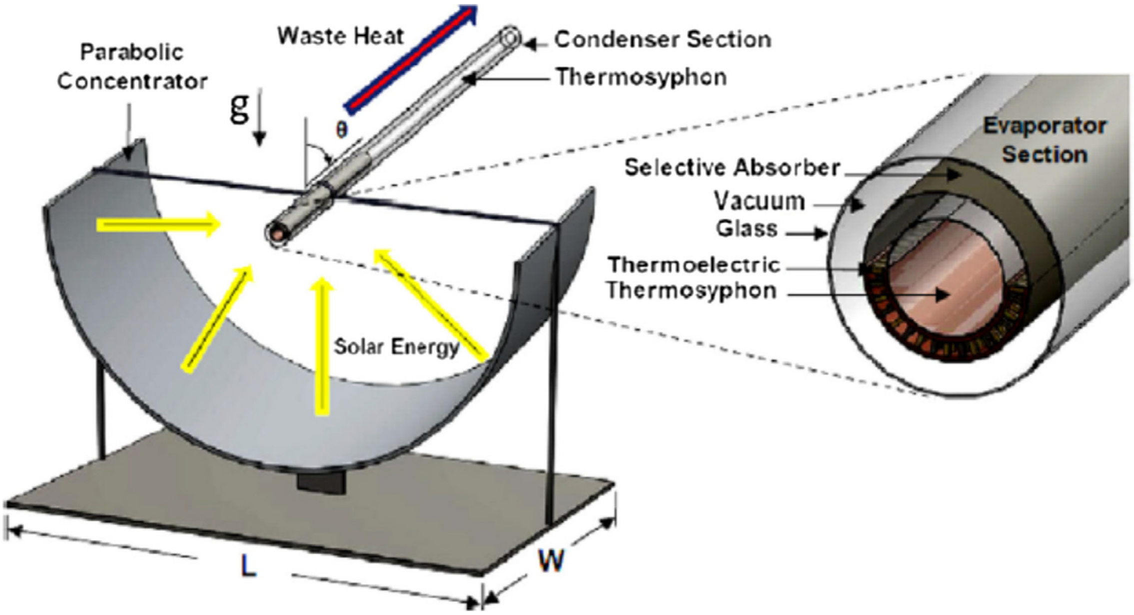

Fig. 21 Schematic of a hybrid solar thermoelectric generator. Adapted from Miljkovic and Wang, 2011

cooling devices increases as the microprocessor's power dissipation increases and the central processing unit expands in size (Putra and Yanuar, 2011). The hybrid cooling system comprising of liquid cooling and the TEC could be thermally beneficial because it can lower the thermal resistance. To facilitate the commercialization of TECs, several works have been carried out to maximize the overall cooling performance of such devices and the possibility of extending their applications to a larger scale. For example, Zhou et al. (Zhou and Yu, 2012) carried out an intensive investigation of the thermal conductance between the hot and low-temperature nodes of the TEC system. Their study revealed that when the total thermal conductance is allocated optimally, a coefficient of performance above 1.5 can be achieved. However, a higher temperature heat exchanger usually determines the overall efficiency of the cooling system (Wang et al., 2013).

The thermoelectric cooling systems are also used for refrigeration purposes, especially where the reliability is more significant than the cost. A typical solar-driven Peltier refrigerator can lower the temperature from 300 K to 278 K in less than 45 min (Abdul-Wahab et al., 2009). Apart from reliability and efficiency, a thermoelectric refrigerator dissipates heat using charge carriers instead of environmentally hazardous freon refrigerants (Dai et al., 2003). One interesting application of such devices is when they are attached to a solar cell for outdoor purposes, as depicted in Fig. 22. During the daytime, the solar cell directly powers the refrigerator via photovoltaic effect and save some portion of the electrical energy in storage like a battery, which can ultimately be used at night. The excess energy stored in the battery can also be utilized during cloudy or rainy conditions to power the refrigerator, as depicted in Fig. 23. However, the coefficient of performance (COP) of such devices may not be as high as the traditional compressor-based systems. Thermoelectric refrigerators have been used for many within and out of space applications. It has equally found applications in industries, aerospace, military and laboratories for different purposes. For instance, when used in the military, TECs can be used as a microclimate controller to remove heat from the soldiers' body while in combat, thereby enhancing the mission duration and the soldier's performance. The coefficient of performance of the present-day thermoelectric refrigerators typically ranges between 0.3 and 0.7. However, COP can reach up to unity if the device extracts heat from a surface hotter than the ambient temperature (Hamid Elsheikh et al., 2014).

Furthermore, thermoelectric materials can be used for air conditioning purposes. The thermoelectric air conditioners are reliable, simple, and environmentally friendly with easy installation. An attractive feature of such devices is the ability to switch between cooling and heating easily, which only requires the reversal of the input current. However, their low COP and high cost limit their domestic usage at present

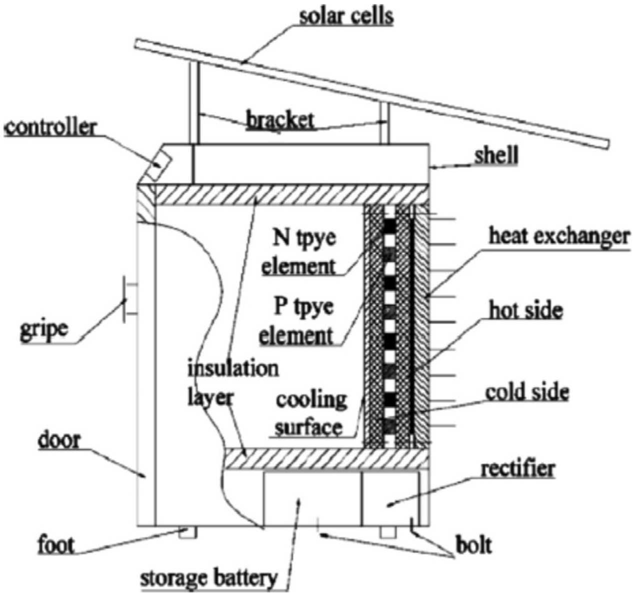

Fig. 22 Schematic of a solar-powered thermoelectric refrigeration system. () Adapted from Dai et al., 2003

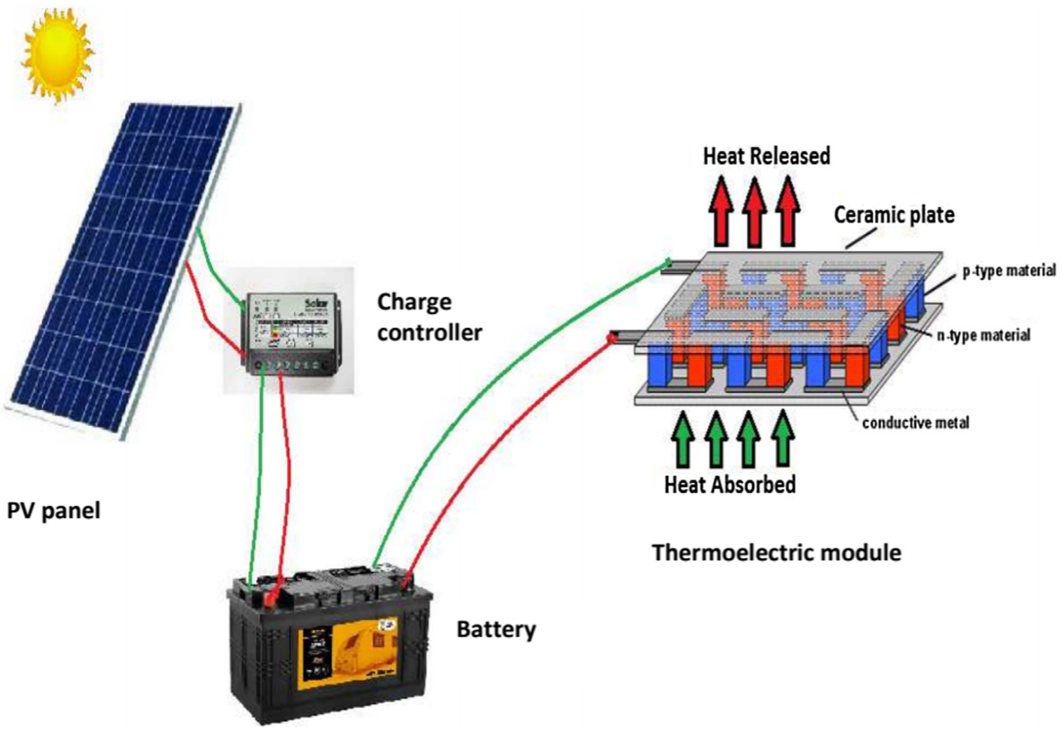

Fig. 23 Solar TE refrigeration architecture. () Adapted from Irshad et al., 2019

(Shen et al., 2013). Meanwhile, these devices still have potential markets for small enclosures like aircraft cabin, submarines, and cars where the power consumption is not high and the efficiency and safety are consequential (Riffat and Qiu, 2004).

5.3. *Thermal energy sensors*

In the last two decades, Seebeck and Peltier effects have been utilized to develop novel thermal energy sensors such as infrared sensors, fluid-flow sensors, water-condensation detectors, cryogenic heat-flux sensors, and power ultrasound effects (Riffat and Ma, 2003). These devices usually operate based on heat-electrical-signals interconversions. The performance of such thermal energy sensors has tremendously increased compared to the traditional thermal sensors.

For example, infrared sensors operate on the notion that mass releases heat, which can then be detected via the Seebeck effect. The released heat manifests as a temperature gradient that produces electrical voltage. Thus, responsivity, which is the ratio of the voltage to the radiated power, noise voltage, and time constant, is the main sensor parameter. A low-cost thermoelectric infrared sensor was developed by Hirota et al. (Hirota et al., 2007). They recorded responsivity reaching up to 3900 V/W. In terms of compatibility, the most effective infrared sensor reported is the thin-film type. Meanwhile, most infrared sensors can be able to operate within 7 – 14 μm range. These sensors find applications in intrusion alarm sensors, infrared gas analysis, and non-contact temperature measurements (Chen and Wu, 2019; Huang et al., 2020).

Thermoelectric devices can be used as cryogenic heat flux sensors. Some commercially obtained Te modules were used down to 60 K for radiant heat flux measurement for possible cryogenic applications. A sensitivity of 27 $\mu V/(W/m^2)$ at 80 K was observed using the 127P/N junction module, which is more than five times the sensitivity of a conventional heat flux sensor. Thermoelectric microsensors can also be employed for the detection of water condensation. The operation of such devices is based on thermal oscillation created at a junction by the Peltier effect. The water droplet reaching the junction perturbs the thermal oscillation, which causes a shift in the frequency. Thus, the formation of a mist can be projected in advance (Riffat and Ma, 2003).

5.4. *Aerospace applications*

Thermoelectric power sources are considered one of the best options for extraterrestrial energy demand since sophisticated self-running power sources that do not rely on solar sources is highly important. For instance, Jupiter and Mars's solar illumination is as low as 4% and 45%, respectively, even lower for some other planets. In 1961, the united states space mission utilized a radioisotope TEG to generate electricity in their spacecraft. Recently, the Jet propulsion laboratory in California has developed skutterudite alloys with a high figure of merit (0.9 – 1.5) in the temperature range 300 – 900 K. The materials are to be used in advanced radioisotopes power systems to support NASA's extraterrestrial missions (El-Genk et al., 2006). The use of SiGe unicouples in the top while skutterudite in the bottom array was proposed for TE modules to be integrated into the radioisotopes power system. However, sublimation of antimony near the hot junction becomes the major impediment to using skutterudites in such systems. Currently, the Boeing research team considers using TEGs in commercial aircraft (Hamid Elsheikh et al., 2014) to reduce fuel consumption and minimize carbon emissions.

6. Summary and outlook

In summary, we presented a review of the advances in developing inorganic thermoelectric materials and the existing impediments to their large-scale applications. The possibility of decoupling the relevant parameters defining the thermoelectric efficiency provides an optimistic outlook for designing even better TE materials soon. Recent investigations based on high-performance inorganic thermoelectric materials, majorly chalcogenides, Heusler compounds, clathrates, and skutterudites revealed the possibility of achieving higher TE efficiency. The paper highlighted different techniques to improve the thermoelectric figure of merit of materials and how to integrate them in the same material to boost the performance. We also highlighted various sample fabrication techniques related to the power output of TE materials and further discussed novel mechanisms employed by researchers to simultaneously improve the TE parameters using a multi-scale approach. On this note, the all-scale hierarchical approach creates a new window for TE materials development as they provide a path for suppressing phonons motions which are majorly responsible for the lattice thermal conduction. Apart from efforts to improve the TE efficiency by modifying the intrinsic properties, we have shown how the performance of the materials can be enhanced through the proper architectural design of the TE systems. On the other hand, the stability issues of some of the materials possessing a high figure of merit still need to be addressed, while for the stable compounds, the efficiency needs to be enhanced. Finally, some prospects of the TE materials and their various applications have been highlighted. Since more than 50% of the energy produced globally is depleted as a waste-heat, the use of thermoelectrics to convert such otherwise wasted-heat to useful energy is paramount.

Declaration of Competing Interest

The authors declare that they have no known competing financial interests or personal relationships that could have appeared to influence the work reported in this paper.

Acknowledgment

This work is supported by the King Fahd University of Petroleum and Minerals under project # DF191032. M.A. Gondal and Y.S. Wudil acknowledge the support by King Abdullah City for Atomic and Renewable Energy (K.A.CARE) under the Senior Fellowship Scheme.

References

Wu, Y., Nan, P., Chen, Z., Zeng, Z., Lin, S., Zhang, X., Dong, H., Chen, Z., Gu, H., Li, W., Chen, Y., Ge, B., Pei, Y., 2020. Manipulation of Band Degeneracy and Lattice Strain for Extraordinary PbTe Thermoelectrics. Research. 2020, 1–12 https://doi.org/10.34133/2020/8151059.

Heo, S.H., Jo, S., Kim, H.S., Choi, G., Song, J.Y., Kang, J.Y., Park, N.J., Ban, H.W., Kim, F., Jeong, H., Jung, J., Jang, J., Lee, W.B., Shin, H., Son, J.S., 2019. Composition change-driven texturing and doping in solution-processed SnSe thermoelectric thin films. Nat. Commun. 10. https://doi.org/10.1038/s41467-019-08883-x.

V. Pavan Kumar, A.R. Supka, P. Lemoine, O.I. Lebedev, B. Raveau, K. Suekuni, V. Nassif, R. Al Rahal Al Orabi, M. Fornari, E. Guilmeau, High Power Factors of Thermoelectric Colusites Cu 26 T 2 Ge 6 S 32 (T = Cr, Mo, W): Toward Functionalization of the Conductive "Cu–S" Network, Adv. Energy Mater. 9 (2019) 1803249. https://doi.org/10.1002/aenm.201803249.

Hsieh, Y.-Y., Zhang, Y., Zhang, L., Fang, Y., Kanakaraaj, S.N., Bahk, J.-H., Shanov, V., 2019. High thermoelectric power-factor composites based on flexible three-dimensional graphene and polyaniline. Nanoscale. 11, 6552–6560. https://doi.org/10.1039/C8NR10537E.

Ahmad, K., Wan, C., Al-Eshaikh, M.A., Kadachi, A.N., 2019. Enhanced thermoelectric performance of Bi2Te3 based graphene nanocomposites. Appl. Surf. Sci. 474, 2–8. https://doi.org/10.1016/J.APSUSC.2018.10.163.

J. Mao, H. Zhu, Z. Ding, Z. Liu, G.A. Gamage, G. Chen, Z. Ren, High thermoelectric cooling performance of n-type Mg3Bi2-based materials, Science (80-.). 365 (2019) 495–498. https://doi.org/10.1126/science.aax7792.

Kleinke, H., 2010. New bulk Materials for Thermoelectric Power Generation: Clathrates and Complex Antimonides †. Chem. Mater. 22, 604–611. https://doi.org/10.1021/cm901591d.

Qian, X., Wu, H., Wang, D., Zhang, Y., Wang, J., Wang, G., Zheng, L., Pennycook, S.J., Zhao, L.D., 2019. Synergistically optimizing interdependent thermoelectric parameters of n-type PbSe through alloying CdSe. Energy Environ. Sci. 12, 1969–1978. https://doi.org/10.1039/c8ee03386b.

Xi, L., Pan, S., Li, X., Xu, Y., Ni, J., Sun, X., Yang, J., Luo, J., Xi, J., Zhu, W., Li, X., Jiang, D., Dronskowski, R., Shi, X., Snyder, G.J., Zhang, W., 2018. Discovery of High-Performance Thermoelectric Chalcogenides through Reliable High-Throughput Material Screening. J. Am. Chem. Soc. 140, 10785–10793. https://doi.org/10.1021/jacs.8b04704.

Liu, B., Rajagopal, D., 2019. Life-cycle energy and climate benefits of energy recovery from wastes and biomass residues in the United States. Nat. Energy. 4, 700–708. https://doi.org/10.1038/s41560-019-0430-2.

Salhi, B., Wudil, Y.S., Hossain, M.K., Al-Ahmed, A., Al-Sulaiman, F.A., 2018. Review of recent developments and persistent challenges in stability of perovskite solar cells. Renew. Sustain. Energy Rev. 90, 210–222. https://doi.org/10.1016/J.RSER.2018.03.058.

H.J. Nolas, G. S.; Sharp, J.; Goldsmid, Thermoelectrics: Basic Principles and New Materials Developments - G.S. Nolas, J. Sharp, J. Goldsmid - Google Books, n.d. https://books.google.com.sa/books?hl=en&lr=&id=QKDzCAAAQBAJ&oi=fnd&pg=PA1&dq=Nolas,+G.+S.%3B+Sharp,+J.%3B+Goldsmid,+H.+J.+Thermoelectrics:+Basic+Principles+and+New+Materials+Developments%3B+Springer:+New+York,+2001.&ots=waNssqf65m&sig=pG0VXikPXQ5oUVIYDBkp (accessed September 11, 2019).

Wudil, Y.S., Gondal, M.A., Rao, S.G., Kunwar, S., Alsayoud, A.Q., 2020. Substrate temperature-dependent thermoelectric figure of merit of nanocrystalline Bi2Te3 and Bi2Te2.7Se0.3 prepared using pulsed laser deposition supported by DFT study. Ceram. Int. https://doi.org/10.1016/j.ceramint.2020.06.196.

N. Mott, H. Jones, The theory of the properties of metals and alloys, (1958).

Rao, A.M., Ji, X., Tritt, T.M., 2006. Properties of nanostructured one-dimensional and composite thermoelectric materials. MRS Bull. 31, 218–223. https://doi.org/10.1557/mrs2006.48.

G.A. Slack, Design concepts for improved thermoelectric materials, in: Mater. Res. Soc. Symp. - Proc., MRS, 1997: pp. 47–54. https://doi.org/10.1557/proc-478-47.

Wei, K., Neu, J.N., Lai, Y., Chen, K.W., Hobbis, D., Nolas, G.S., Graf, D.E., Siegrist, T., Baumbach, R.E., 2019. Enhanced thermoelectric performance of heavy-fermion compounds YbTM2Zn20 (TM = Co, Rh, Ir) at low temperatures. Sci. Adv. 5. https://doi.org/10.1126/sciadv.aaw6183.

Wudil, Y.S., Gondal, M.A., Rao, S.G., Kunwar, S., 2019. Thermal conductivity of PLD-grown thermoelectric Bi2Te2.7Se0.3 films using temperature-dependent Raman spectroscopy technique. Ceram. Int. https://doi.org/10.1016/j.ceramint.2019.11.219.

Mahmoudinezhad, S., Cotfas, P.A., Cotfas, D.T., Rosendahl, L.A., Rezania, A., 2020. Response of thermoelectric generators to Bi2Te3 and Zn4Sb3 energy harvester materials under variant solar radiation. Renew. Energy. 146, 2488–2498. https://doi.org/10.1016/j.renene.2019.08.080.

Mohammadnia, A., Ziapour, B.M., Sedaghati, F., Rosendahl, L., Rezania, A., 2020. Utilizing thermoelectric generator as cavity temperature controller for temperature management in dish-Stirling engine. Appl. Therm. Eng. 165. https://doi.org/10.1016/j.applthermaleng.2019.114568.

Houshfar, E., 2020. Thermodynamic analysis and multi-criteria optimization of a waste-to-energy plant integrated with thermoelectric generator. Energy Convers. Manag. 205. https://doi.org/10.1016/j.enconman.2019.112207.

Cui, Y.J., Wang, B.L., Wang, K.F., Zheng, L., 2019. Power output evaluation of a porous annular thermoelectric generator for waste heat harvesting. Int. J. Heat Mass Transf. 137, 979–989. https://doi.org/10.1016/j.ijheatmasstransfer.2019.03.157.

Allison, L.K., Andrew, T.L., 2019. A Wearable All-Fabric Thermoelectric Generator. Adv. Mater. Technol. 4, 1800615. https://doi.org/10.1002/admt.201800615.

Zhao, X., Han, W., Zhao, C., Wang, S., Kong, F., Ji, X., Li, Z., Shen, X., 2019. Fabrication of Transparent Paper-Based Flexible Thermoelectric Generator for Wearable Energy Harvester Using Modified Distributor Printing Technology. ACS Appl. Mater. Interfaces. 11, 10301–10309. https://doi.org/10.1021/acsami.8b21716.

Karthick, K., Suresh, S., Hussain, M.M.M.D., Ali, H.M., Kumar, C. S.S., 2019. Evaluation of solar thermal system configurations for thermoelectric generator applications: A critical review. Sol. Energy. 188, 111–142. https://doi.org/10.1016/j.solener.2019.05.075.

Yuan, Z., Tang, X., Liu, Y., Xu, Z., Liu, K., Li, J., Zhang, Z., Wang, H., 2019. Improving the performance of a screen-printed micro-radioisotope thermoelectric generator through stacking integration. J. Power Sources. 414, 509–516. https://doi.org/10.1016/j.jpowsour.2019.01.040.

Marefati, M., Mehrpooya, M., 2019. Introducing and investigation of a combined molten carbonate fuel cell, thermoelectric generator, linear fresnel solar reflector and power turbine combined heating and power process. J. Clean. Prod. 240. https://doi.org/10.1016/j.jclepro.2019.118247.

Angeline, A.A., Asirvatham, L.G., Hemanth, D.J., Jayakumar, J., Wongwises, S., 2019. Performance prediction of hybrid thermoelectric generator with high accuracy using artificial neural networks. Sustain. Energy Technol. Assessments. 33, 53–60. https://doi.org/10.1016/j.seta.2019.02.008.

Elmoughni, H.M., Menon, A.K., Wolfe, R.M.W., Yee, S.K., 2019. A Textile-Integrated Polymer Thermoelectric Generator for Body Heat Harvesting. Adv. Mater. Technol. 4, 1800708. https://doi.org/10.1002/admt.201800708.

Karthick, K., Suresh, S., Singh, H., Joy, G.C., Dhanuskodi, R., 2019. Theoretical and experimental evaluation of thermal interface materials and other influencing parameters for thermoelectric generator system. Renew. Energy. 134, 25–43. https://doi.org/10.1016/j.renene.2018.10.109.

Pourkiaei, S.M., Ahmadi, M.H., Sadeghzadeh, M., Moosavi, S., Pourfayaz, F., Chen, L., Pour Yazdi, M.A., Kumar, R., 2019. Thermoelectric cooler and thermoelectric generator devices: A review of present and potential applications, modeling and materials. Energy. 186. https://doi.org/10.1016/j.energy.2019.07.179.

Zhou, Y., Zhang, S., Xu, X., Liu, W., Zhang, S., Li, G., He, J., 2020. Dynamic piezo-thermoelectric generator for simultaneously harvesting mechanical and thermal energies. Nano Energy. 69. https://doi.org/10.1016/j.nanoen.2019.104397.

Kong, D., Zhu, W., Guo, Z., Deng, Y., 2019. High-performance flexible Bi2Te3 films based wearable thermoelectric generator for energy harvesting. Energy. 175, 292–299. https://doi.org/10.1016/j.energy.2019.03.060.

Yang, K., Cho, K., Yang, S., Park, Y., Kim, S., 2019. A laterally designed all-in-one energy device using a thermoelectric generator-coupled micro supercapacitor. Nano Energy. 60, 667–672. https://doi.org/10.1016/j.nanoen.2019.04.016.

Rodrigo, P.M., Valera, A., Fernández, E.F., Almonacid, F.M., 2019. Performance and economic limits of passively cooled hybrid thermoelectric generator-concentrator photovoltaic modules. Appl. Energy. 238, 1150–1162. https://doi.org/10.1016/j.apenergy.2019.01.132.

Choi, H., Kim, Y.J., Song, J., Kim, C.S., Lee, G.S., Kim, S., Park, J., Yim, S.H., Park, S.H., Hwang, H.R., Hong, M., Veluswamy, P., Cho, B.J., 2019. UV-Curable Silver Electrode for Screen-Printed Thermoelectric Generator. Adv. Funct. Mater. 29, 1901505. https://doi.org/10.1002/adfm.201901505.

Kanimba, E., Tian, Z., 2019. A new dimensionless number for thermoelectric generator performance. Appl. Therm. Eng. 152, 858–864. https://doi.org/10.1016/j.applthermaleng.2019.02.093.

Toberer, E., 2016. Solar thermoelectric generators: Pushing the efficiency up. Nat. Energy. 1. https://doi.org/10.1038/nenergy.2016.172.

Beretta, D., Neophytou, N., Hodges, J.M., Kanatzidis, M.G., Narducci, D., Martin-Gonzalez, M., Beekman, M., Balke, B., Cerretti, G., Tremel, W., Zevalkink, A., Hofmann, A.I., Müller, C., Dörling, B., Campoy-Quiles, M., Caironi, M., 2019. Thermoelectrics: From history, a window to the future. Mater. Sci. Eng. R Reports. 138. https://doi.org/10.1016/j.mser.2018.09.001.

W. He, D. Wang, H. Wu, Y. Xiao, Y. Zhang, D. He, Y. Feng, Y.J. Hao, J.F. Dong, R. Chetty, L. Hao, D. Chen, J. Qin, Q. Yang, X. Li, J.M. Song, Y. Zhu, W. Xu, C. Niu, X. Li, G. Wang, C. Liu, M. Ohta, S.J. Pennycook, J. He, J.F. Li, L.D. Zhao, High thermoelectric performance in low-cost SnS0.91Se0.09 crystals, Science (80-.). 365 (2019) 1418–1424. https://doi.org/10.1126/science.aax5123.

Wudil, Y.S., Gondal, M.A., Rao, S.G., Kunwar, S., Alsayoud, A.Q., 2020. Improved thermoelectric performance of ternary Cu/Ni/Bi2Te2.7Se0.3 nanocomposite prepared by pulsed laser deposition. Mater. Chem. Phys. https://doi.org/10.1016/j.matchemphys.2020.123321 123321.

L.E. Bell, Cooling, heating, generating power, and recovering waste heat with thermoelectric systems, Science (80-.). 321 (2008) 1457–1461. https://doi.org/10.1126/science.1158899.

Pichanusakorn, P., Bandaru, P., 2010. Nanostructured thermoelectrics. Mater. Sci. Eng. R Reports. 67, 19–63. https://doi.org/10.1016/j.mser.2009.10.001.

Alam, H., Ramakrishna, S., 2013. A review on the enhancement of figure of merit from bulk to nano-thermoelectric materials. Nano Energy. 2, 190–212. https://doi.org/10.1016/j.nanoen.2012.10.005.

G.J. SNYDER, E.S. TOBERER, Complex thermoelectric materials, in: Mater. Sustain. Energy, Co-Published with Macmillan Publishers Ltd, UK, 2010: pp. 101–110. https://doi.org/10.1142/9789814317665_0016.

D.R.-Crcp.B. Raton, undefined 2005, CRC handbook of thermoelectrics. 1995, (n.d.).

Goldsmid, H.J., 2009. Introduction to Thermoelectricity (Springer Series in Materials Science). https://doi.org/10.1007/978-3-642-00716-3.

Dylla, M.T., Kuo, J.J., Witting, I., Snyder, G.J., 2019. Grain Boundary Engineering Nanostructured $SrTiO_3$ for Thermoelectric Applications. Adv. Mater. Interfaces. 6, 1900222. https://doi.org/10.1002/admi.201900222.

Ge, Z.H., Chong, X., Feng, D., Zhang, Y.X., Qiu, Y., Xie, L., Guan, P.W., Feng, J., He, J., 2019. Achieving an excellent thermoelectric performance in nanostructured copper sulfide bulk via a fast doping strategy. Mater. Today Phys. 8, 71–77. https://doi.org/10.1016/j.mtphys.2019.01.003.

Alagar Nedunchezhian, A.S., Sidharth, D., Devi, N.Y., Rajkumar, R., Rajasekaran, P., Arivanandhan, M., Anbalagan, G., Jayavel, R., 2019. Effect of Bismuth substitution on the enhancement of thermoelectric power factor of nanostructured Bi x Co 3–x O 4. Ceram. Int. 45, 6782–6787. https://doi.org/10.1016/j.ceramint.2018.12.170.

Wang, Y., Liu, W.-D., Gao, H., Wang, L.-J., Li, M., Shi, X.-L., Hong, M., Wang, H., Zou, J., Chen, Z.-G., 2019. High Porosity in Nanostructured *n* -Type Bi $_2$ Te $_3$ Obtaining Ultralow Lattice Thermal Conductivity. ACS Appl. Mater. Interfaces. 11, 31237–31244. https://doi.org/10.1021/acsami.9b12079.

Wu, Y., Lou, Q., Qiu, Y., Guo, J., Mei, Z.Y., Xu, X., Feng, J., He, J., Ge, Z.H., 2019. Highly enhanced thermoelectric properties of nanostructured Bi2S3 bulk materials: Via carrier modification and multi-scale phonon scattering. Inorg. Chem. Front. 6, 1374–1381. https://doi.org/10.1039/c9qi00213h.

K.F. Hsu, S. Loo, F. Guo, W. Chen, J.S. Dyck, C. Uher, T. Hogan, E.K. Polychroniadis, M.G. Kanatzidis, Cubic AgPbmSbTe2 + m: Bulk Thermoelectric Materials with High Figure of Merit, Science (80-.). 303 (2004) 818–821. https://doi.org/10.1126/science.1092963.

Kang, H.B., Poudel, B., Li, W., Lee, H., Saparamadu, U., Nozariasbmarz, A., Kang, M.G., Gupta, A., Heremans, J.J., Priya, S., 2020. Decoupled phononic-electronic transport in multi-phase n-type half-Heusler nanocomposites enabling efficient high temperature power generation. Mater. Today. 36, 63–72. https://doi.org/10.1016/j.mattod.2020.01.002.

Venkatasubramanian, R., Siivola, E., Colpitts, T., O'Quinn, B., 2001. Thin-film thermoelectric devices with high room-temperature figures of merit. Nature. 413, 597–602. https://doi.org/10.1038/35098012.

Balandin, A., Wang, K.L., 1998. Effect of phonon confinement on the thermoelectric figure of merit of quantum wells. J. Appl. Phys. 84, 6149–6153. https://doi.org/10.1063/1.368928.

Li, G., He, J., An, Q., Morozov, S.I., Hao, S., Zhai, P., Zhang, Q., Goddard, W.A., Snyder, G.J., 2019. Dramatically reduced lattice thermal conductivity of Mg 2 Si thermoelectric material from nanotwinning. Acta Mater. 169, 9–14. https://doi.org/10.1016/j.actamat.2019.02.041.

Wang, Y., Liu, W.-D., Shi, X.-L., Hong, M., Wang, L.-J., Li, M., Wang, H., Zou, J., Chen, Z.-G., 2019. Enhanced thermoelectric properties of nanostructured n-type Bi2Te3 by suppressing Te vacancy through non-equilibrium fast reaction. Chem. Eng. J. https://doi.org/10.1016/j.cej.2019.123513 123513.

X. Hu, J. Hu, X. an Fan, B. Feng, Z. Pan, P. Liu, Y. Zhang, R. Li, Z. He, G. Li, Y. Li, Artificial porous structure: An effective method to improve thermoelectric performance of Bi2Te3 based alloys, J. Solid State Chem. (2019) 121060. https://doi.org/10.1016/j.jssc.2019.121060.

Zhang, J., Huang, L., Zhu, C., Zhou, C., Jabar, B., Li, J., Zhu, X., Wang, L., Song, C., Xin, H., Li, D., Qin, X., 2019. Design of Domain Structure and Realization of Ultralow Thermal Conductivity for Record-High Thermoelectric Performance in Chalcopyrite. Adv. Mater., 1905210 https://doi.org/10.1002/adma.201905210.

Zhou, J., Jin, C., Seol, J.H., Li, X., Shi, L., 2005. Thermoelectric properties of individual electrodeposited bismuth telluride nanowires. Appl. Phys. Lett. 87, 1–3. https://doi.org/10.1063/1.2058217.

Lee, S.M., Cahill, D.G., Venkatasubramanian, R., 1997. Thermal conductivity of Si-Ge superlattices. Appl. Phys. Lett. 70, 2957–2959. https://doi.org/10.1063/1.118755.

Kim, W., Zide, J., Gossard, A., Klenov, D., Stemmer, S., Shakouri, A., Majumdar, A., 2006. Thermal conductivity reduction and thermoelectric figure of merit increase by embedding nanoparticles in crystalline semiconductors. Phys. Rev. Lett. 96. https://doi.org/10.1103/PhysRevLett.96.045901.

Wang, C., Ma, Z., Lei, J., Zhang, D., Chen, Y., Wang, Y., Wang, J., Cheng, Z.X., 2020. Core-shell nanostructures introduce multiple potential barriers to enhance energy filtering for the improvement of thermoelectric properties of SnTe. Nanoscale. https://doi.org/10.1039/C9NR09331A.

Marinho, A.A., Costa, N.P., Pereira, L.F.C., Brito, F.A., Chesman, C., 2019. Thermoelectric properties of BiSbTe alloy nanofilms produced by DC sputtering: experiments and modeling. J. Mater. Sci. https://doi.org/10.1007/s10853-019-04188-y.

Sivaprahasam, D., Chandrasekhar, S.B., Kashyap, S., Kumar, A., Gopalan, R., 2019. Thermal conductivity of nanostructured Fe0.04Co0.96Sb3 skutterudite. Mater. Lett. 252, 231–234. https://doi.org/10.1016/j.matlet.2019.05.140.

Gainza, J., Serrano-Sánchez, F., Gharsallah, M., Carrascoso, F., Bermúdez, J., Dura, O.J., Mompean, F.J., Biskup, N., Meléndez, J. J., Martínez, J.L., Alonso, J.A., Nemes, N.M., 2019. Evidence of nanostructuring and reduced thermal conductivity in n-type Sb-alloyed SnSe thermoelectric polycrystals. J. Appl. Phys. 126. https://doi.org/10.1063/1.5108569.

Fitriani, R., Ovik, B.D., Long, M.C., Barma, M., Riaz, M.F.M., Sabri, S.M., Said, R., 2016. Saidur, A review on nanostructures of high-temperature thermoelectric materials for waste heat recovery. Renew. Sustain. Energy Rev. 64, 635–659. https://doi.org/10.1016/j.rser.2016.06.035.

Yin, Y., Baskaran, K., Tiwari, A., 2019. A Review of Strategies for Developing Promising Thermoelectric Materials by Controlling Thermal Conduction. Phys. Status Solidi. 216, 1800904. https://doi.org/10.1002/pssa.201800904.

W. Lu, S. Li, R. Xu, J. Zhang, D. Li, Z. Feng, Y. Zhang, G. Tang, Boosting Thermoelectric Performance of SnSe via Tailoring Band Structure, Suppressing Bipolar Thermal Conductivity, and Introducing Large Mass Fluctuation, ACS Appl. Mater. Interfaces. (2019) acsami.9b17811. https://doi.org/10.1021/acsami.9b17811.

Hooshmand Zaferani, S., Ghomashchi, R., Vashaee, D., 2019. Strategies for engineering phonon transport in Heusler thermoelectric compounds. Renew. Sustain. Energy Rev. 112, 158–169. https://doi.org/10.1016/j.rser.2019.05.051.

Biswas, R., Mukherjee, S., Mallik, R.C., Vitta, S., Dasgupta, T., 2019. Ultralow thermal conductivity and low charge carrier scattering potential in Zn 1–x Cd x Sb solid solutions for thermoelectric application. Mater. Today Energy. 12, 107–113. https://doi.org/10.1016/j.mtener.2018.12.014.

Kang, H.B., Saparamadu, U., Nozariasbmarz, A., Li, W., Zhu, H., Poudel, B., Priya, S., 2020. Understanding Oxidation Resistance of Half-Heusler Alloys for in-Air High Temperature Sustainable Thermoelectric Generators. ACS Appl. Mater. Interfaces. 12, 36706–36714. https://doi.org/10.1021/acsami.0c08413.

Shen, Q., Chen, L., Goto, T., Hirai, T., Yang, J., Meisner, G.P., Uher, C., 2001. Effects of partial substitution of Ni by Pd on the thermoelectric properties of ZrNiSn-based half-Heusler compounds. Appl. Phys. Lett. 79, 4165–4167. https://doi.org/10.1063/1.1425459.

Browning, V.M., Poon, S.J., Tritt, T.M., Pope, A.L., Bhattacharya, S., Volkov, P., Song, J.G., Ponnambalam, V., Ehrlich, A.C., 1999. Thermoelectric properties of the half-Heusler compound (Zr, Hf)(Ni, Pd)Sn. Mater. Res. Soc. Symp. - Proc. 545, 403–412. https://doi.org/10.1557/proc-545-403.

Zhao, L.D., Wu, H.J., Hao, S.Q., Wu, C.I., Zhou, X.Y., Biswas, K., He, J.Q., Hogan, T.P., Uher, C., Wolverton, C., Dravid, V.P., Kanatzidis, M.G., 2013. All-scale hierarchical thermoelectrics: MgTe in PbTe facilitates valence band convergence and suppresses bipolar thermal transport for high performance. Energy Environ. Sci. 6, 3346–3355. https://doi.org/10.1039/c3ee42187b.

Biswas, K., He, J., Blum, I.D., Wu, C.I., Hogan, T.P., Seidman, D. N., Dravid, V.P., Kanatzidis, M.G., 2012. High-performance bulk thermoelectrics with all-scale hierarchical architectures. Nature. 489, 414–418. https://doi.org/10.1038/nature11439.

Zhao, L.D., Dravid, V.P., Kanatzidis, M.G., 2014. The panoscopic approach to high performance thermoelectrics. Energy Environ. Sci. 7, 251–268. https://doi.org/10.1039/c3ee43099e.

T. Li, J. Yu, G. Nie, B.-P. Zhang, Q. Sun, The Ultralow Thermal Conductivity and Ultrahigh Thermoelectric Performance of Fluorinated Sn2Bi Sheet in Room Temperature, Nano Energy. (n.d.). https://doi.org/10.1016/j.nanoen.2019.104283.

Banik, A., Shenoy, U.S., Anand, S., Waghmare, U.V., Biswas, K., 2015. Mg alloying in SnTe facilitates valence band convergence and optimizes thermoelectric properties. Chem. Mater. 27, 581–587. https://doi.org/10.1021/cm504112m.

Pei, Y., Wang, H., Snyder, G.J., 2012. Band engineering of thermoelectric materials. Adv. Mater. 24, 6125–6135. https://doi.org/10.1002/adma.201202919.

Lalonde, A.D., Pei, Y., Wang, H., Jeffrey Snyder, G., 2011. Lead telluride alloy thermoelectrics. Mater. Today. 14, 526–532. https://doi.org/10.1016/S1369-7021(11)70278-4.

Zhao, L.D., Hao, S., Lo, S.H., Wu, C.I., Zhou, X., Lee, Y., Li, H., Biswas, K., Hogan, T.P., Uher, C., Wolverton, C., Dravid, V.P., Kanatzidis, M.G., 2013. High thermoelectric performance via hierarchical compositionally alloyed nanostructures. J. Am. Chem. Soc. 135, 7364–7370. https://doi.org/10.1021/ja403134b.

Zhao, L.D., Lo, S.H., He, J., Li, H., Biswas, K., Androulakis, J., Wu, C.I., Hogan, T.P., Chung, D.Y., Dravid, V.P., Kanatzidis, M.G., 2011. High performance thermoelectrics from earth-abundant materials: Enhanced figure of merit in PbS by second phase nanostructures. J. Am. Chem. Soc. 133, 20476–20487. https://doi.org/10.1021/ja208658w.

Shenoy, U.S., Bhat, D.K., 2019. Electronic structure engineering of tin telluride through co-doping of bismuth and indium for high performance thermoelectrics: A synergistic effect leading to a record high room temperature ZT in tin telluride. J. Mater. Chem. C. 7, 4817–4821. https://doi.org/10.1039/c9tc01184f.

D'Souza, R., Cao, J., Querales-Flores, J.D., Fahy, S., Savić, I., 2020. Electron-phonon scattering and thermoelectric transport in p -type PbTe from first principles. Phys. Rev. B. 102,. https://doi.org/10.1103/physrevb.102.115204 115204.

J.P. Heremans, V. Jovovic, E.S. Toberer, A. Saramat, K. Kurosaki, A. Charoenphakdee, S. Yamanaka, G.J. Snyder, Enhancement of thermoelectric efficiency in PbTe by distortion of the electronic density of states, Science (80-.). 321 (2008) 554–557. https://doi.org/10.1126/science.1159725.

Heremans, J.P., Wiendlocha, B., Chamoire, A.M., 2012. Resonant levels in bulk thermoelectric semiconductors. Energy Environ. Sci. 5, 5510–5530. https://doi.org/10.1039/c1ee02612g.

Zhou, M., Gibbs, Z.M., Wang, H., Han, Y., Li, L., Snyder, G.J., 2016. Thermoelectric performance of co-doped SnTe with resonant levels. Appl. Phys. Lett. 109,. https://doi.org/10.1063/1.4959845 042102.

Zhang, Q., Liao, B., Lan, Y., Lukas, K., Liu, W., Esfarjani, K., Opeil, C., Broido, D., Chen, G., Ren, Z., 2013. High thermoelectric performance by resonant dopant indium in nanostructured SnTe. Proc. Natl. Acad. Sci. U. S. A. 110, 13261–13266. https://doi.org/10.1073/pnas.1305735110.

Ma, Z., Lei, J., Zhang, D., Wang, C., Wang, J., Cheng, Z., Wang, Y., 2019. Enhancement of thermoelectric properties in pd-in co-doped snte and its phase transition behavior. ACS Appl. Mater. Interfaces. 11, 33792–33802. https://doi.org/10.1021/acsami.9b08564.

Zhu, W., Huang, Z., Chu, M., Li, S., Zhang, Y., Ao, W., Wang, R., Luo, J., Liu, F., Xiao, Y., Pan, F., 2019. Enhanced thermoelectric performance through optimizing structure of anionic framework in AgCuTe-based materials. Chem. Eng. J. https://doi.org/10.1016/j.cej.2019.123917 123917.

Zhang, J., Liu, X., Liu, Q., Xia, S., 2019. Structure transition and thermoelectric properties related to AZn(1–x)/2CuxSb (A = Ca, Eu, Sr; $0 < x < 1$) Zintl phases. J. Alloys Compd. https://doi.org/10.1016/j.jallcom.2019.152508.

Gascoin, F., Ottensmann, S., Stark, D., Haïle, S.M., Snyder, G.J., 2005. Zintl Phases as Thermoelectric Materials: Tuned Transport Properties of the Compounds CaxYb1-xZn2Sb2. Adv. Funct. Mater. 15, 1860–1864. https://doi.org/10.1002/adfm.200500043.

Zhao, L.D., Zhang, X., Wu, H., Tan, G., Pei, Y., Xiao, Y., Chang, C., Wu, D., Chi, H., Zheng, L., Gong, S., Uher, C., He, J., Kanatzidis, M.G., 2016. Enhanced Thermoelectric Properties in the Counter-Doped SnTe System with Strained Endotaxial SrTe. J. Am. Chem. Soc. 138, 2366–2373. https://doi.org/10.1021/jacs.5b13276.

Khitun, A., Balandin, A., Wang, K.L., Chen, G., 2000. Enhancement of the thermoelectric figure of merit of Si1-xGex quantum wires due to spatial confinement of acoustic phonons. Phys. E Low-Dimensional Syst. Nanostructures. 8, 13–18. https://doi.org/10.1016/S1386-9477(00)00119-3.

Balandin, A.A., Lazarenkova, O.L., 2003. Mechanism for thermoelectric figure-of-merit enhancement in regimented quantum dot superlattices. Appl. Phys. Lett. 82, 415–417. https://doi.org/10.1063/1.1539905.

M.S. Dresselhaus, G. Dresselhaus, X. Sun, Z. Zhang, S.B. Cronin, T. Koga, Low-dimensional thermoelectric materials, in: Phys. Solid State, American Institute of Physics Inc., 1999: pp. 679–682. https://doi.org/10.1134/1.1130849.

Hicks, L., Harman, T., 1996. Experimental study of the effect of quantum-well structures on the thermoelectric figure of merit. Phys. Rev. B - Condens. Matter Mater. Phys. 53, R10493–R10496. https://doi.org/10.1103/PhysRevB.53.R10493.

Dresselhaus, M.S., Chen, G., Tang, M.Y., Yang, R.G., Lee, H., Wang, D.Z., Ren, Z.F., Fleurial, J.-P., Gogna, P., 2007. New Directions for Low-Dimensional Thermoelectric Materials. Adv. Mater. 19, 1043–1053. https://doi.org/10.1002/adma.200600527.

Parbatani, A., Song, E.S., Claypoole, J., Yu, B., 2019. High performance broadband bismuth telluride tetradymite topological insulator photodiode. Nanotechnology. 30,. https://doi.org/10.1088/1361-6528/aafc84 165201.

Li, J.M., Li, D., Song, C.J., Wang, L., Xin, H.X., Zhang, J., Qin, X. Y., 2019. Realized high power factor and thermoelectric performance in Cu3SbSe4. Intermetallics. 109, 68–73. https://doi.org/10.1016/J.INTERMET.2019.03.009.

Li, S., Liu, Y., Liu, F., He, D., He, J., Luo, J., Xiao, Y., Pan, F., 2018. Effective atomic interface engineering in Bi2Te2.7Se0.3 thermoelectric material by atomic-layer-deposition approach. Nano Energy. 49, 257–266. https://doi.org/10.1016/J.NANOEN.2018.04.047.

Vikram, D.D., Johnson, A., 2018. Alam, Enhanced thermoelectric performance of Mg2Si1-xSnx codoped with Bi and Cr. Phys. Rev. B. 98. https://doi.org/10.1103/PhysRevB.98.115204.

Chen, T.-H., Chen, P.-H., Chen, C.-H., 2018. Laser co-ablation of bismuth antimony telluride and diamond-like carbon nanocomposites for enhanced thermoelectric performance. J. Mater. Chem. A. 6, 982–990. https://doi.org/10.1039/C7TA08701B.

Ge, Z.-H., Ji, Y.-H., Qiu, Y., Chong, X., Feng, J., He, J., 2018. Enhanced thermoelectric properties of bismuth telluride bulk achieved by telluride-spilling during the spark plasma sintering process. Scr. Mater. 143, 90–93. https://doi.org/10.1016/J.SCRIPTAMAT.2017.09.020.

Jin, M., Chen, Z., Tan, X., Shao, H., Liu, G., Hu, H., Xu, J., Yu, B., Shen, H., Xu, J., Jiang, H., Pei, Y., Jiang, J., 2018. Charge Transport in Thermoelectric SnSe Single Crystals. ACS Energy Lett. 3, 689–694. https://doi.org/10.1021/acsenergylett.7b01259.

Ramirez, D.C., Macario, L.R., Cheng, X., Cino, M., Walsh, D., Tseng, Y.C., Kleinke, H., 2020. Large Scale Solid State Synthetic Technique for High Performance Thermoelectric Materials: Magnesium-Silicide-Stannide. ACS Appl. Energy Mater. 3, 2130–2136. https://doi.org/10.1021/acsaem.9b02146.

Mamur, H., Bhuiyan, M.R.A., Korkmaz, F., Nil, M., 2018. A review on bismuth telluride (Bi 2 Te 3) nanostructure for thermoelectric applications. Renew. Sustain. Energy Rev. 82, 4159–4169. https://doi.org/10.1016/j.rser.2017.10.112.

Guo, W., Ma, J., Zheng, W., 2016. Bi2Te3 nanoflowers assembled of defective nanosheets with enhanced thermoelectric performance. J. Alloys Compd. 659, 170–177. https://doi.org/10.1016/j.jallcom.2015.10.228.

Zhang, Y., Hu, L.P., Zhu, T.J., Xie, J., Zhao, X.B., 2013. High Yield Bi_2Te_3 Single Crystal Nanosheets with Uniform Morphology via a Solvothermal Synthesis. Cryst. Growth Des. 13, 645–651. https://doi.org/10.1021/cg3013156.

Liang, Y., Wang, W., Zeng, B., Zhang, G., Huang, J., Li, J., Li, T., Song, Y., Zhang, X., 2011. Raman scattering investigation of Bi2Te3 hexagonal nanoplates prepared by a solvothermal process in the absence of NaOH. J. Alloys Compd. 509, 5147–5151. https://doi.org/10.1016/j.jallcom.2011.02.015.

Y. Deng, X. song Zhou, G. dan Wei, J. Liu, C.W. Nan, S. jing Zhao, Solvothermal preparation and characterization of nanocrystalline Bi2Te3 powder with different morphology, J. Phys. Chem. Solids. 63 (2002) 2119–2121. https://doi.org/10.1016/S0022-3697(02)00261-5.

Mntungwa, N., Rajasekhar, P.V.S.R., Ramasamy, K., Revaprasadu, N., 2014. A simple route to Bi2Se3 and Bi2Te 3 nanocrystals. Superlattices Microstruct. 69, 226–230. https://doi.org/10.1016/j.spmi.2014.02.021.

Wu, F., Song, H., Gao, F., Shi, W., Jia, J., Hu, X., 2013. Effects of different morphologies of Bi2Te3 nanopowders on thermoelectric properties. J. Electron. Mater. 42, 1140–1145. https://doi.org/10.1007/s11664-013-2541-z.

Kim, H.J., Han, M.K., Kim, H.Y., Lee, W., Kim, S.J., 2012. Morphology controlled synthesis of nanostructured Bi2Te 3. Bull. Korean Chem. Soc. 33, 3977–3980. https://doi.org/10.5012/bkcs.2012.33.12.3977.

Li, Y., Zhao, Q., Wang, Y.G., Bi, K., 2011. Synthesis and characterization of Bi2Te3/polyaniline composites. Mater. Sci. Semicond. Process. 14, 219–222. https://doi.org/10.1016/j.mssp.2011.02.019.

Chandra, S., Biswas, K., 2019. Realization of High Thermoelectric Figure of Merit in Solution Synthesized 2D SnSe Nanoplates via Ge Alloying. J. Am. Chem. Soc. 141, 6141–6145. https://doi.org/10.1021/jacs.9b01396.

Mi, J.-L., Lock, N., Sun, T., Christensen, M., Søndergaard, M., Hald, P., Hng, H.H., Ma, J., Iversen, B.B., 2010. Biomolecule-Assisted Hydrothermal Synthesis and Self-Assembly of Bi_2Te_3 Nanostring-Cluster Hierarchical Structure. ACS Nano. 4, 2523–2530. https://doi.org/10.1021/nn100267q.

Zhao, Q., Wang, Y.G., 2010. A facile two-step hydrothermal route for the synthesis of low-dimensional structured Bi 2 Te 3 nanocrystals with various morphologies. J. Alloys Compd. 497, 57–61. https://doi.org/10.1016/j.jallcom.2010.03.077.

Wang, S., Li, H., Lu, R., Zheng, G., Tang, X., 2013. Metal nanoparticle decorated n-type Bi2Te3-based materials with enhanced thermoelectric performances. Nanotechnology. 24. https://doi.org/10.1088/0957-4484/24/28/285702.

Chen, X., Liu, L., Dong, Y., Wang, L., Chen, L., Jiang, W., 2012. Preparation of nano-sized Bi2Te3 thermoelectric material powders by cryogenic grinding. Prog. Nat. Sci. Mater. Int. 22, 201–206. https://doi.org/10.1016/j.pnsc.2012.04.006.

Gupta, S., Neeleshwar, S., Kumar, V., Chen, Y.Y., 2012. ADVANCED MATERIALS Letters Synthesis of bismuth telluride nanostructures by refluxing method. Res. Artic. Adv. Mat. Lett. 2012, 50–54. https://doi.org/10.5185/amlett.2011.7285.

P. Srivastava, K. Singh, Structural and thermal properties of chemically synthesized Bi 2Te3 nanoparticles, in: J. Therm. Anal. Calorim., 2012: pp. 523–527. https://doi.org/10.1007/s10973-012-2553-6.

Kim, K.T., Lee, H.M., Kim, D.W., Kim, K.J., Ha, G.H., Lee, G.G., 2010. Bismuth-telluride thermoelectric nanoparticles synthesized by using a polyol process. J. Korean Phys. Soc. 57, 1037–1040. https://doi.org/10.3938/jkps.57.1037.

Kim, C., Kim, D.H., Han, Y.S., Chung, J.S., Park, S.H., Kim, H., 2011. Fabrication of bismuth telluride nanoparticles using a chemical synthetic process and their thermoelectric evaluations. Powder Technol. 214, 463–468. https://doi.org/10.1016/j.powtec.2011.08.049.

Scheele, M., Oeschler, N., Meier, K., Kornowski, A., Klinke, C., Weller, H., 2009. Synthesis and Thermoelectric Characterization of Bi_2Te_3 Nanoparticles. Adv. Funct. Mater. 19, 3476–3483. https://doi.org/10.1002/adfm.200901261.

Zakeri, M., Allahkarami, M., Kavei, G., Khanmohammadian, A., Rahimipour, M.R., 2009. Synthesis of nanocrystalline Bi2Te3 via mechanical alloying. J. Mater. Process. Technol. 209, 96–101. https://doi.org/10.1016/j.jmatprotec.2008.01.027.

Tan, G., Shi, F., Hao, S., Zhao, L.D., Chi, H., Zhang, X., Uher, C., Wolverton, C., Dravid, V.P., Kanatzidis, M.G., 2016. Non-equilibrium processing leads to record high thermoelectric figure of merit in PbTe-SrTe. Nat. Commun. 7. https://doi.org/10.1038/ncomms12167.

Nassary, M.M., Shaban, H.T., El-Sadek, M.S., 2009. Semiconductor parameters of Bi2Te3 single crystal. Mater. Chem. Phys. 113, 385–388. https://doi.org/10.1016/j.matchemphys.2008.07.106.

Liu, Y., Zhou, M., He, J., 2016. Towards higher thermoelectric performance of Bi2Te3 via defect engineering. Scr. Mater. 111, 39–43. https://doi.org/10.1016/j.scriptamat.2015.06.031.

Ashalley, E., Chen, H., Tong, X., Li, H., Wang, Z.M., 2015. Bismuth telluride nanostructures: preparation, thermoelectric properties and topological insulating effect. Front. Mater. Sci. 9, 103–125. https://doi.org/10.1007/s11706-015-0285-9.

Liu, W., Yan, X., Chen, G., Ren, Z., 2012. Recent advances in thermoelectric nanocomposites. Nano Energy. 1, 42–56. https://doi.org/10.1016/j.nanoen.2011.10.001.

Bhattacharya, S., Pope, A.L., Littleton IV, R.T., Tritt, T.M., Ponnambalam, V., Xia, Y., Poon, S.J., 2000. Effect of Sb doping on the thermoelectric properties of Ti-based half-Heusler compounds, TiNiSn1-xSbx. Appl. Phys. Lett. 77, 2476–2478. https://doi.org/10.1063/1.1318237.

Hinterleitner, B., Knapp, I., Poneder, M., Shi, Y., Müller, H., Eguchi, G., Eisenmenger-Sittner, C., Stöger-Pollach, M., Kakefuda, Y., Kawamoto, N., Guo, Q., Baba, T., Mori, T., Ullah, S., Chen, X.Q., Bauer, E., 2019. Thermoelectric performance of a metastable thin-film Heusler alloy. Nature. https://doi.org/10.1038/s41586-019-1751-9.

Rogl, G., Ghosh, S., Wang, L., Bursik, J., Grytsiv, A., Kerber, M., Bauer, E., Mallik, R.C., Chen, X.-Q., Zehetbauer, M., Rogl, P., 2020. Half-Heusler alloys: Enhancement of ZT after severe plastic deformation (ultra-low thermal conductivity). Acta Mater. 183, 285–300. https://doi.org/10.1016/j.actamat.2019.11.010.

Li, S., Zhu, H., Mao, J., Feng, Z., Li, X., Chen, C., Cao, F., Liu, X., Singh, D.J., Ren, Z., Zhang, Q., 2019. n-Type TaCoSn-Based Half-Heuslers as Promising Thermoelectric Materials. ACS Appl. Mater. Interfaces. 11, 41321–41329. https://doi.org/10.1021/acsami.9b13603.

Sekimoto, T., Kurosaki, K., Muta, H., Yamanaka, S., 2005. Thermoelectric Properties of (Ti, Zr, Hf)CoSb Type Half-Heusler Compounds. Mater. Trans. 46, 1481–1484. https://doi.org/10.2320/matertrans.46.1481.

Wu, T., Jiang, W., Li, X., Bai, S., Liufu, S., Chen, L., 2009. Effects of Ge doping on the thermoelectric properties of TiCoSb-based p-type half-Heusler compounds. J. Alloys Compd. 467, 590–594. https://doi.org/10.1016/j.jallcom.2007.12.055.

Qiu, P., Huang, X., Chen, X., Chen, L., 2009. Enhanced thermoelectric performance by the combination of alloying and doping in TiCoSb-based half-Heusler compounds. J. Appl. Phys. 106. https://doi.org/10.1063/1.3238363.

Chauhan, N.S., Bathula, S., Vishwakarma, A., Bhardwaj, R., Johari, K.K., Gahtori, B., Dhar, A., 2019. Enhanced thermoelectric performance in p-type ZrCoSb based half-Heusler alloys employing nanostructuring and compositional modulation. J. Mater. 5, 94–102. https://doi.org/10.1016/j.jmat.2018.11.003.

Voronin, A.I., Serhiienko, I.A., Ashim, Y.Z., Kurichenko, V.L., Novitskii, A.P., Inerbaev, T.M., Umetsu, R., Khovaylo, V.V., 2019. Electrical Transport Properties of Nb and Ga Double Substituted Fe2VAl Heusler Compounds. Semiconductors. 53, 125–128. https://doi.org/10.1134/S1063782619130207.

Van Du, N., Rahman, J.U., Meang, E.J., Lim, C.H., Shin, W.H., Seo, W.S., Huy, P.T., Kim, M.H., Lee, S., 2019. Synthesis and thermoelectric properties of Ti-substituted (Hf0.5Zr0.5)1-xTix-NiSn0.998Sb0.002 Half-Heusler compounds. J. Alloys Compd. 773, 1141–1145. https://doi.org/10.1016/j.jallcom.2018.09.268.

El-Khouly, A., Novitskii, A., Adam, A.M., Sedegov, A., Kalugina, A., Pankratova, D., Karpenkov, D., Khovaylo, V., 2020. Transport and thermoelectric properties of Hf-doped FeVSb half-Heusler alloys. J. Alloys Compd. 820,. https://doi.org/10.1016/j.jallcom.2019.153413 153413.

H. Luo, Q. Li, K. Sun, S. Liu, Z. Liang, Magnetic properties and site preference of Ru in Heusler alloys Fe2V1-xRuxSi (x = 0.25, 0.5, 0.75, 1), J. Magn. Magn. Mater. 496 (2020). https://doi.org/10.1016/j.jmmm.2019.165908.

Yan, X., Joshi, G., Liu, W., Lan, Y., Wang, H., Lee, S., Simonson, J. W., Poon, S.J., Tritt, T.M., Chen, G., Ren, Z.F., 2011. Enhanced Thermoelectric Figure of Merit of p-Type Half-Heuslers. Nano Lett. 11, 556–560. https://doi.org/10.1021/nl104138t.

He, Q., Hao, Q., Wang, X., Yang, J., Lan, Y., Yan, X., Yu, B., Ma, Y., Poudel, B., Joshi, G., Wang, D., Chen, G., Ren, Z., 2008. Nanostructured thermoelectric skutterudite Co 1-xNi xSb 3 alloys. J. Nanosci. Nanotechnol. 8, 4003–4006. https://doi.org/10.1166/jnn.2008.469.

Wood, C., 1988. Materials for thermoelectric energy conversion. Reports Prog. Phys. 51, 459–539. https://doi.org/10.1088/0034-4885/51/4/001.

Graziosi, P., Kumarasinghe, C., Neophytou, N., 2019. Impact of the scattering physics on the power factor of complex thermoelectric materials. J. Appl. Phys. 126. https://doi.org/10.1063/1.5116793.

SLACK, G. A., New Materials and Performance Limits for Thermoelectric Cooling, CRC Handb. Thermoelectr. (1995) 407–440.

Nolas, G.S., Poon, J., Kanatzidis, M., 2006. Recent developments in bulk thermoelectric materials. MRS Bull. 31, 199–205. https://doi.org/10.1557/mrs2006.45.

Kurosaki, K., Kosuga, A., Muta, H., Uno, M., Yamanaka, S., 2005. Ag9TlTe5: A high-performance thermoelectric bulk material with extremely low thermal conductivity. Appl. Phys. Lett. 87. https://doi.org/10.1063/1.2009828.

Kim, S.J., Hu, S., Uher, C., Hogan, T., Huang, B., Corbett, J.D., Kanatzidis, M.G., 2000. Structure and thermoelectric properties of Ba6Ge(25–x), Ba6Ge23Sn2, and Ba6Ge22In3: Zintl phases with a chiral clathrate structure. J. Solid State Chem. 153, 321–329. https://doi.org/10.1006/jssc.2000.8777.

Okamoto, N.L., Oh, M.W., Nishii, T., Tanaka, K., Inui, H., 2006. Crystal structure and thermoelectric properties of the type-I clathrate compound Ba8Ge43 with an ordered arrangement of Ge vacancies. J. Appl. Phys. 99. https://doi.org/10.1063/1.2169869.

Nolas, G.S., Cohn, J.L., Slack, G.A., Schujman, S.B., 1998. Semiconducting Ge clathrates: Promising candidates for thermoelectric applications. Appl. Phys. Lett. 73, 178–180. https://doi.org/10.1063/1.121747.

Iversen, B.B., Palmqvist, A.E.C., Cox, D.E., Nolas, G.S., Stucky, G. D., Blake, N.P., Metiu, H., 2000. Why are clathrates good candidates for thermoelectric materials?. J. Solid State Chem. 149, 455–458. https://doi.org/10.1006/jssc.1999.8534.

Bentien, A., Christensen, M., Bryan, J.D., Sanchez, A., Paschen, S., Steglich, F., Stucky, G.D., Iversen, B.B., 2004. Thermal conductivity of thermoelectric clathrates. Phys. Rev. B - Condens. Matter Mater. Phys. 69. https://doi.org/10.1103/PhysRevB.69.045107.

Hou, X., Zhou, Y., Wang, L., Zhang, W., Zhang, W., Chen, L., 2009. Growth and thermoelectric properties of Ba8Ga16Ge30 clathrate crystals. J. Alloys Compd. 482, 544–547. https://doi.org/10.1016/j.jallcom.2009.04.072.

Wang, L., Chen, L.D., Chen, X.H., Bin Zhang, W., 2009. Synthesis and thermoelectric properties of n-type Sr8Ga 16-xGe30-y clathrates with different Ga/Ge ratios, J. Phys. D. Appl. Phys. 42. https://doi.org/10.1088/0022-3727/42/4/045113.

Deng, S., Saiga, Y., Suekuni, K., Takabatake, T., 2010. Enhancement of thermoelectric efficiency in type-VIII clathrate Ba 8Ga16Sn30 by Al substitution for Ga. J. Appl. Phys. 108. https://doi.org/10.1063/1.3490776.

S. Deng, Y. Saiga, K.K.-J. of A. Physics, undefined 2010, Toshiro Takabatake-High Thermoelectric Performance of Cu Substitution Type VIII Clathrates Ba8Ga16-xCuxGe30 Single Crystals, (n.d.).

Bobev, S., Sevov, S.C., 2001. Clathrate III of Group 14 Exists After All. J. Am. Chem. Soc. 123, 3389–3390. https://doi.org/10.1021/ja010010f.

Shi, X., Zhang, W., Chen, L.D., Yang, J., 2005. Filling fraction limit for intrinsic voids in crystals: Doping in skutterudites. Phys. Rev. Lett. 95. https://doi.org/10.1103/PhysRevLett.95.185503.

Nie, G., Li, W., Guo, J., Yamamoto, A., Kimura, K., Zhang, X., Isaacs, E.B., Dravid, V., Wolverton, C., Kanatzidis, M.G., Priya, S., 2019. High performance thermoelectric module through isotype bulk heterojunction engineering of skutterudite materials. Nano Energy. https://doi.org/10.1016/j.nanoen.2019.104193.

Qin, D., Wu, H., Cai, S., Zhu, J., Cui, B., Yin, L., Qin, H., Shi, W., Zhang, Y., Zhang, Q., Liu, W., Cao, J., Pennycook, S.J., Cai, W., Sui, J., 2019. Enhanced Thermoelectric and Mechanical Properties in Yb$_{0.3}$ Co$_{4}$ Sb$_{12}$ with In Situ Formed CoSi Nanoprecipitates. Adv. Energy Mater. 9, 1902435. https://doi.org/10.1002/aenm.201902435.

Tanahashi, H., Ohta, Y., Uchida, H., Itsumi, Y., Kasama, A., Matsubara, K., 2002. Formation of Cerium-Filled Skutterudite Thermoelectric Materials Sintered from Gas-Atomized Powder. Mater. Trans. 43, 1214–1219. https://doi.org/10.2320/matertrans.43.1214.

J. Junga, S. Urb, I.K.-J. of C.P. Research, undefined 2009, Thermoelectric properties of SnzCo4Sb11. 2Te0. 8 skutterudites, (n.d.).

Shi, X., Yang, J., Salvador, J.R., Chi, M., Cho, J.Y., Wang, H., Bai, S., Yang, J., Zhang, W., Chen, L., 2011. Multiple-Filled Skutterudites: High Thermoelectric Figure of Merit through Separately Optimizing Electrical and Thermal Transports. J. Am. Chem. Soc. 133, 7837–7846. https://doi.org/10.1021/ja111199y.

G.J. Snyder, E.S. Toberer, Complex thermoelectric materials, in: Mater. Sustain. Energy A Collect. Peer-Reviewed Res. Rev. Artic. from Nat. Publ. Gr., World Scientific Publishing Co., 2010: pp. 101–110. https://doi.org/10.1142/9789814317665_0016.

Zhang, F., Chen, C., Yao, H., Bai, F., Yin, L., Li, X., Li, S., Xue, W., Wang, Y., Cao, F., Liu, X., Sui, J., Zhang, Q., 2019. High-Performance N-type Mg$_{3}$ Sb$_{2}$ towards Thermoelectric Application near Room Temperature. Adv. Funct. Mater., 1906143 https://doi.org/10.1002/adfm.201906143.

Mohammadnia, A., Rezania, A., Ziapour, B.M., Sedaghati, F., Rosendahl, L., 2020. Hybrid energy harvesting system to maximize power generation from solar energy. Energy Convers. Manag. 205,. https://doi.org/10.1016/j.enconman.2019.112352 112352.

Rahman, S.M.A., Hachicha, A.A., Ghenai, C., Saidur, R., Said, Z., 2020. Performance and life cycle analysis of a novel portable solar thermoelectric refrigerator. Case Stud. Therm. Eng. 19,. https://doi.org/10.1016/j.csite.2020.100599 100599.

Luo, X., Guo, Q., Tao, Z., Liang, Y., Liu, Z., 2020. Modified phase change materials used for thermal management of a novel solar thermoelectric generator. Energy Convers. Manag. 208,. https://doi.org/10.1016/j.enconman.2019.112459 112459.

A. Riahi, A. Ben Haj Ali, A. Fadhel, A. Guizani, M. Balghouthi, Performance investigation of a concentrating photovoltaic thermal hybrid solar system combined with thermoelectric generators, Energy Convers. Manag. 205 (2020) 112377. https://doi.org/10.1016/j.enconman.2019.112377.

Y. Sargolzaeiaval, V. Padmanabhan Ramesh, T. V. Neumann, V. Misra, D. Vashaee, M.D. Dickey, M.C. Öztürk, Flexible thermoelectric generators for body heat harvesting – Enhanced device performance using high thermal conductivity elastomer encapsulation on liquid metal interconnects, Appl. Energy. 262 (2020) 114370. https://doi.org/10.1016/j.apenergy.2019.114370.

Jia, X., Guo, Q., 2020. Design study of Bismuth-Telluride-based thermoelectric generators based on thermoelectric and mechanical performance. Energy. 190,. https://doi.org/10.1016/j.energy.2019.116226 116226.

Kishore, R.A., Nozariasbmarz, A., Poudel, B., Priya, S., 2020. High-Performance Thermoelectric Generators for Field Deployments. ACS Appl. Mater. Interfaces. https://doi.org/10.1021/acsami.9b21299.

Ishaq, H., Islam, S., Dincer, I., Yilbas, B.S., 2020. Development and performance investigation of a biomass gasification based integrated system with thermoelectric generators. J. Clean. Prod. https://doi.org/10.1016/j.jclepro.2020.120625 120625.

Araiz, M., Casi, Á., Catalán, L., Martínez, Á., Astrain, D., 2020. Prospects of waste-heat recovery from a real industry using thermoelectric generators: Economic and power output analysis. Energy Convers. Manag. 205,. https://doi.org/10.1016/j.enconman.2019.112376 112376.

Lv, S., Liu, M., He, W., Li, X., Gong, W., Shen, S., 2020. Study of thermal insulation materials influence on the performance of thermoelectric generators by creating a significant effective temperature difference. Energy Convers. Manag. 207,. https://doi.org/10.1016/j.enconman.2020.112516 112516.

Riffat, S.B., Ma, X., 2003. Thermoelectrics: A review of present and potential applications. Appl. Therm. Eng. 23, 913–935. https://doi.org/10.1016/S1359-4311(03)00012-7.

Hamid Elsheikh, M., Shnawah, D.A., Sabri, M.F.M., Said, S.B.M., Haji Hassan, M., Ali Bashir, M.B., Mohamad, M., 2014. A review on thermoelectric renewable energy: Principle parameters that affect their performance, Renew. Sustain. Energy Rev. 30, 337–355. https://doi.org/10.1016/j.rser.2013.10.027.

Brito, F.P., Pacheco, N., Vieira, R., Martins, J., Martins, L., Teixeira, J., Goncalves, L.M., Oliveira, J., Hall, M.J., 2020. Efficiency improvement of vehicles using temperature controlled exhaust thermoelectric generators. Energy Convers. Manag. 203,. https://doi.org/10.1016/j.enconman.2019.112255 112255.

S. Shoeibi, N. Rahbar, A. Abedini Esfahlani, H. Kargarsharifabad, Application of simultaneous thermoelectric cooling and heating to improve the performance of a solar still: An experimental study and exergy analysis, Appl. Energy. 263 (2020) 114581. https://doi.org/10.1016/j.apenergy.2020.114581.

Cai, Y., Wang, L., Wang, W.W., Liu, D., Zhao, F.Y., 2020. Solar energy harvesting potential of a photovoltaic-thermoelectric cooling and power generation system: Bidirectional modeling and performance optimization. J. Clean. Prod. 254,. https://doi.org/10.1016/j.jclepro.2020.120150 120150.

Zhao, D., Yin, X., Xu, J., Tan, G., Yang, R., 2020. Radiative sky cooling-assisted thermoelectric cooling system for building applications. Energy. 190,. https://doi.org/10.1016/j.energy.2019.116322 116322.

Wang, H., Liang, X., Wang, J., Jiao, S., Xue, D., 2020. Multifunctional inorganic nanomaterials for energy applications. Nanoscale. 12, 14–42. https://doi.org/10.1039/c9nr07008g.

Meng, H., An, M., Luo, T., Yang, N., 2020. Thermoelectric applications of chalcogenides. Chalcogenide, Elsevier, 31–56. https://doi.org/10.1016/b978-0-08-102687-8.00002-6.

Gholikhani, M., Roshani, H., Dessouky, S., Papagiannakis, A.T., 2020. A critical review of roadway energy harvesting technologies. Appl. Energy. 261,. https://doi.org/10.1016/j.apenergy.2019.114388 114388.

Saha, C.R., Huda, M.N., Mumtaz, A., Debnath, A., Thomas, S., Jinks, R., 2020. Photovoltaic (PV) and thermo-electric energy harvesters for charging applications. Microelectronics J. 96,. https://doi.org/10.1016/j.mejo.2019.104685 104685.

Yu, K., Zhou, Y., Liu, Y., Liu, F., Hu, L., Ao, W., Zhang, C., Li, Y., Li, J., Xie, H., 2020. Near-room-temperature thermoelectric materials and their application prospects in geothermal power generation. Geomech. Geophys. Geo-Energy Geo-Resources. 6, 1–25. https://doi.org/10.1007/s40948-019-00134-z.

N. Pryds, R. Bjørk, Oxide thermoelectrics: From materials to module, in: Adv. Ceram. Energy Convers. Storage, Elsevier, 2020: pp. 131–156. https://doi.org/10.1016/b978-0-08-102726-4.00004-1.

Rodriguez, R., Preindl, M., Cotton, J.S., Emadi, A., 2019. Review and Trends of Thermoelectric Generator Heat Recovery in Automotive Applications. IEEE Trans. Veh. Technol. 68, 5366–5378. https://doi.org/10.1109/TVT.2019.2908150.

Vullers, R.J.M., van Schaijk, R., Doms, I., Van Hoof, C., Mertens, R., 2009. Micropower energy harvesting. Solid. State. Electron. 53, 684–693. https://doi.org/10.1016/j.sse.2008.12.011.

Wang, Y., Yang, L., Shi, X.L., Shi, X., Chen, L., Dargusch, M.S., Zou, J., Chen, Z.G., 2019. Flexible Thermoelectric Materials and Generators: Challenges and Innovations. Adv. Mater. 31, 1807916. https://doi.org/10.1002/adma.201807916.

Soleimani, Z., Zoras, S., Ceranic, B., Shahzad, S., Cui, Y., 2020. A review on recent developments of thermoelectric materials for room-temperature applications. Sustain. Energy Technol. Assessments. 37,. https://doi.org/10.1016/j.seta.2019.100604 100604.

Sharma, V., Kagdada, H.L., Jha, P.K., Śpiewak, P., Kurzydłowski, K.J., 2020. Thermal transport properties of boron nitride based materials: A review. Renew. Sustain. Energy Rev. 120,. https://doi.org/10.1016/j.rser.2019.109622 109622.

M. Wolf, R. Hinterding, A. Feldhoff, High Power Factor vs. High zT—A Review of Thermoelectric Materials for High-Temperature Application, Entropy. 21 (2019) 1058. https://doi.org/10.3390/e21111058.

Jaziri, N., Boughamoura, A., Müller, J., Mezghani, B., Tounsi, F., Ismail, M., 2019. A comprehensive review of Thermoelectric Generators: Technologies and common applications. Energy Reports. https://doi.org/10.1016/j.egyr.2019.12.011.

Jiang, B., Liu, X., Wang, Q., Cui, J., Jia, B., Zhu, Y., Feng, J., Qiu, Y., Gu, M., Ge, Z., He, J., 2020. Realizing high-efficiency power generation in low-cost PbS-based thermoelectric materials. Energy Environ. Sci. 13, 579–591. https://doi.org/10.1039/c9ee03410b.

Nozariasbmarz, A., Collins, H., Dsouza, K., Polash, M.H., Hosseini, M., Hyland, M., Liu, J., Malhotra, A., Ortiz, F.M., Mohaddes, F., Ramesh, V.P., Sargolzaeiaval, Y., Snouwaert, N., Özturk, M.C., Vashaee, D., 2020. Review of wearable thermoelectric energy harvesting: From body temperature to electronic systems. Appl. Energy. 258,. https://doi.org/10.1016/j.apenergy.2019.114069 114069.

Zhang, Y., Park, S.-J., 2019. Flexible Organic Thermoelectric Materials and Devices for Wearable Green Energy Harvesting. Polymers (Basel). 11, 909. https://doi.org/10.3390/polym11050909.

Cai, B., Hu, H., Zhuang, H.L., Li, J.F., 2019. Promising materials for thermoelectric applications. J. Alloys Compd. 806, 471–486. https://doi.org/10.1016/j.jallcom.2019.07.147.

Yu, C., Chau, K.T., 2009. Thermoelectric automotive waste heat energy recovery using maximum power point tracking. Energy Convers. Manag. 50, 1506–1512. https://doi.org/10.1016/j.enconman.2009.02.015.

Hsu, C.T., Huang, G.Y., Chu, H.S., Yu, B., Yao, D.J., 2011. Experiments and simulations on low-temperature waste heat harvesting system by thermoelectric power generators. Appl. Energy. 88, 1291–1297. https://doi.org/10.1016/j.apenergy.2010.10.005.

Karri, M.A., Thacher, E.F., Helenbrook, B.T., 2011. Exhaust energy conversion by thermoelectric generator: Two case studies. Energy Convers. Manag. 52, 1596–1611. https://doi.org/10.1016/j.enconman.2010.10.013.

Gou, X., Yang, S., Xiao, H., Ou, Q., 2013. A dynamic model for thermoelectric generator applied in waste heat recovery. Energy. 52, 201–209. https://doi.org/10.1016/j.energy.2013.01.040.

Suter, C., Tomeš, P., Weidenkaff, A., Steinfeld, A., 2010. Heat Transfer and Geometrical Analysis of Thermoelectric Converters Driven by Concentrated Solar Radiation. Materials (Basel). 3, 2735–2752. https://doi.org/10.3390/ma3042735.

He, W., Su, Y., Wang, Y.Q., Riffat, S.B., Ji, J., 2012. A study on incorporation of thermoelectric modules with evacuated-tube heat-pipe solar collectors. Renew. Energy. 37, 142–149. https://doi.org/10.1016/j.renene.2011.06.002.

Miljkovic, N., Wang, E.N., 2011. Modeling and optimization of hybrid solar thermoelectric systems with thermosyphons. Sol. Energy. 85, 2843–2855. https://doi.org/10.1016/j.solener.2011.08.021.

Zhang, Y., Heo, Y.-J., Park, M., Park, S.-J., 2019. Recent Advances in Organic Thermoelectric Materials: Principle Mechanisms and Emerging Carbon-Based Green Energy Materials. Polymers (Basel). 11, 167. https://doi.org/10.3390/polym11010167.

P. Eklund, S. Kerdsongpanya, B. Alling, Transition-Metal-Nitride-Based Thin Films as Novel Thermoelectric Materials, in: Thermoelectr. Thin Film., Springer International Publishing, 2019: pp. 121–138. https://doi.org/10.1007/978-3-030-20043-5_6.

Li, D., Gong, Y., Chen, Y., Lin, J., Khan, Q., Zhang, Y., Li, Y., Zhang, H., Xie, H., 2020. Recent Progress of Two-Dimensional Thermoelectric Materials. Nano-Micro Lett. 12, 1–40. https://doi.org/10.1007/s40820-020-0374-x.

Sun, Y., Di, C.A., Xu, W., Zhu, D., 2019. Advances in n-Type Organic Thermoelectric Materials and Devices. Adv. Electron. Mater. 5, 1800825. https://doi.org/10.1002/aelm.201800825.

Putri, Y.E., Said, S.M., Diantoro, M., 2019. Nanoarchitectured titanium complexes for thermal mitigation in thermoelectric materials. Renew. Sustain. Energy Rev. 101, 346–360. https://doi.org/10.1016/j.rser.2018.10.006.

Zhao, K., Qiu, P., Shi, X., Chen, L., 2019. Recent Advances in Liquid-Like Thermoelectric Materials. Adv. Funct. Mater. 30, 1903867. https://doi.org/10.1002/adfm.201903867.

Di Liu, W., Yang, L., Chen, Z.G., Zou, J., 2020. Promising and Eco-Friendly Cu2X-Based Thermoelectric Materials: Progress and Applications. Adv. Mater. 32, 1905703. https://doi.org/10.1002/adma.201905703.

P. MohanKumar, V. Jagadeesh Babu, A. Subramanian, A. Bandla, N. Thakor, S. Ramakrishna, H. Wei, Thermoelectric Materials—Strategies for Improving Device Performance and Its Medical Applications, Sci. 1 (2019) 37. https://doi.org/10.3390/sci1020037.

Li, C., Jiang, F., Liu, C., Liu, P., Xu, J., 2019. Present and future thermoelectric materials toward wearable energy harvesting. Appl. Mater. Today. 15, 543–557. https://doi.org/10.1016/j.apmt.2019.04.007.

Liu, X., Wang, Z., 2019. Printable Thermoelectric Materials and Applications. Front. Mater. 6, 88. https://doi.org/10.3389/fmats.2019.00088.

Chein, R., Huang, G., 2004. Thermoelectric cooler application in electronic cooling. Appl. Therm. Eng. 24, 2207–2217. https://doi.org/10.1016/j.applthermaleng.2004.03.001.

Putra, N., Yanuar, F.N., 2011. Iskandar, Application of nanofluids to a heat pipe liquid-block and the thermoelectric cooling of electronic equipment. Exp. Therm. Fluid Sci. 35, 1274–1281. https://doi.org/10.1016/j.expthermflusci.2011.04.015.

Y. Zhou, J. Yu, Design optimization of thermoelectric cooling systems for applications in electronic devices, in: Int. J. Refrig., Elsevier, 2012: pp. 1139–1144. https://doi.org/10.1016/j.ijrefrig.2011.12.003.

Wang, X., Yu, J., Ma, M., 2013. Optimization of heat sink configuration for thermoelectric cooling system based on entropy generation analysis. Int. J. Heat Mass Transf. 63, 361–365. https://doi.org/10.1016/j.ijheatmasstransfer.2013.03.078.

S.A. Abdul-Wahab, A. Elkamel, A.M. Al-Damkhi, I.A. Al-Habsi, H. S. Al-Rubai'ey', A.K. Al-Battashi, A.R. Al-Tamimi, K.H. Al-Mamari, M.U. Chutani, Design and experimental investigation of portable solar thermoelectric refrigerator, Renew. Energy. 34 (2009) 30–34. https://doi.org/10.1016/j.renene.2008.04.026.

Dai, Y.J., Wang, R.Z., Ni, L., 2003. Experimental investigation on a thermoelectric refrigerator driven by solar cells. Renew. Energy. 28, 949–959. https://doi.org/10.1016/S0960-1481(02)00055-1.

Shen, L., Xiao, F., Chen, H., Wang, S., 2013. Investigation of a novel thermoelectric radiant air-conditioning system. Energy Build. 59, 123–132. https://doi.org/10.1016/j.enbuild.2012.12.041.

Riffat, S.B., Qiu, G., 2004. Comparative investigation of thermoelectric air-conditioners versus vapour compression and absorption air-conditioners. Appl. Therm. Eng. 24, 1979–1993. https://doi.org/10.1016/j.applthermaleng.2004.02.010.

Hirota, M., Nakajima, Y., Saito, M., Uchiyama, M., 2007. 120 × 90 element thermoelectric infrared focal plane array with precisely patterned Au-black absorber. Sensors Actuators, A Phys. 135, 146–151. https://doi.org/10.1016/j.sna.2006.06.058.

Chen, S.-J., Wu, Y.-C., 2019. Active Thermoelectric Vacuum Sensor Based on Frequency Modulation. Micromachines. 11, 15. https://doi.org/10.3390/mi11010015.

Huang, L., Chen, J., Yu, Z., Tang, D., 2020. Self-Powered Temperature Sensor with Seebeck Effect Transduction for Photothermal-Thermoelectric Coupled Immunoassay. Anal. Chem. 92, 2809–2814. https://doi.org/10.1021/acs.analchem.9b05218.

El-Genk, M.S., Saber, H.H., Caillat, T., Sakamoto, J., 2006. Tests results and performance comparisons of coated and un-coated skutterudite based segmented unicouples. Energy Convers. Manag. 47, 174–200. https://doi.org/10.1016/j.enconman.2005.03.023.

Ma, Z., Wang, C., Chen, Y., Li, L., Li, S., Wang, J., Zhao, H., 2021. Ultra-high thermoelectric performance in SnTe by the integration of several optimization strategies. Mater. Today Phys. 17,. https://doi.org/10.1016/j.mtphys.2021.100350 100350.

J.-W.G. Bos, Recent developments in half-Heusler thermoelectric materials, in: Thermoelectr. Energy Convers., Elsevier, 2021: pp. 125–142. https://doi.org/10.1016/b978-0-12-818535-3.00014-1.

Y. Tsai, P. Wei, L. Chang, K. Wang, C. Yang, Y. Lai, C. Hsing, C. Wei, J. He, G.J. Snyder, H. Wu, Thermoelectric Materials: Compositional Fluctuations Locked by Athermal Transformation Yielding High Thermoelectric Performance in GeTe (Adv. Mater. 1/2021), Adv. Mater. 33 (2021) 2170008. https://doi.org/10.1002/adma.202170008.

Yang, J., Xi, L., Qiu, W., Wu, L., Shi, X., Chen, L., Yang, J., Zhang, W., Uher, C., Singh, D.J., 2016. On the tuning of electrical and thermal transport in thermoelectrics: An integrated theory-experiment perspective. Npj Comput. Mater. 2, 1–17. https://doi.org/10.1038/npjcompumats.2015.15.

Song, S.W., Mao, J., Bordelon, M., He, R., Wang, Y.M., Shuai, J., Sun, J.Y., Lei, X.B., Ren, Z.S., Chen, S., Wilson, S., Nielsch, K., Zhang, Q.Y., Ren, Z.F., 2019. Joint effect of magnesium and yttrium on enhancing thermoelectric properties of n-type Zintl Mg 3 + δ Y 0.02 Sb 1.5 Bi 0.5. Mater. Today Phys. 8, 25–33. https://doi.org/10.1016/j.mtphys.2018.12.004.

Wu, Y., Chen, Z., Nan, P., Xiong, F., Lin, S., Zhang, X., Chen, Y., Chen, L., Ge, B., Pei, Y., 2019. Lattice Strain Advances Thermoelectrics. Joule. 3, 1276–1288. https://doi.org/10.1016/j.joule.2019.02.008.

Vining, C.B., 2009. An inconvenient truth about thermoelectrics. Nat. Mater. 8, 83–85. https://doi.org/10.1038/nmat2361.

Saidur, R., Rezaei, M., Muzammil, W.K., Hassan, M.H., Paria, S., Hasanuzzaman, M., 2012. Technologies to recover exhaust heat from internal combustion engines. Renew. Sustain. Energy Rev. 16, 5649–5659. https://doi.org/10.1016/j.rser.2012.05.018.

Hyland, M., Hunter, H., Liu, J., Veety, E., Vashaee, D., 2016. Wearable thermoelectric generators for human body heat harvesting. Appl. Energy. 182, 518–524. https://doi.org/10.1016/j.apenergy.2016.08.150.

Irshad, K., Habib, K., Saidur, R., Kareem, M.W., Saha, B.B., 2019. Study of thermoelectric and photovoltaic facade system for energy efficient building development: A review. J. Clean. Prod. 209, 1376–1395. https://doi.org/10.1016/J.JCLEPRO.2018.09.245.